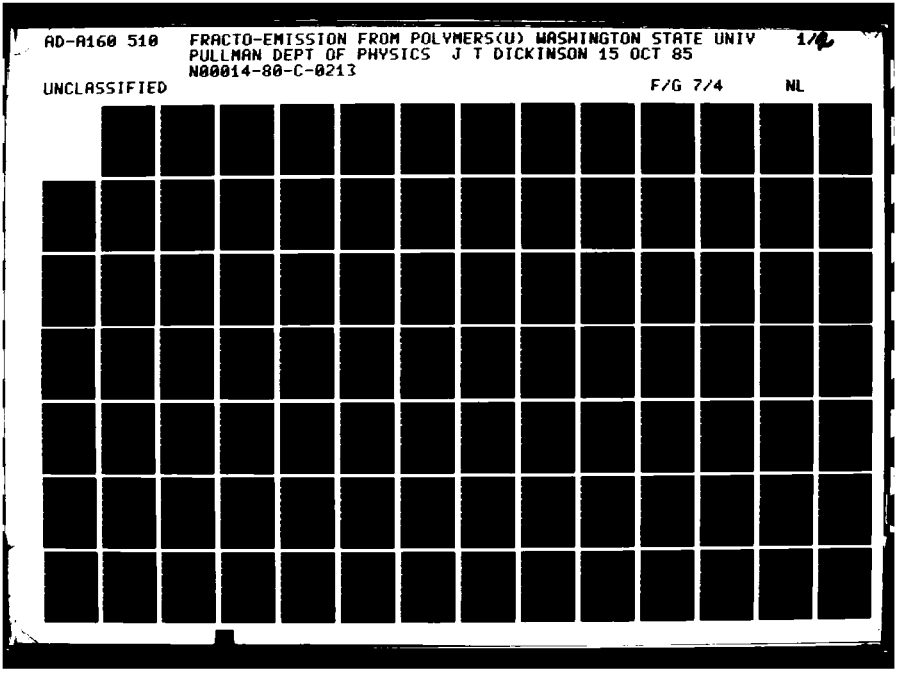
AD-A160 510 FRACTO-EMISSION FROM POLYMERS(U) WASHINGTON STATE UNIV 1/2
PULLMAN DEPT OF PHYSICS J T DICKINSON 15 OCT 85
N00014-80-C-0213
UNCLASSIFIED F/G 7/4 NL

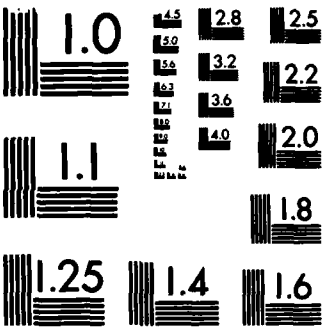

UNCLASSIFIED

SECURITY CLASSIFICATION OF THIS PAGE (When Data Entered)

(12)

REPORT DOCUMENTATION PAGE		READ INSTRUCTIONS BEFORE COMPLETING FORM
1. REPORT NUMBER	2. GOVT ACCESSION NO.	3. RECIPIENT'S CATALOG NUMBER
4. TITLE (and Subtitle) Fracto-Emission from Polymers		5. TYPE OF REPORT & PERIOD COVERED Annual Technical Report June, 1984 - June 1985
		6. PERFORMING ORG. REPORT NUMBER
7. AUTHOR(s) J. Thomas Dickinson		8. CONTRACT OR GRANT NUMBER(s) N00014-80-C-0213
PERFORMING ORGANIZATION NAME AND ADDRESS Department of Physics Washington State University Pullman, WA 99164-2814		10. PROGRAM ELEMENT, PROJECT, TASK AREA & WORK UNIT NUMBERS NR 659-803
1. CONTROLLING OFFICE NAME AND ADDRESS Office of Naval Research Propulsion and Energetics Program Arlington, VA 22217		12. REPORT DATE October 15, 1985
		13. NUMBER OF PAGES 115
4. MONITORING AGENCY NAME & ADDRESS(if different from Controlling Office)		15. SECURITY CLASS. (of this report) Unclassified
		15a. DECLASSIFICATION/DOWNGRADING SCHEDULE

AD-A160 510

5. DISTRIBUTION STATEMENT (of this Report)

Approved for public release; distribution unlimited

17. DISTRIBUTION STATEMENT (of the abstract entered in Block 20, if different from Report)

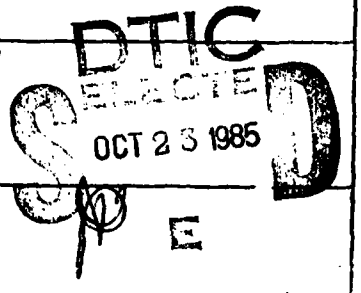

18. SUPPLEMENTARY NOTES

19. KEY WORDS (Continue on reverse side if necessary and identify by block number) fracture, crack propagation, fracture surfaces, interfacial failure, exo-emission, electron emission, positive ion emission, photon emission, tribo-luminescence, radio-wave emission, fracto-emission, surface charging, fracture-induced breakdown, gaseous discharges, electrical breakdown, fracture of: Polymers, propellents, elastomers, rubber, MgO, and PETN. Electron beam damage, induced fracture, Kevlar.

20. ABSTRACT (Continue on reverse side if necessary and identify by block number) Progress in the investigation of fracto-emission (FE) from polymers is reported. Measurements characterizing the FE, experiments concerning FE mechanisms, and studies of factors influencing FE are discussed. This work includes: measurements of fracto-emission from model propellents, a metal-polymer interface, the peeling of pressure sensitive adhesives, and single crystal MgO. We report also the electron induced fracture of single filaments of a polymer, Kevlar-49.

DTIC FILE COPY

DD FORM 1 JAN 73 1473 EDITION OF 1 NOV 65 IS OBSOLETE

Unclassified

SECURITY CLASSIFICATION OF THIS PAGE (When Data Entered)

OFFICE OF NAVAL RESEARCH
Contract N00014-80-C-0213
Project NR 092-558

Annual Technical Report
October 1985

FRACTO-EMISSION FROM POLYMERS

J. Thomas Dickinson

Department of Physics
Washington State University
Pullman, Washington 99164-2814

TABLE OF CONTENTS

I. TECHNICAL SUMMARY

Crack propagation through an insulating material or at an interface produces regions of high electronic and chemical activity on the freshly-created surfaces. This activity causes the emission of particles, i.e. electrons, ions, and neutral species, as well as photons, from the surfaces both during and after crack propagation. This emission is called fracto-emission (FE), and in many ways serves as a probe of the electronic and chemical activity of the fracture surfaces. The work described in this report represents the results of our research activity from June 1, 1984 to May 31, 1985. Our primary goals have been to further characterize FE from polymers, crystalline materials, and from interfaces, to further our understanding of the FE mechanisms, and to examine the dependence of FE on the nature of the fracture event and material properties.

In this report we present our results on: the fracto-emission from model propellents with a variety of formulations, the fracto-emission from a metal-polymer interface with and without an externally applied electric field, the photon and radiowave emission from peeling pressure sensitive adhesives, the detection of atom and molecular emission (neutral charge) emitted from the fracture of inorganic single crystals, and a study of the effect of electron bombardment of single fibers of a polymer. In addition, we discuss briefly the work in progress in several areas related to the above projects: the fracto-emission mechanisms from single crystal inorganics, the neutral emission from both polymers and inorganics, the fracto-emission from explosive crystals, a number of interfacial failure studies (including the fracture of particulate-filled binders), and further work in the area of radiation induced fracture.

values, an electron beam focused onto a polymeric fiber (Kevlar-49) in tension can cause the fiber to fail. Calculations of the temperature of the fiber due to energy deposition during bombardment is well below the temperatures when the fiber should yield. We conclude that the fracture is dominated by electrons producing bond scissions in critical load carrying chains.

Finally, in Section VIII we outline our work in progress on several areas related to the above projects: the fracto-emission from single crystal inorganics, the neutral emission from both polymers and inorganics, the fracto-emission from explosive crystals, a number of interfacial failure studies (including the fracture of particulate-filled binders), and further work in the area of radiation induced fracture.

Participants in this Work

J. Thomas Dickinson, Principal Investigator
L. C. Jensen, Research Physicist
M. H. Miles, Associate Professor of Physics
E. E. Donaldson, Professor of Physics
M. K. Klakken, Research Assistant, M. S. Degree, Pursuing Ph.D.
X. Shen, Research Assistant, M. S. Degree.
J. Bye, Research Assistant, M. S. Degree.
L. A. K'Singam, Research Assistant, M. S. Degree.

Visitors Contributing to this Work

Dr. Alan Gent, Institute of Polymer Science, University of Akron
Dr. Friedemann Freund, Institute of Geochemistry, University of Koln

III. ELECTRON AND PHOTON EMISSION ACCOMPANYING FRACTURE OF CYCLOTRIMETHYLENE TRINITRAMINE (RDX) FILLED POLYMERIC BINDERS

J. T. Dickinson, M. H. Miles, and L. C. Jensen
Department of Physics
Washington State University
Pullman, WA 99164-2814

ABSTRACT

Electron and photon emission was examined during tensile loading and compressional impact of cyclotrimethylene trinitramine (RDX) loaded polymeric binders. These materials are model formulations produced by at the Naval Weapons Center for a study of the effects of surface interactions and mechanical properties of plastic bonded explosives on explosive sensitivity. In these fracto-emission studies we observe considerable differences in the emission intensity and time dependence for different material formulation and loading conditions.

INTRODUCTION

Dynamic fracture of polymers or interfacial failure produces regions of high electronic and chemical activity on the freshly-created surfaces. The various excitations of the fracture surface can lead to the emission of particles; i.e., electrons, ions, neutral species, and photons both during and after crack propagation. This emission is collectively referred to as "fracto-emission". In several of our papers we have outlined current models for the observed emission [1-6]. In particular, we have shown that the unique condition of fracture at interfaces of dissimilar materials can lead to FE of high intensity, long duration, and other distinguishing characteristics.

The work presented here involves measurements of the electron and photon emission during and following fracture and mechanical impact of model propellant materials. The formulations used were produced at the Naval Weapons Center (NWC) as part of a study carried out by R. Y. Yee and E. C. Martin, NWC, on the effects of surface interactions and mechanical properties of plastic bonded explosives on explosive sensitivity. The compositions of

Table 1. (Continued).

TABLE 2. Composition of R45M/IPDI Formulations.

Material	Weight percent			
	BLX-1	BLX-2	BLX-3	BLX-11
R45M	23.20	18.55	23.20	23.20
IPDI	1.74	1.39	1.74	1.74
Triphenyl bismuth	0.03	0.03	0.03	0.30
Octanoic acid	0.03	0.03	0.03	0.30
RDX (class A)	22.56	0.00	0.00	0.00
RDX (screened class A)	0.00	32.00	30.00	30.00
RDX (class E)	52.50	48.00	45.00	45.00
Total RDX	75.00	80.00	75.00	75.00
NCO/OH[a]	0.95	0.95	0.95	0.95
Shore A hardness	58.00	65.00	63.00	...

[a]Isocyanate/hydroxyl ratio.

TABLE 3. Composition of GAP Formulations.

Material	Weight percent			
	BLX-4	BLX-7	BLX-8	BLX-9
GAP	4.95	26.73	26.72	9.18
N-100[a]	1.30	4.68	4.68	2.09
TMETN	18.70	0.00	0.00	0.00
BTTN	0.00	0.00	0.00	22.63
Plasticizer/polymer	3.00	0.00	0.00	2.00
RS-5[b]	0.00	0.00	0.00	0.20
T-12[c]	0.005	0.005	0.005	0.005
Octanoic acid	0.00	0.00	0.05	0.00
RDX (screened class A)	44.91	27.43	27.43	39.54
RDX (class E)	29.94	41.15	41.15	26.36
Total RDX	74.80	68.60	68.60	65.90
NCO/OH	1.50	1.00	1.00	1.30
Shore A hardness	12.00	...	70.00	48.00

[a]Poly functional isocyanate.

[b]Nitrocellulose.

[c]Dibutyltin dilaurate.

Table 1. (Continued).

NWC TP 6619

TABLE 4. Composition of Acrylic Formulations.

Material	Weight percent BLX-5 and -6
EHA[a]	11.34
VP[b]	7.61
DOM[c]	8.11
TGDMA[d]	0.10
COAA[e]	0.03
t-BPB[f]	0.29
RDX (screened class A)	29.01
RDX (class E)	43.51
Total RDX	72.51
NCO/OH	1.20
Shore A hardness	18.00

[a]2-ethylhexylacrylate.

[b]N-vinyl-2-pyrolidane.

[c]Dioctylmaleate.

[d]Triethyleneglycol dimethacrylate.

[e]Cobaltous acetylacetonate.

[f]Tertiary-butyl perbenzoate.

TABLE 5. Composition of BAMO/THF Formulations.

Material	Weight percent BLX-10
BAMO/THF (5L)	9.90
N-100	1.25
BTTN	22.29
Plasticizer/polymer	2.00
RS-5	0.20
T-12	0.003
Octanoic acid	0.030
RDX (screened class A)	26.53
RDX (class E)	39.80
Total RDX	66.33
NCO/OH	0.95

physics data acquisition techniques were employed to count and store pulses as a function of time.

RESULTS AND DISCUSSION

Slow tensile loading of the notched specimens generally resulted in opening up of the notch followed by crack growth over a time period of a few seconds. Data were usually collected at 0.1 second per channel for a total of 4095 channels, corresponding to a time of 410 seconds. For comparison of intensities, we report total counts detected for a period of 100 s starting with the fracture event. Table 2 below summarizes electron and photon emission for the two types of urethane cross linked polybutadiene specimens tested at the low strain rate. The background count rate for our electron detector is sufficiently low that it can be ignored; the much larger photon detector background count rate was subtracted from the acquired data.

Table 2. Slow Tensile Loading—Notched Sample

Sample Type	Total Electron Count	Peak Electron Count	Total Photon Count	Peak Photon Count
BLX-1	13,000	2,700	40	30
BLX-3	10,000	2,250	<20	< 20

Fig. 1a and 1b show the electron emission from two samples of type BLX-1, where we have plotted approximately 10 s of data. The rise in emission coincides with the onset of crack growth and the most intense emission is occurring during crack growth. The results in Fig. 1b shows more distinct after emission following separation (at approx. 5 s on the time axis). Fig. 2

show similar EE electron emission curves for two BLX-3 specimens. Note the duration of emission in 2b is somewhat longer than in 2a; this is due to a longer time of crack growth for that particular sample. The photon emission for BLX-3 was negligible compared to our detector noise for this strain rate and the BLX-1 material yielded only a small peak during fracture.

The only difference between BLX-1 and BLX-3 is the particle size of the RDX, where BLX-3 contains the smaller particle sizes. Our results indicate that there is a slight dependence on electron and photon emission intensities on this parameter.

Results for the medium speed tensile loading (strain rate of 10/s) are given in Table 3 for four of the formulations.

Table 3. Medium Speed Tensile Loading—Electron, Photon Emission

Sample Type	Total Electron Count (in 100 s)	Peak Electron Count	Total Photon Count (0.1 s)	Peak Photon Count
BLX-1	30,000	11,000	700	600
BLX-3	17,000	8,000	2,000	1,500
BLX-8	81,000	5,000	7,000	700
BLX-9	400	300	1,600	1,500

Clearly, the higher strain rate has resulted in considerably more emission from the two urethane crosslinked polybutadiene formulations (BLX-1 and BLX-3). Fig. 3 shows the electron and photon emission, measured simultaneously, for medium rate loading of BLX-1. One sees a single channel of photon emission in coincidence with the fracture event and the rapid rise

in electron emission. The decay in the electron emission following fracture is much more evident at this higher strain rate. Very similar curve shapes are seen for the BLX-3 formulation, as seen in Fig. 4.

The tensile impact or fast tensile loading results are summarized in Table 4 (strain rate 100/s). The duration of the fracture event is estimated to be on the order of a few ms. To make comparisons of total counts and decay curves with the other strain rates, we did not change the data acquisition rate.

Table 4. Fast Tensile Loading—Electron and Photon Emission

Sample Type	Total Electron Count	Peak Electron Count	Total Photon Count	Peak Photon Count
BLX-1	400,000	60,000	5,000	3,000
BLX-3	24,000	8,500	2,300	900
BLX-4	1,500	1,300	200	100
BLX-6	2,500	1,000	1,900	1,200
BLX-8	5,300	1,700	700	400
BLX-9	250	200	100	20

In the cases of BLX-1 and BLX-3, we again observe substantial increases in emission intensity with strain rate. On the contrary, BLX-8 and BLX-9 both show decreases in emission intensity. Also, BLX-1 (containing larger RDX particles) tended to be much more emissive than BLX-3.

Fig. 5 shows the electron emission and photon emission (plotted on different time scales) for BLX-1. Both peaks occurred in coincidence with the fracture event and the photon emission shows an observable decay curve shown

on the faster time scale (0.01 s/channel). Electron emission curves for BLX-3, BLX-4, and BLX-6 from fast tensile loading are shown in Fig. 6.

Compressional impact was the final form of loading examined in this study. Such impact of the samples lead to considerable plastic deformation with expansion of the material out of the "vise" which produces considerable tensile deformation on the outer surfaces. In Table 5, we summarize the compressional impact results.

Table 5. Electron and Photon Emission - Compressional Impact

Sample Type	Total Electron Count	Peak Electron Count	Total Photon Count	Peak Photon Count
BLX-1	300,000	40,000	30,000	700
BLX-3	600,000	9,000	30,000	600
BLX-4	1,000	300	1,000	200
BLX-6	2,000	300	1,000	400
BLX-8	2,000	1,000	30,000	1,000
BLX-9	2,000	1,000	100	100

The measured peak electron emission is, on the average, reduced compared to Table 4, yet very strong, sustained emission follows impact. In general, the electron emission decayed slower following compressional impact than for tension. Fig. 7a and 7b show the electron emission for compressional impact of BLX-1 and BLX-3, illustrating the missing "peak". It is possible that the deformation of the material during impact tends to depress the emission because new surfaces are being pushed together rather than opening up, as is the case in tension. We therefore suspect that the geometry for this form of loading is actually very poor for electrons escaping the

material, so that the actual emission may be considerably higher. Fig. 8 show the electron emission from BLX-6 and BLX-9, loaded in compressional impact. The lower intensities and shorter decays can be seen.

One piece of previously unpublished data indicates the importance of the interface in the BLX-1 and BLX-3 formulations. In 1983, a small amount of unfilled R45M/IPDI of very similar composition to these formulations was provided to us by NWC. We tested the material immediately for electron emission under the condition of slow tension; the results are shown in Fig. 9. The arrow indicates the onset of elongation; the time of fracture is also shown. The most important thing to notice is that the emission intensity is small: 100 s of emission totals approx. 500 counts.

We have previously shown that for a number of filled polymers, the occurrence of interfacial failure greatly enhances charged particle and photon emission. This is because of the charge separation that occurs when dissimilar materials are separated. Such an effect leads to charge induced phenomena such as electrical breakdown in the crack tip, causing excitation of the surfaces and a number of particle and photon emission processes [1-6]. It appears that similar effects are occurring in the filled R45M/IPDI specimens, and we expect in the other binders, also, albeit, at lower levels of activity.

CONCLUSIONS

We have shown that under various loading conditions, the plastic bonded explosives studied here lead to detectable electron and photon emission accompanying and following fracture. In general, the BLX-1 and BLX-3 formulations were more emissive, with slight differences between them for various loading conditions. Of the remaining formulations tested, BLX-8 was the next highest. When these results are compared with the mechanical

properties of these materials measured at NWC [7], we find some interesting correlations. We feel the two most important parameters which correlate with our tensile test results are the tensile stress for the onset of dewetting and the tensile stress at failure, which mechanically are themselves intimately related. BLX-1, BLX-3, and BLX-8 showed considerably higher values for these stresses. These higher stresses can lead to much more energetic and rapid detachment of the binder from the filler particles. This should be more effective in producing charge separation on the fracture surfaces and therefore induces more emission. With the addition to the plasticizer BTTN to the GAP-RDX (BLX-8) formulation, the tensile stress at fracture was reduced by 60%. This was accompanied by a 80% drop in the peak electron emission.

These formulations exhibited considerable dependence in their emission intensities with the rate of loading. This has proven to be the case for a number of materials studied to date, including filled elastomers and epoxies, as well as single crystals of inorganic and organic compounds. Higher rates of loading tends to cause more "damage" to the material, and again results in faster separation between the freshly created fracture surfaces. Both consequences can contribute to the increase in emission intensity. Furthermore, as the loading becomes increasingly violent, the onset of localized instabilities may also arise and contribute to the emission of particles. It is of considerable interest to try more severe loading conditions and examine the possible influence of higher rates of deformation on the various fracto-emission components.

REFERENCES

1. J. T. Dickinson, L. B. Brix, and L. C. Jensen, J. Phys. Chem. 88, 1698 (1984).

2. J. T. Dickinson and L. C. Jensen, J. Poly. Sci.: Poly. Phys. Ed. 23, 873 (1985).

3. J. T. Dickinson, L. C. Jensen, and A. Jahan-Latibari, J. Vac Sci. and Technol. A 2, 1112 (1984).

4. H. Miles and J. T. Dickinson, Appl. Phys. Lett. 41, 924 (1982).

5. J. T. Dickinson, M. H. Miles, W. L. Elban, and R. G. Rosemeier, J. Appl. Phys. 55, 3994 (1984).

6. M. H. Miles, J. T. Dickinson, and L. C. Jensen, J. Appl. Phys. 57, 5048 (1985).

7. R. Y. Yee and E. C. Martin, "Effects of Surface Interactions and Mechanical Properties of Plastic Bonded Explosives on Explosive Sensitivity. Part 2: Model Formulation", Naval Weapons Center Technical Publication 6619, March, 1985.

FIGURE CAPTIONS

Fig. 1. a) and b). Electron emission accompanying slow tensile testing of two BLX-1 samples. The emission intensity is plotted on a log scale.

Fig. 2. a) and b). Electron emission accompanying slow tensile testing of two BLX-3 samples.

Fig. 3. Simultaneous measurements of the electron and photon emission for medium rate of tensile testing on a BLX-1 sample.

Fig. 4. Simultaneous measurements of the electron and photon emission for medium rate of tensile testing on a BLX-3 sample.

Fig. 5. The electron and photon emission accompanying fast tensile testing of BLX-1. Note the different time scales.

Fig. 6. Electron emission curves for BLX-3, BLX-4, and BLX-6 samples under fast tensile test conditions.

Fig. 7. Electron emission accompanying impact compression of a) BLX-1 and b) BLX-3.

Fig. 8. Electron emission for BLX-6 and BLX-9 loaded in compressional impact.

Fig. 9. Electron emission for unfilled R43M/IPDM (urethane crosslinked polybutadiene) tested in slow tension.

ELECTRON EMISSION - SLOW TENSILE

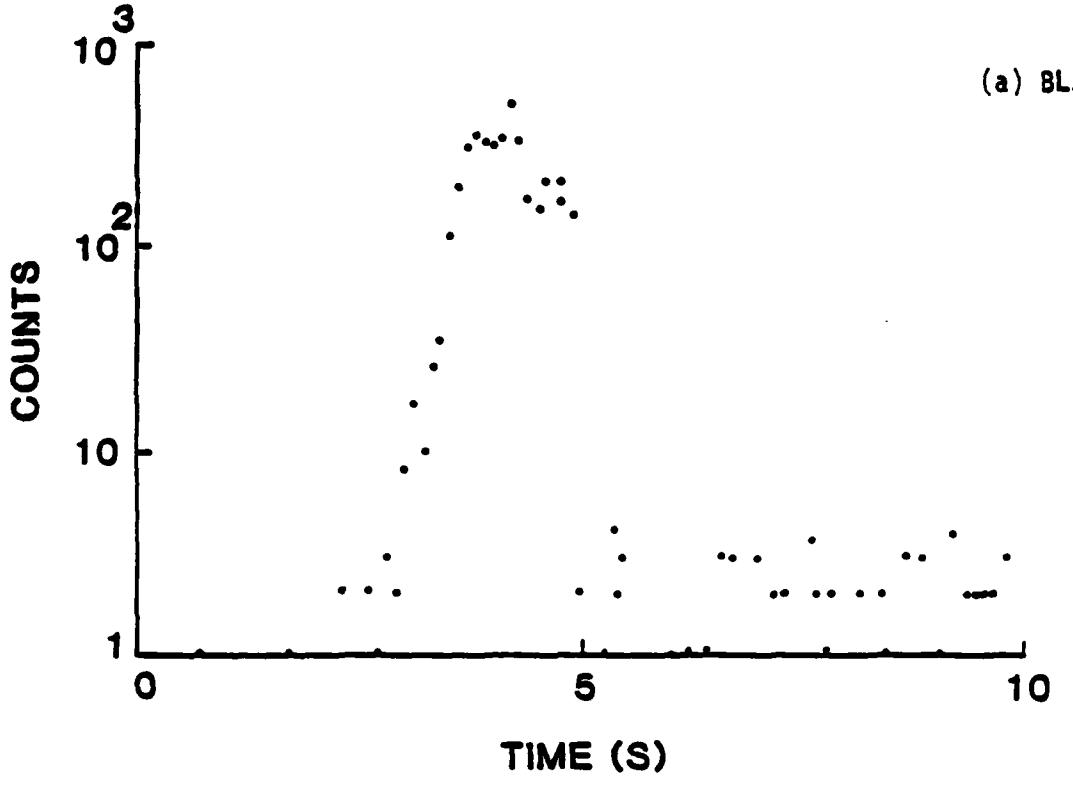

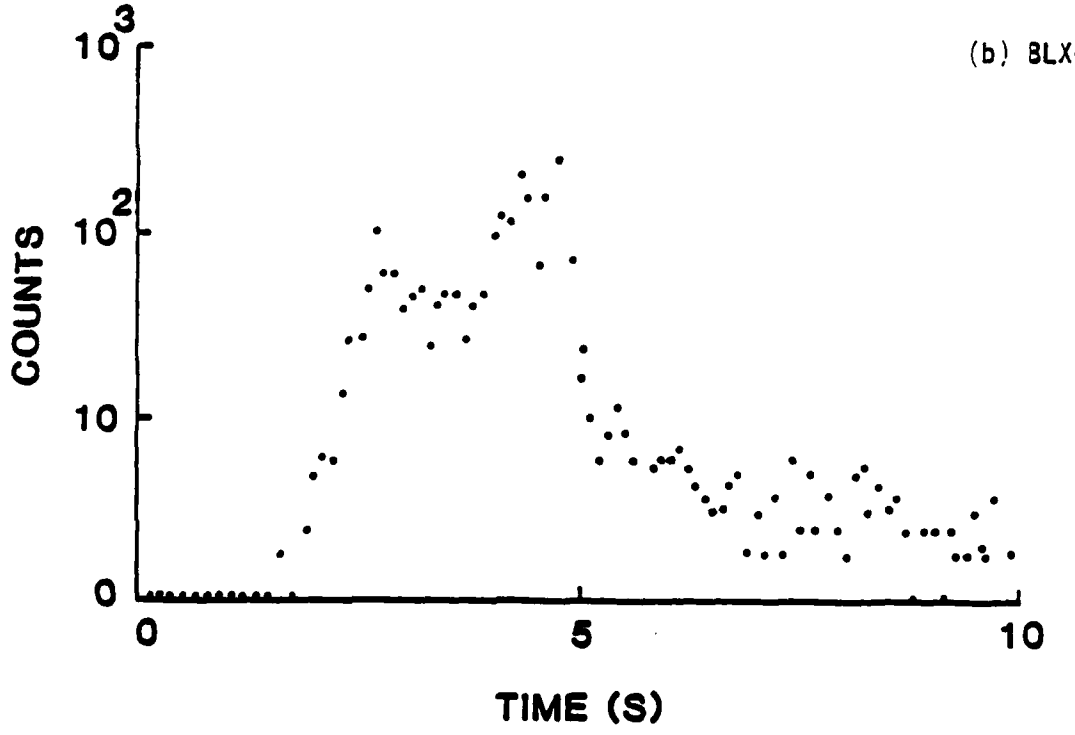

Fig. III-1

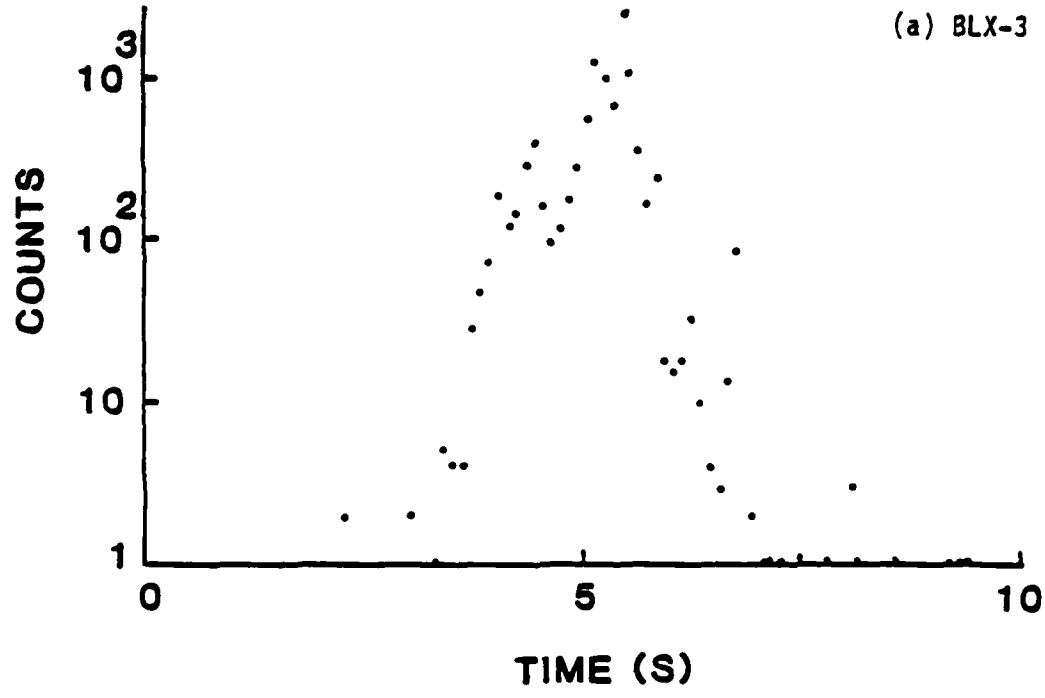
(a) BLX-3
COUNTS
10^3
10^2
10
1
0
5
10
TIME (S)

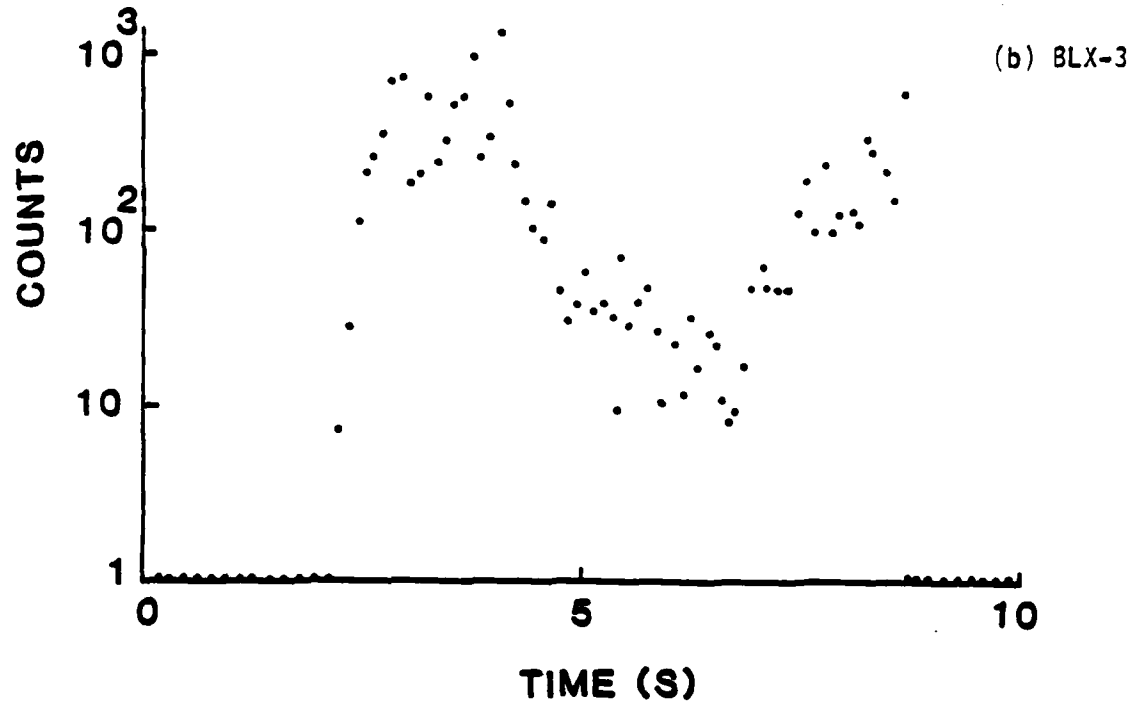
(b) BLX-3
COUNTS
10^3
10^2
10
1
0
5
10
TIME (S)

Fig. III-2

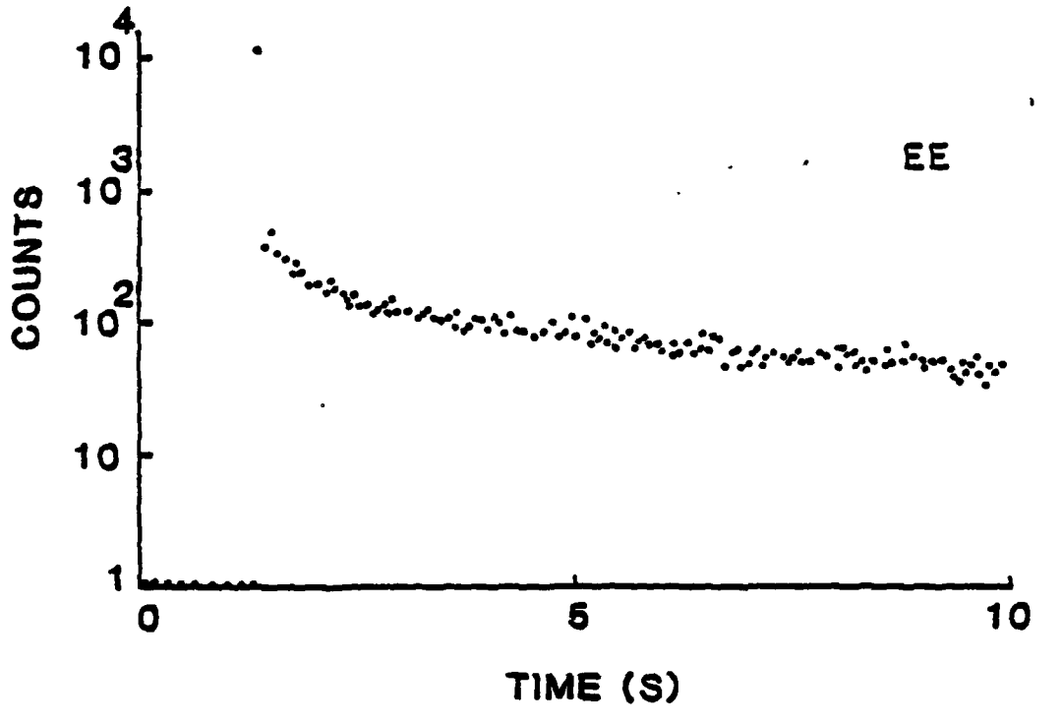
EE
COUNTS
10^4
10^3
10^2
10
1
0
5
10
TIME (S)

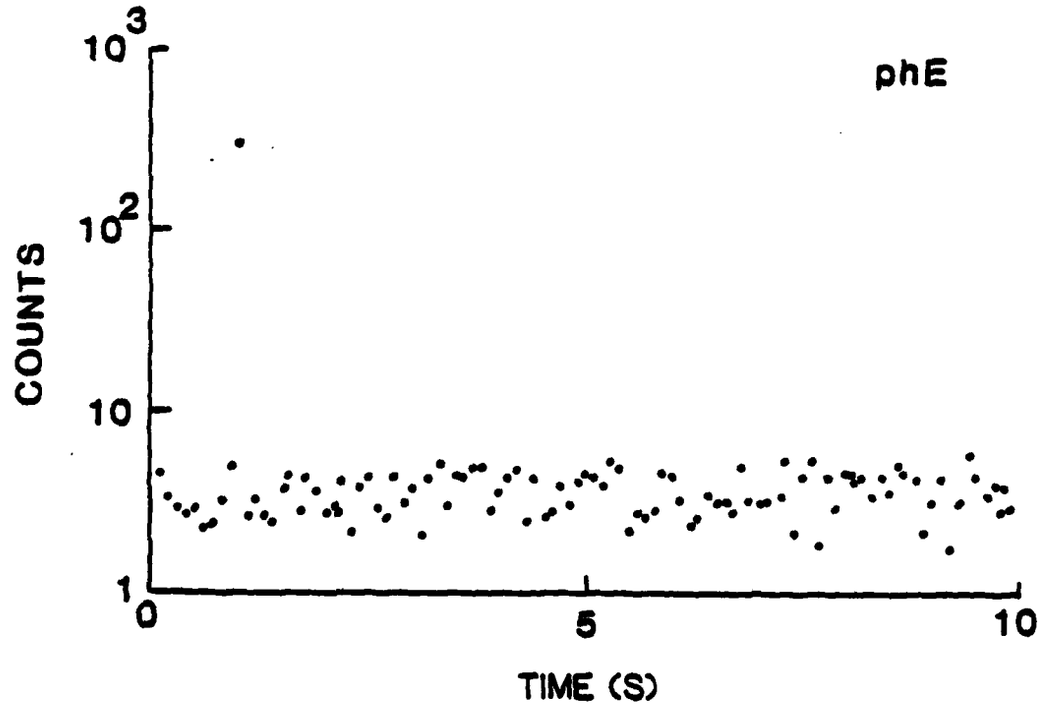
phE
COUNTS
10^3
10^2
10
1
0
5
10
TIME (S)

Fig. III-3

EE AND phE FROM BLX-3

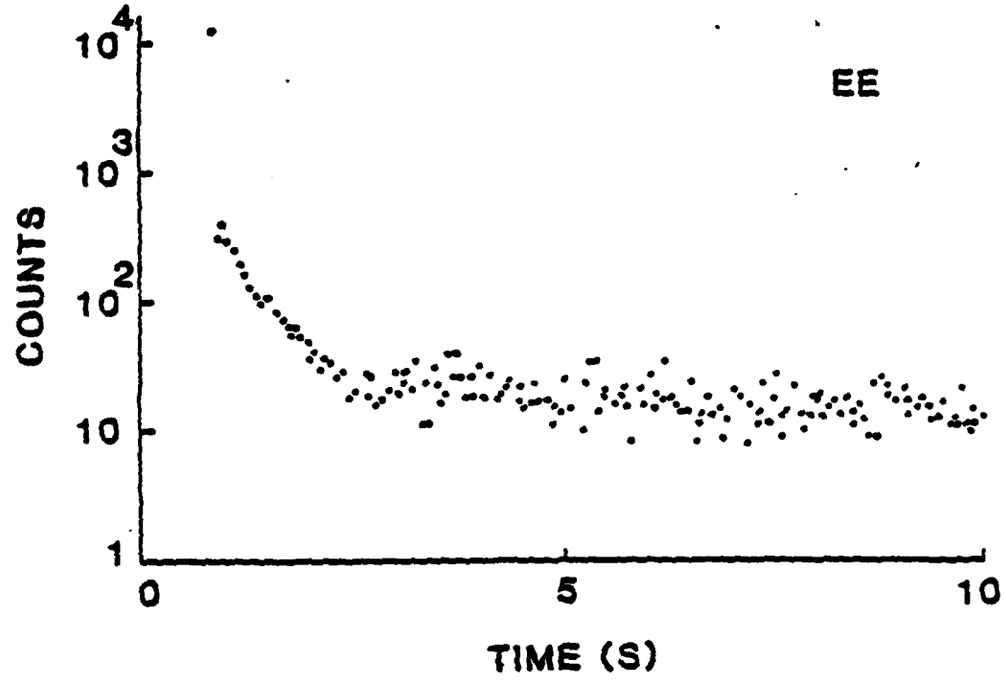

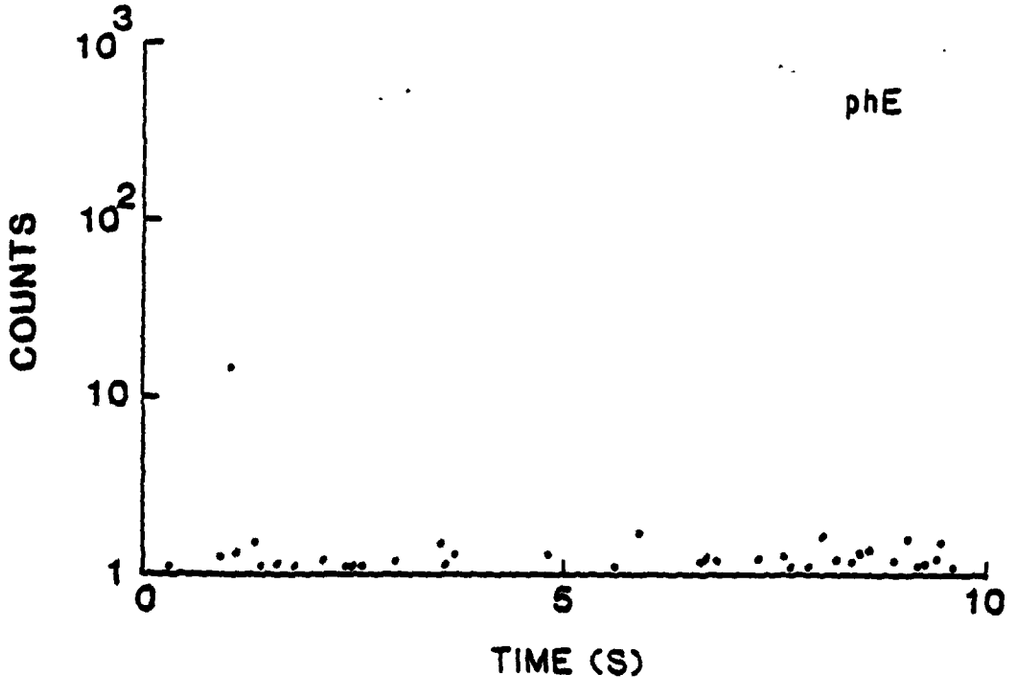

Fig. III-4

EE AND phE FROM BLX-1 - FAST TENSILE

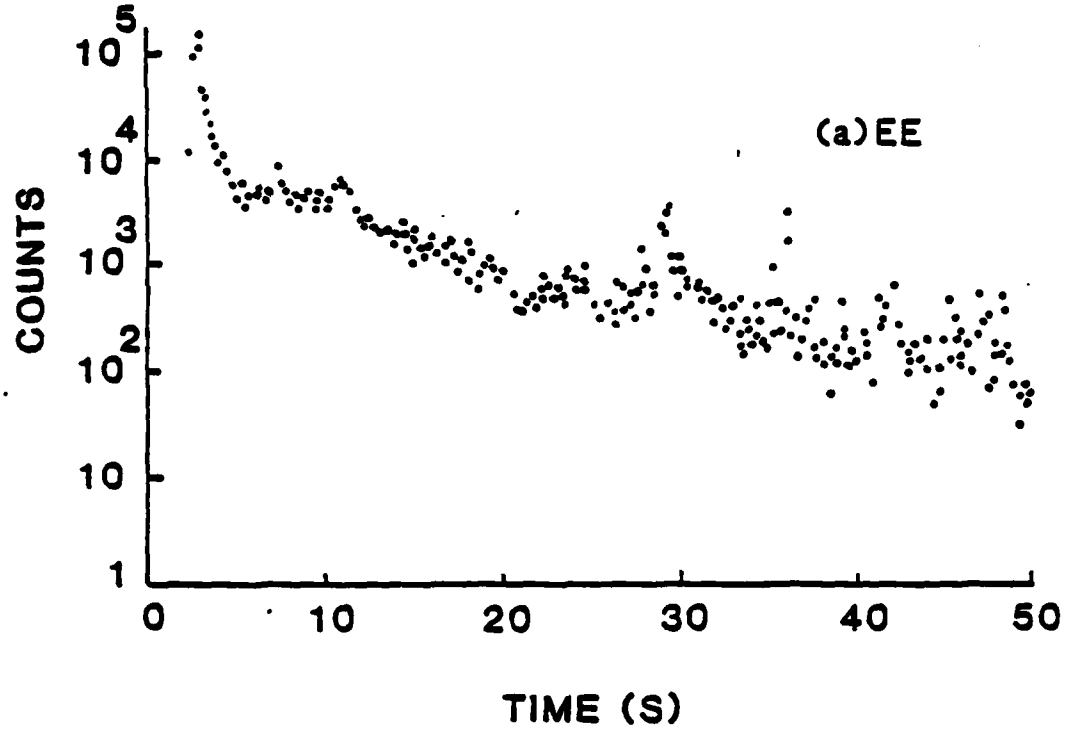

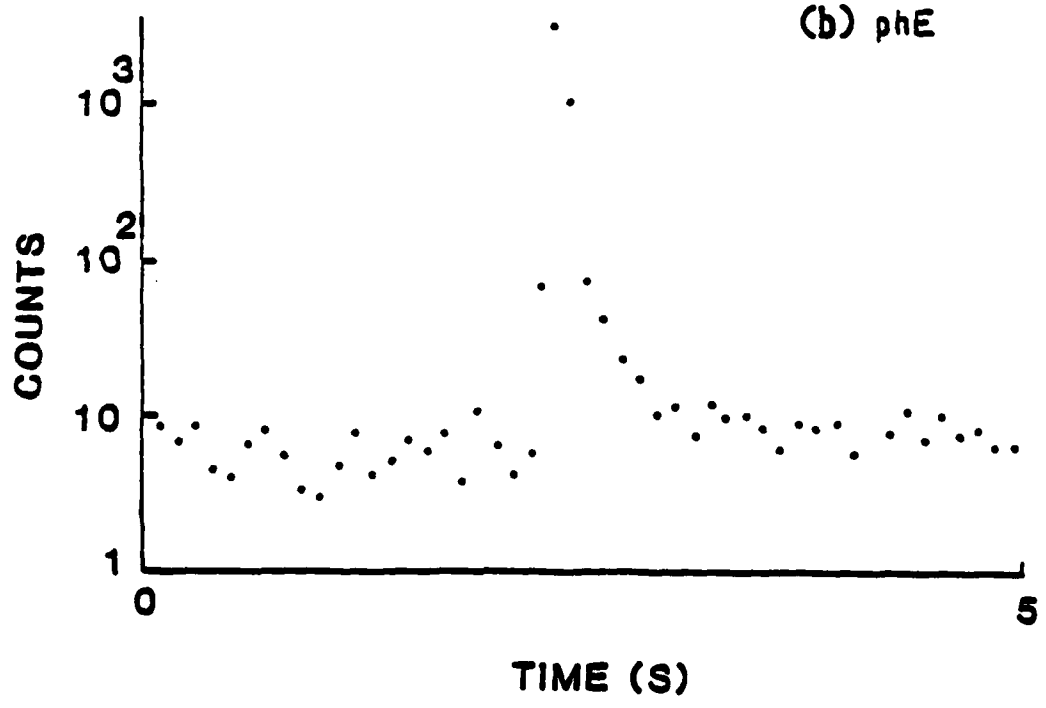

Fig. III-5

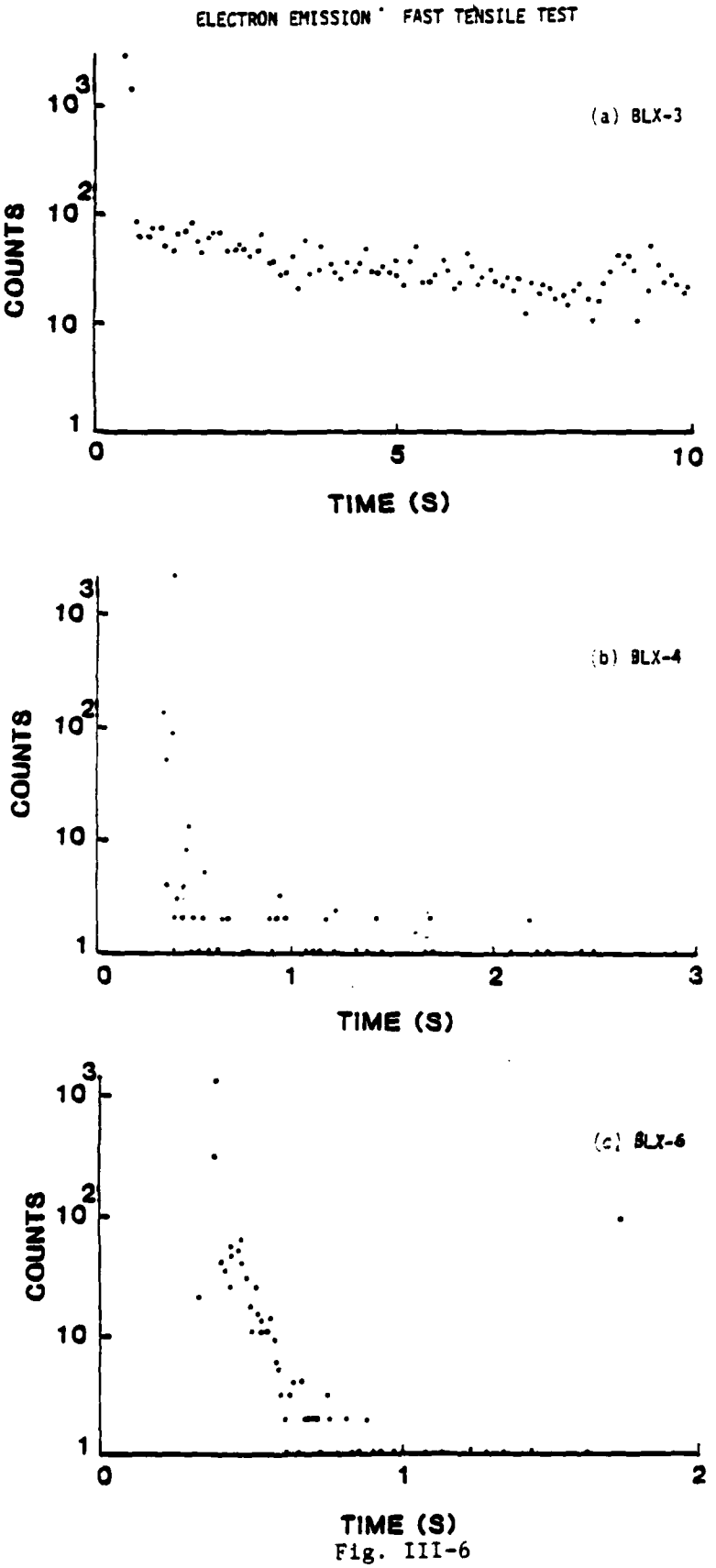
ELECTRON EMISSION · FAST TENSILE TEST
(a) BLX-3
COUNTS
10^3
10^2
10
1
0
5
10
TIME (S)
(b) BLX-4
COUNTS
10^3
10^2
10
1
0
1
2
3
TIME (S)
(c) BLX-6
COUNTS
10^3
10^2
10
1
0
1
2
TIME (S)

Fig. III-6

ELECTRON EMISSION - COMPRESSIONAL IMPACT

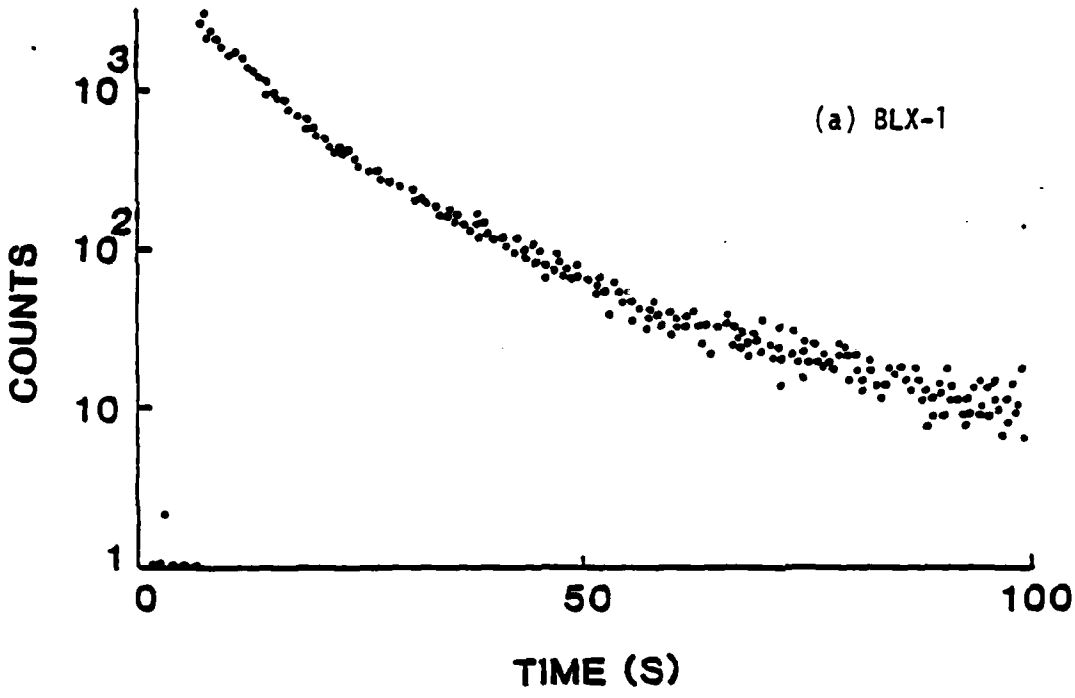

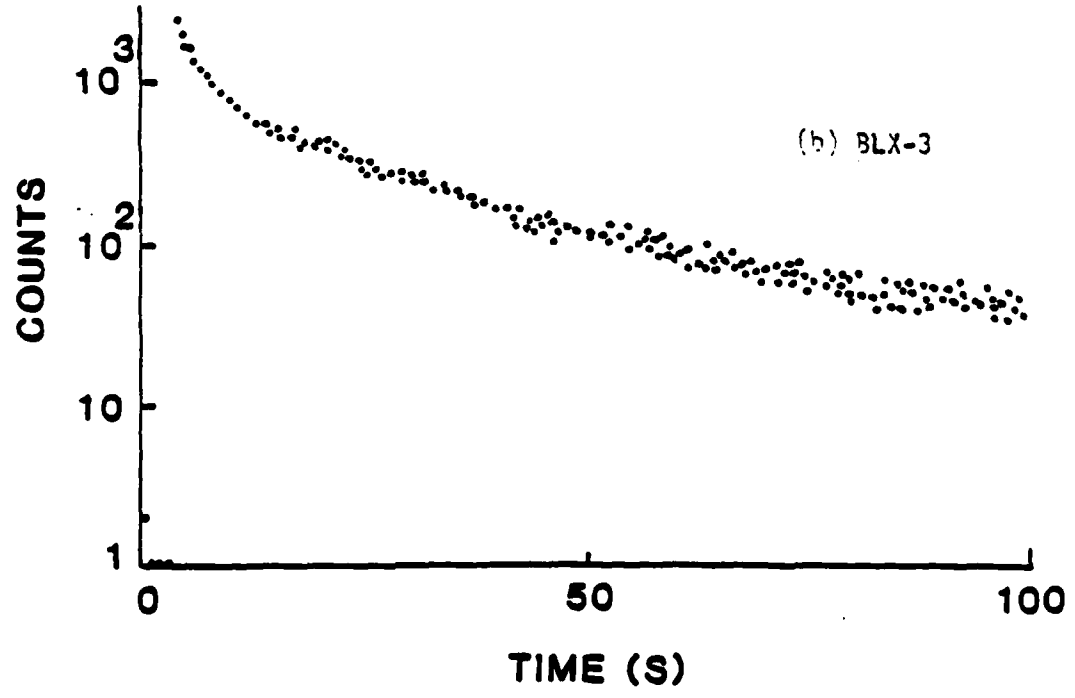

Fig. III-7

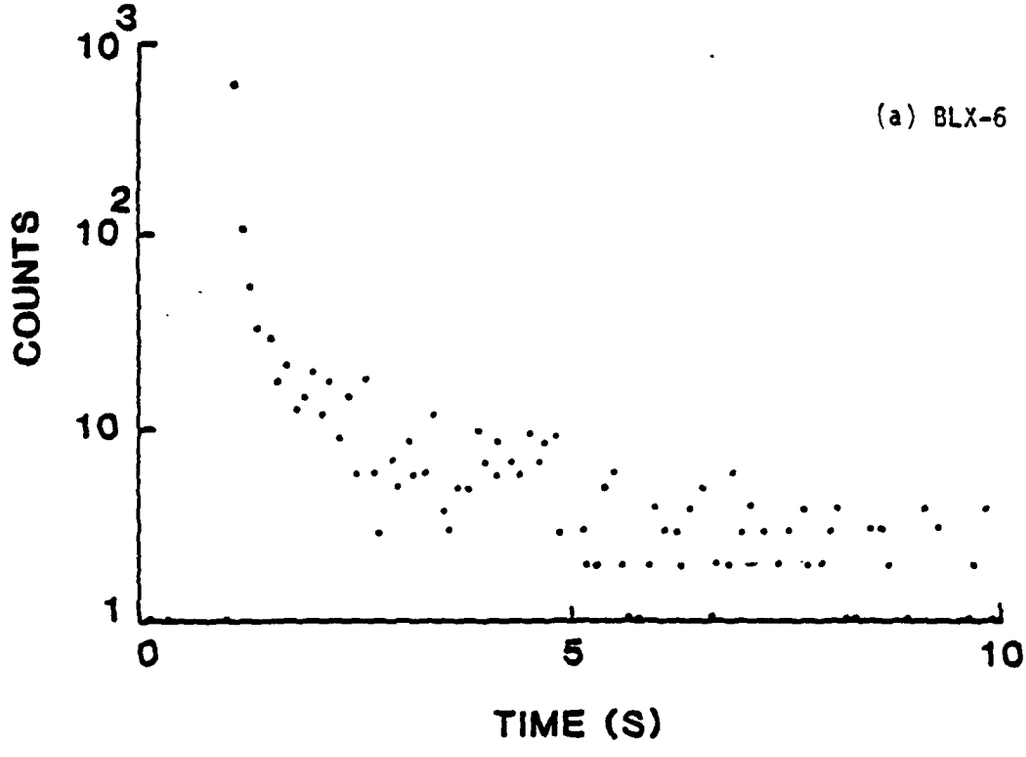
(a) BLX-6
COUNTS
10^3
10^2
10
1
0
5
10
TIME (S)

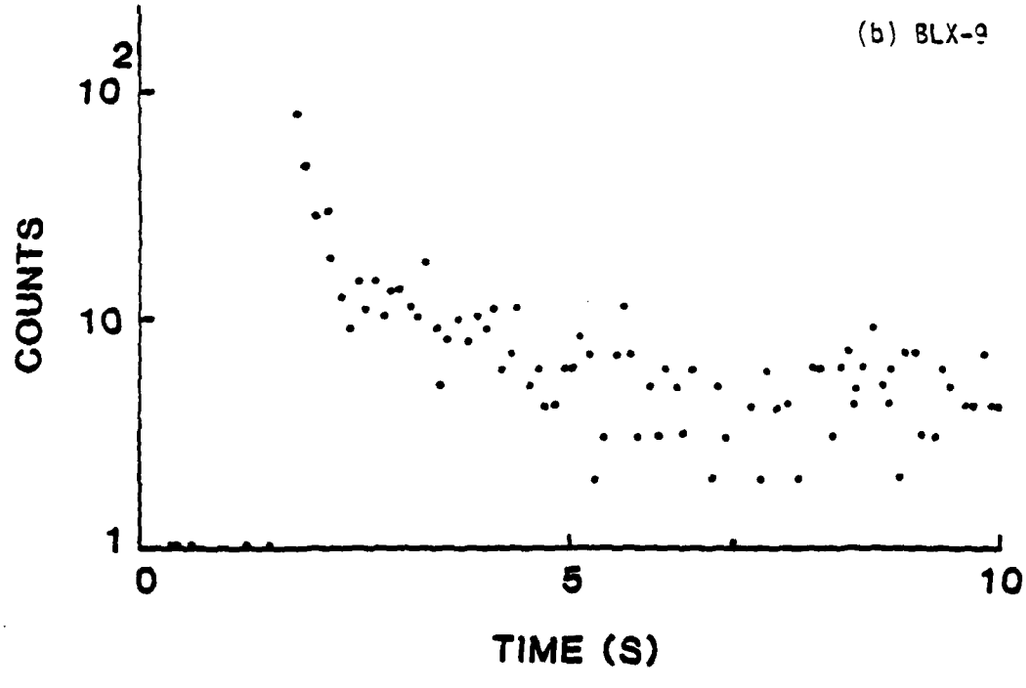
(b) BLX-9
COUNTS
10^2
10
1
0
5
10
TIME (S)

Fig. III-8

ELECTRON EMISSION FROM THE FRACTURE OF UNFILLED
URETHANE CROSS-LINKED POLYBUTADIENE

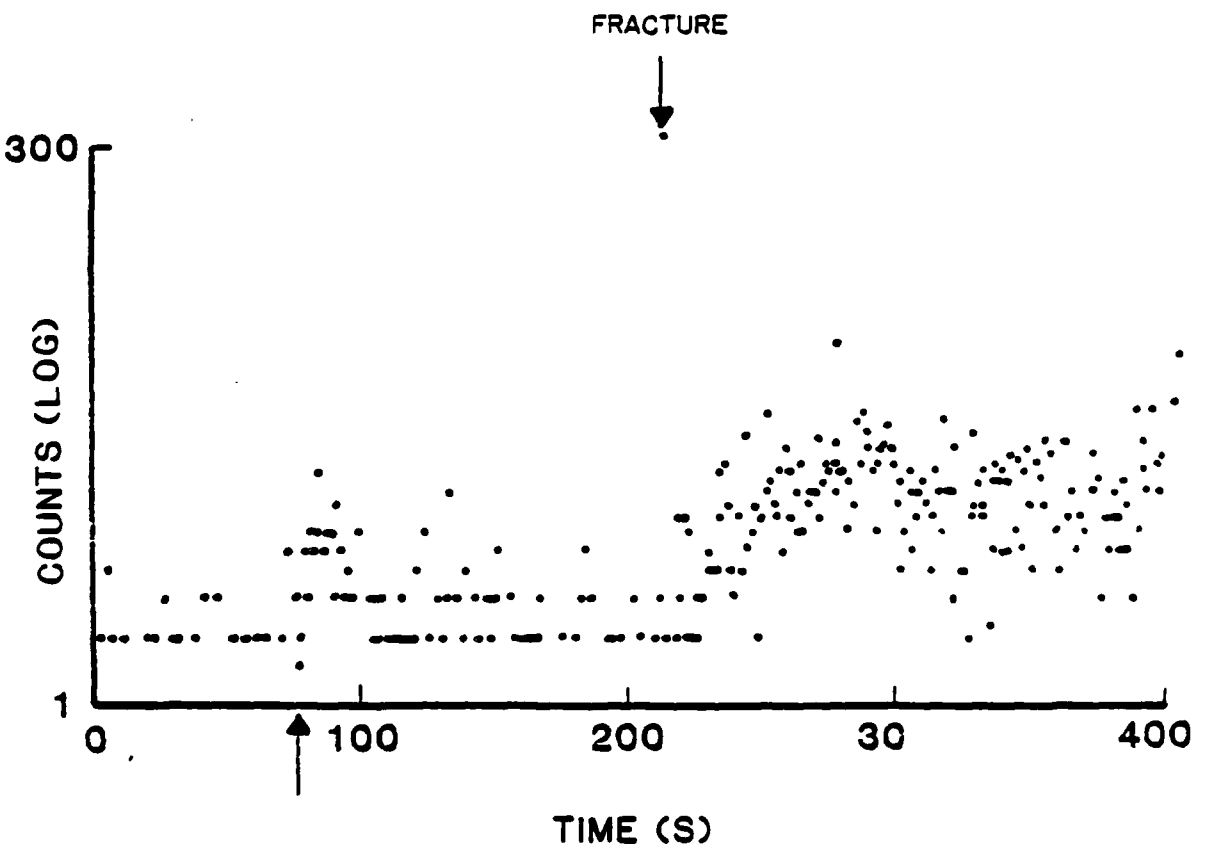

Fig. III-9

IV. FRACTO-EMISSION FROM THE FAILURE OF METAL/EPOXY INTERFACES

(to appear in J. Vacuum Science and Technology)

J. T. Dickinson, L. C. Jensen, and S. K. Bhattacharya
Department of Physics
Washington State University
Pullman, WA 99164-2814

ABSTRACT

We examine the electron emission, photon emission, and long wavelength electromagnetic radiation accompanying the failure of interfaces between aluminum and epoxy. Experimental evidence is given in support of a previously presented model involving fracture induced micro-discharges which excite the fracture surfaces by particle bombardment. We also examine the influence of an applied potential across the fracture surface at an Al/epoxy interface and present evidence for electrical breakdown in vacuum caused by fracto-emission.

INTRODUCTION

When fracture occurs in materials, emission of various types can occur; this emission is particularly apparent when new free surfaces are being formed. The types of emission observed include the release of electrons, ions, neutral molecules, and photons (often referred to as tribo-luminescence). We call such emission "fracto-emission" (FE) to emphasize the fact that some form of crack growth is a requirement for its occurrence.

In recent papers[1-5] we have outlined a physical model for the emission of charged particles following fracture of solids in vacuum, particularly in cases where a high degree of charge separation occurs. For example, when a polymer such as polybutadiene (BR), initially adhering to a glass surface (either in the form of a macroscopic, planar glass surface or small spherical filler particles), is separated in vacuum from the glass, intense long lasting electron emission (EE) and positive ion emission (PIE) are observed.[5,6] In such instances we also observe easily detectable photon emission (phE) and

long wavelength electromagnetic radiation (RE -- for radiowave emission) during fracture indicating the occurrence of a small gaseous discharge in the crack. The necessary gas in the region where this micro-discharge occurs consists of molecules evolving from the sample as the fracture takes place.[7] These gases either come from occluded volatiles or from actual fracture fragments produced by bond scissions. The presence of these gases and an electric field due to charge separation (in the case of dissimilar materials, this is due to contact charging) results in gaseous breakdown in the relatively close dimensions of the crack-tip during fracture.

This micro-discharge causes ionization of the gases in the crack-tip yielding high concentrations of electrons and positive ions which are attracted to and strike the crack walls. Bombardment of the fresh crack walls creates primary excitations, usually explained in insulators in terms of electron-hole production, raising electrons into traps near conduction band energy levels. The recombination of electrons and "holes" is a thermally stimulated process and can yield an emitted electron (thermally stimulated electron emission (TSEE)),[8] via an Auger Process,[9] or a photon, e.g., thermally stimulated luminescence (TSL)[10] (we place quotation marks around hole because at present we do not know the nature of this recombination center in polymers such as polybutadiene and epoxy; it may be simply a positive ion in the polymer, as suggested by Partridge[11] and Bohm[12]). Furthermore, a portion of the electron emission may be attracted back to the fracture surface due to variations in the density and sign of the charge distributions (i.e. charge patches) strike the surface and thereby produce PIE via an electron stimulated desorption (ESD) mechanism.[13] In addition, the positive ions can be neutralized as they escape from the fracture surface and leave in an

excited state (e.g., a metastable molecule), forming a component of FE which we call excited neutral emission (NE^*).[14]

In light of this model, we were lead to two interesting questions related to charge separation which we would like to probe in this paper:

1) Would a metal/epoxy interface yield evidence of intense EE, phE, and RE as expected for a system where charge separation should readily occur?

2) For such interfacial failure, what would be the results of applying an external potential across the interface before and during fracture; i.e., could the E-field lead to stronger charge separation and thus more intense emission?

The results of these studies have considerable relevancy to studying failure mechanisms in bonded aluminum structures and other adhesive systems. In addition, we show for the first time that fracto-emission can actually induce in a vacuum electrical breakdown on a macroscopic scale.

EXPERIMENTAL

The metal epoxy system consisted of two pieces of aluminum 40 mm x 20 mm x 2 mm with a 1 mm x 2 mm x 20 mm gap between them filled with Devcon 5 minute epoxy. One Al piece was machined smooth and cleaned with acetone, presumably with a natural oxide layer formed prior to bonding. The other piece of Al was etched in dilute nitric acid for 12 hours then rinsed in distilled water and cleaned in acetone. A simple mold was used to hold the epoxy resin during curing which was carried out in an oven at 75 C for 8 hours. For testing, the sample was mounted in insulated grips and pulled in tension. A high voltage could be applied to the Al pieces, thus producing a

field in the gap, similar to a parallel plate capacitor filled with a dielectric. Furthermore, due to the Al surface preparation, the failure was always on the unetched side of the epoxy. Thus, we could selectively apply either a positive or negative potential to the unetched side of the capacitor. Unless otherwise stated, the unetched side was at a negative potential and the etched side was grounded.

The EE was detected with a Galileo Electro-optics Channeltron Electron Multiplier (CEM) which produces fast (10ns) pulses with approximately 90% absolute detection efficiency. Background noise counts ranged from one to ten counts/second.

A Thorn EMI 9924QB photomutiplier tube (PMT) with a bialkali photosensitive surface and background count rate of 1000 counts/second, placed within one centimeter of the sample, was used to detect the visible photons. Standard nuclear physics data acquisition techniques were used to count and store the EE and phE pulses as a function of time. All experiments were carried out in a vacuum system at a pressure of 1×10^{-5} Pa.

The electromagnetic waves (RE) were detected with a 20,000 turn solenoid of No. 30 magnet wire placed 2 mm from the sample. Such an antenna couples to a changing B field. It should be emphasized that this arrangement is detecting the near-field electromagnetic emission because of the close proximity of the solenoid to the source. The intensity of these oscillating fields is so weak that we would not be able to detect them at distances of several wavelengths. Such measurements would have to be made to assure absolutely that a true radiation field existed. Our major interest here is finding evidence of a micro-discharge during fracture and we attribute the changing B fields accompanying fracture to such a breakdown. The accompanying burst of photons reinforces this interpretation.[1] The coil was connected to

the input of a wide-band differential amplifier with high common mode rejection to minimize pick-up noise. The ringing frequency of the coil/circuit was 8 kHz; it should be noted that using other coils/circuits, we have detected signals up to 500 kHz. The signal was digitized once every 20 μs and stored on a computer over the duration of the experiment (approximately 100 ms). In some cases, the RE signal was squared so that the appearance of a positive rise provided a sensitive probe of the occurrence of RE and the initial rise of the RE signal could be correlated in time with the EE. For some applications, it was necessary to reduce substantially the amplifier gains to prevent saturation when the RE signals were very large.

RESULTS AND DISCUSSION

As intended, the fracture of the Al/epoxy samples always occurred at the interface between the unetched metal surface and the epoxy. The accompanying emission, EE, phE and RE, with 0 V applied across the sample, is shown in Fig. 1. On this time scale the digitized RE signal, which has been squared and the background subtracted, shows up as a single point lined up in time with the other signals. The EE and phE signals (shown on a log scale) are typical of the emission from many materials[1-6] involving adhesive failure (and therefore charge separation due to contact charging) with an intense peak during fracture and continued emission for many minutes after fracture. In Fig. 2, we show the effect on the EE when a potential difference of 1500 V is applied across the sample as compared to 0 V; (the high voltage was removed a few seconds after fracture) With the potential, the emission intensity increases two orders of magnitude over the EE with 0 V. Note that the time dependence of the decay curves remains the same. With a potential difference applied to the sample, the discharge events appear to be stronger and/or occur

more frequently, presumably due to higher surface potentials and charge separation compared to zero external field. More discharge events and possibly more intense events during the fracture leads to more bombardment of the surface and thus more intense, longer lasting emission decay curves.

Comparing the results shown in Fig. 3, we see the increase in the intensity of EE, RE, and phE for 0 V and 500 V applied across the sample during fracture. All sensitivities, amplifier gains, etc. are the same for both situations. The EE data was multichannel scaled at a time interval of 2 μs/ch, while simultaneously the phE and RE were digitized at a rate of 1 μs/ch. Every tenth channel of the data is displayed in Fig. 3. When the sample with the 500 V applied was fractured the EE intensity during and immediately following fracture was so high that it completely saturated the CEM for approximately 5 ms, at which time it begins to recover and shows count rates well above 4 Mhz (8 counts/channel). This saturation occurs at countrates above 20 Mhz (40 counts/channel) because the CEM gain drops due to the excessive demand for current. The gain decreases to the point where the output pulses are below a discriminator level and therefore the count rate recorded drops essentially to zero. Once the count rate decreases, the CEM recovers which produces the increasing signals at times of 2 ms (0 V) and 4 ms (500 V). On a slower time scale, the resulting EE data shows the normal decay curve with the total number of electron counts approximately ten times greater for the 500 V sample compared to the sample broken with no voltage applied. The RE signal went from 30 mV peak-to-peak to more than 1 volt peak-to-peak (actually saturated), and the phE increased considerably. Thus we observe "coincidence" in the onset of all three types of emission for both voltages, plus significant increases in the intensity of all three signals when the voltages are present.

A closer look at the phE accompanying failure of the Al/Epoxy interface vs applied voltage at higher voltage across the dielectric and higher PMT gain is shown in Fig. 4. The flat peak in the phE in Fig. 4 at the higher voltages was due to amplifier saturation. With increasing potential, we see on this fast time scale the initial phE stays relatively unchanged. This light is the "naturally occurring" phE from failure of the interface. However, with increasing potentials, additional phE occurs which increases dramatically in intensity and occurs earlier in time relative to crack growth, which we have shown to be aligned in time with the initial rise of the phE. Above a few hundred volts, the phE intensities are far too intense for the PMT. What is occurring is fracture-induced electrical breakdown. Time exposures of the sample taken during fracture with a 35 mm camera and Ektachrome film (ASA 400) show that this breakdown is occurring in the gap between the fracture surfaces. These potentials are far too small to produce vacuum breakdown without the assistance of the fracture event. We propose that the combination of the relatively intense charged particle emission and neutral particle emission accompanying fracture is responsible for triggering this resulting electrical breakdown. In earlier work,[15] we showed that fracture could induce electrical breakdown in air by a similar mechanism.

Finally, we mention that with variations in the applied potential, the intensities of EE decay tails also tended to increase. Furthermore, when we reversed the polarity, with the unetched Al positive, (over a range of 200-1500 V) the EE and phE increased to a slightly higher degree than with the negative potential. It is possible that at lower potentials, manipulation of the surface charges on the metal/epoxy interfaces might lead to a decrease in the emission intensities compared to 0 V. Also, at one potential and polarity (-1500 V) we determined that there was a linear increase in the EE

intensity with increased strength of the bonded joint as measured with stress gauge.

CONCLUSION

To summarize, we have examined the EE and phE from two systems wherein the interface between a dielectric in good contact with a metal surface undergoes failure. Our results show the following:

1) In the case of 0 volts applied across the dielectric, we obtained on a slow time scale "coincident" rise in EE, phE, and RE with fracture. Both the EE and phE also exhibited slow decay similar to the results we have reported earlier on other interfacial failure systems.[6] Earlier studies[5] show that this after-emission is a thermally stimulated process and is fit by a simple trap model.

2) In the case of the Al/epoxy system, when an external electric field is added, we found that the after-emission is substantially increased due to a more intense discharge that occurs during fracture.

3) At voltages of a few hundred volts across 1 mm gaps of epoxy, fracture actually induced electrical breakdown which could sustain itself for several hundred microseconds after fracture; this breakdown occurred in the gap between the fracture surfaces, i.e., between the metal and epoxy.

4) The instant of breakdown occurred <u>during</u> fracture and in time moved closer to the onset of fracture with increasing applied voltage. We propose that this breakdown is triggered by the electron and ion emission accompanying fracture.

5) The intensities of the EE and phE after-emission were found to depend on the magnitude of the applied potential and the polarity. Also, with -1500 V applied, there was also a linear dependence of the EE intensity on the strength of the joint.

ACKNOWLEDGMENTS

We wish to thank W. D. Williams, Sandia National Laboratories, and E. E. Donaldson, Washington State University, for helpful discussions.

This work was supported by , McDonnell Douglas Independent Development Fund, Sandia National Laboratories, and the Office of Naval Research Power Program under Contract N00014-80-C-0213, NR 659-803.

REFERENCES

1. J. T. Dickinson, L. C. Jensen, and A. Jahan-Latibari, J. Vac. Sci. and Technol. A 2, 1112 (1984).

2. J. T. Dickinson, L. B. Brix, and L. C. Jensen, J. Phys. Chem. 88, 1698 (1984).

3. J. T. Dickinson, L. C. Jensen, and A. Jahan-Latibari, J. Mat. Sci. 19, 1510 (1984).

4. J. T. Dickinson, J. Mat. Sci. 19, 2426 (1984).

5. J. T. Dickinson and L. C. Jensen, J. Poly. Sci.: Poly. Phys. Ed., to be published.

6. J. T. Dickinson, in Adhesives Chemistry -- Developments and Trends, L. H. Lee, ed., (Plenum Publishers, New York), to be published.

7. L. A. Larson, J. T. Dickinson, P. F. Braunlich, and D. B. Snyder, J. Vac. Sci. and Technol. 16, 590 (1979).

8. H. Glaefeke, in Thermally Stimulated Relaxation in Solids, ed. by P. Braunlich (Springer Verlag, Berlin, 1979), p. 229.

9. V. Bichevin and H. Kaambre, Phys. Status Solidi (A) 4, K235 (1971).

10. R. Chen and Y. Kirsh, Analysis of Thermally Stimulated Processes (Pergamon Press, Oxford, 1981) pp. 16-23.

11. R. H. Partridge, in The Radiation Chemistry of Macromolecules, Vol.I, ed. by M. Dole (Academic Press, New York, 1973), Chapter 10.

12. G. G. A. Bohm, J. Polm. Sci., 14, 437 (1976).

13. M. L. Knotek, Physics Today 37(9), 24 (1984).

14. J. T. Dickinson, L. C. Jensen, and M. K. Park, Appl. Phys. Lett. 41 443 (1982).

15. M. L. Klakken, J. T. Dickinson, and L. C. Jensen, IEEE Trans. on Electrical Insulation, to be published.

FIGURE CAPTIONS

Fig. 1. Simultaneous emission of electrons (EE), photons (phE), and long wavelength radiation (RE) accompanying the fracture of an Al/Epoxy interface. The intensities are plotted on a logarithmic scale.

Fig. 2. The decaying "tails" of the electron emission accompanying failure of Al/Epoxy interfaces for 0 V and 500 V applied across the dielectric. Immediately following fracture the voltage was quickly reduced to 0. The data shown here begins 5 seconds after fracture and removal of the voltage.

Fig. 3. EE, phE, and RE, taken with the same sensitivities and detector positions, are shown for two Al/Epoxy samples fractured with 0 V and 500 V applied across the interface, respectively . The arrows indicate the onset of fracture. The "window" on the 0 V RE shows the small ringing signal in more detail. Note that a number of the signals are saturated. The large increase in intensity is due to electrical breakdown in the crack during and following fracture.

Fig. 4. The build-up of the intensity of the fracture-induced electrical breakdown during failure of the Al/Epoxy interface with increasing voltage across the dielectric can be seen in the accompanying phE shown here.

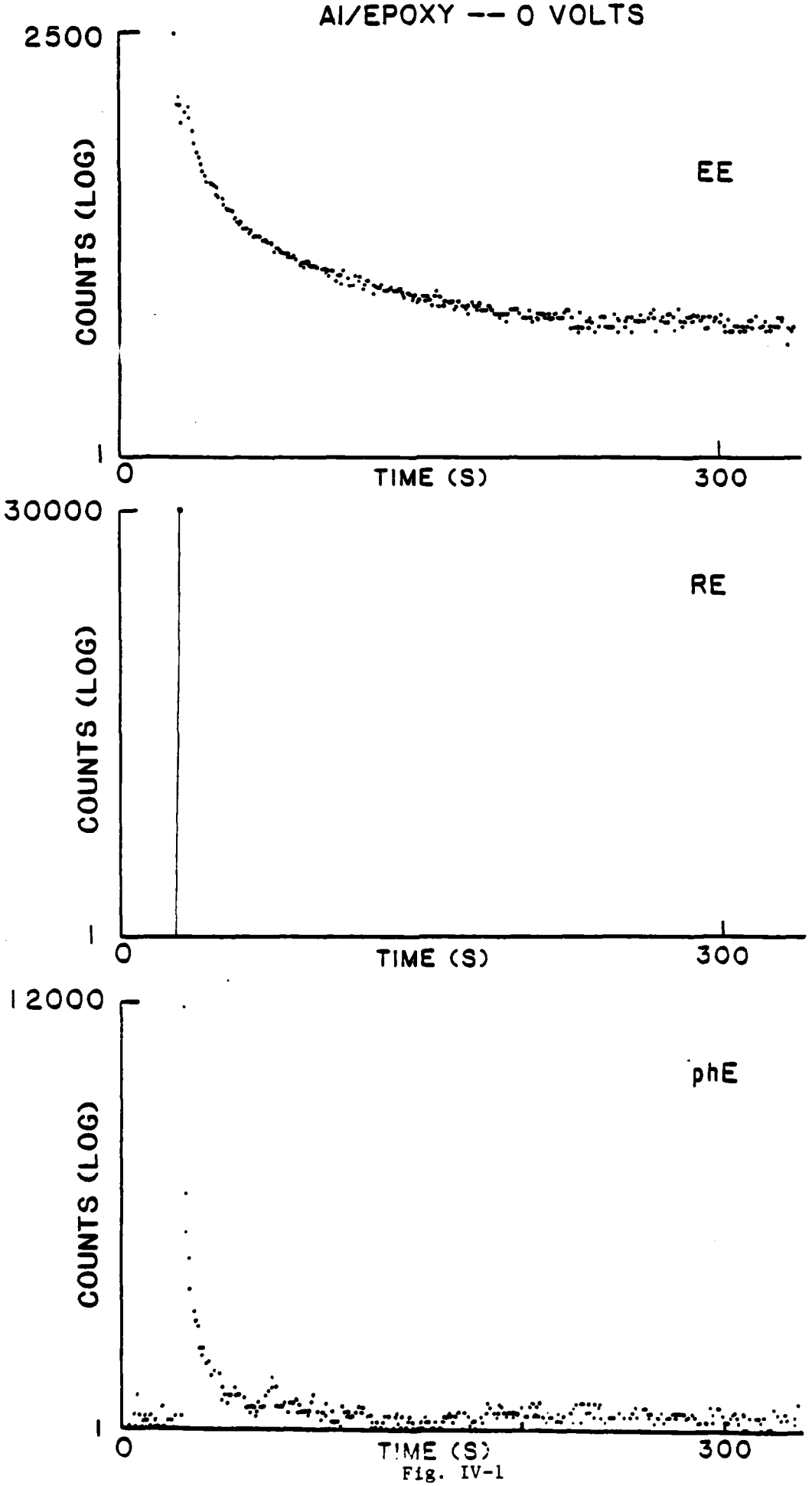
Al/EPOXY -- 0 VOLTS
2500
COUNTS (LOG)
1
EE
0
TIME (S)
300
30000
COUNTS (LOG)
1
RE
0
TIME (S)
300
12000
COUNTS (LOG)
1
phE
0
TIME (S)
300

Fig. IV-1

METAL/EPOXY INTERFACE

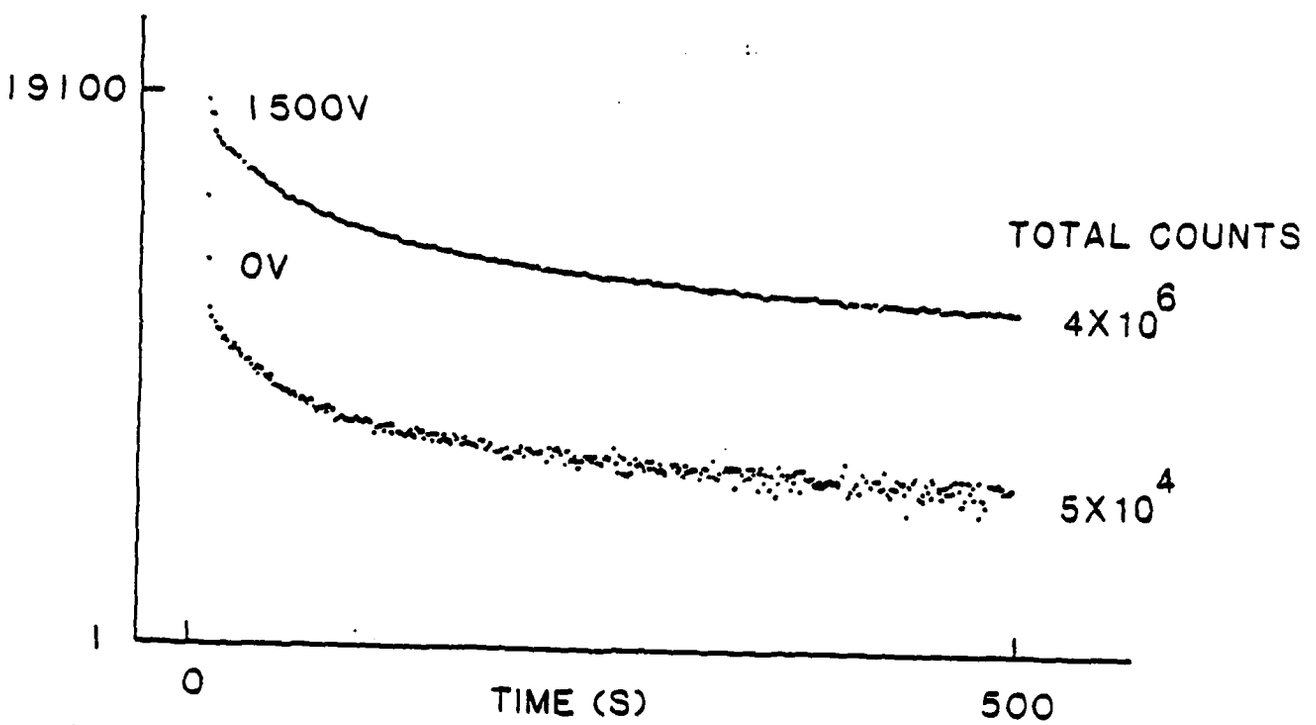

Fig. IV-2

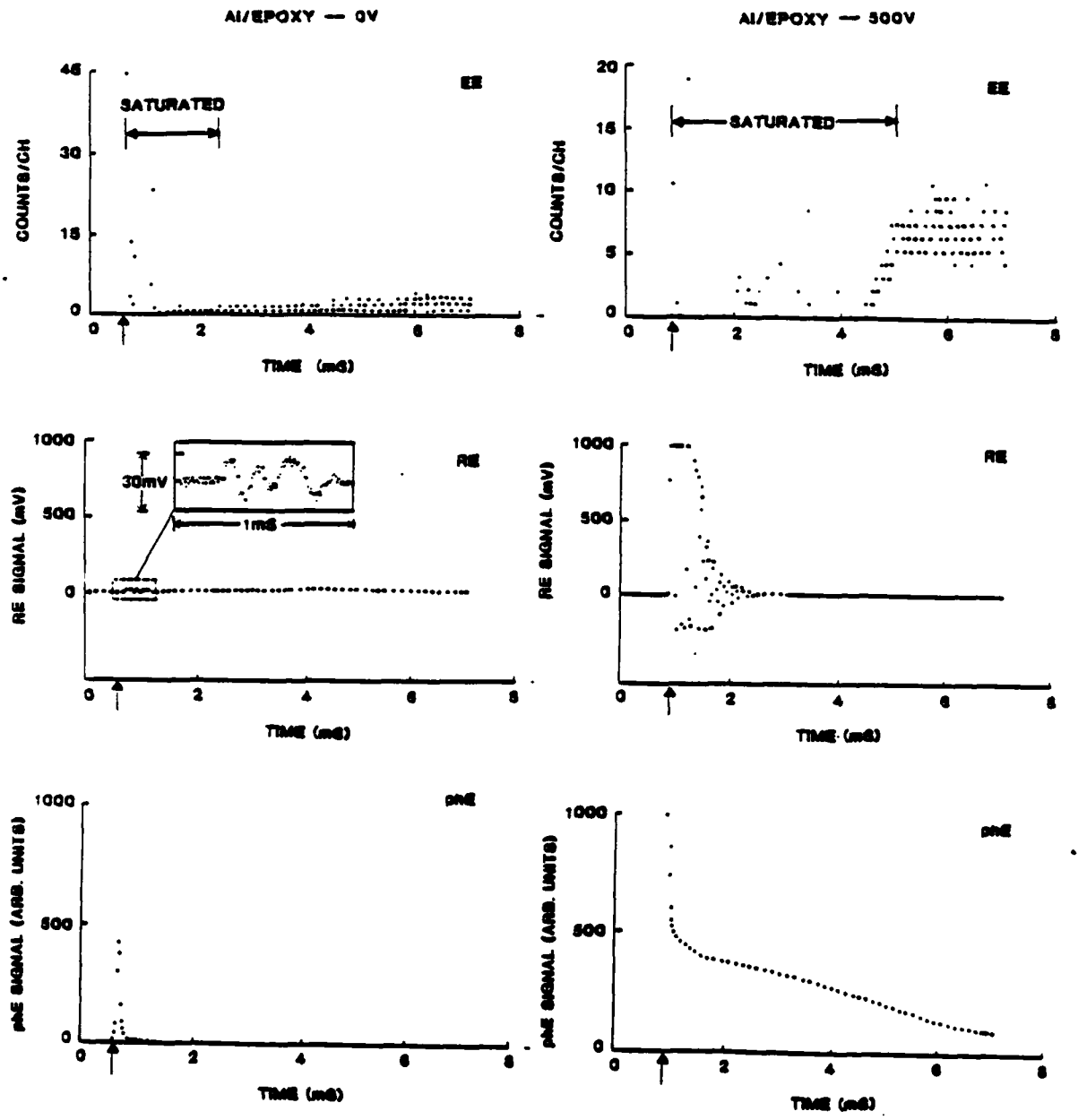
Al/EPOXY — 0V
Al/EPOXY — 500V
EE
RE
pRE
SATURATED
COUNTS/CH
RE SIGNAL (mV)
pRE SIGNAL (ARB. UNITS)
TIME (mS)
30mV
1mS

Fig. IV-3

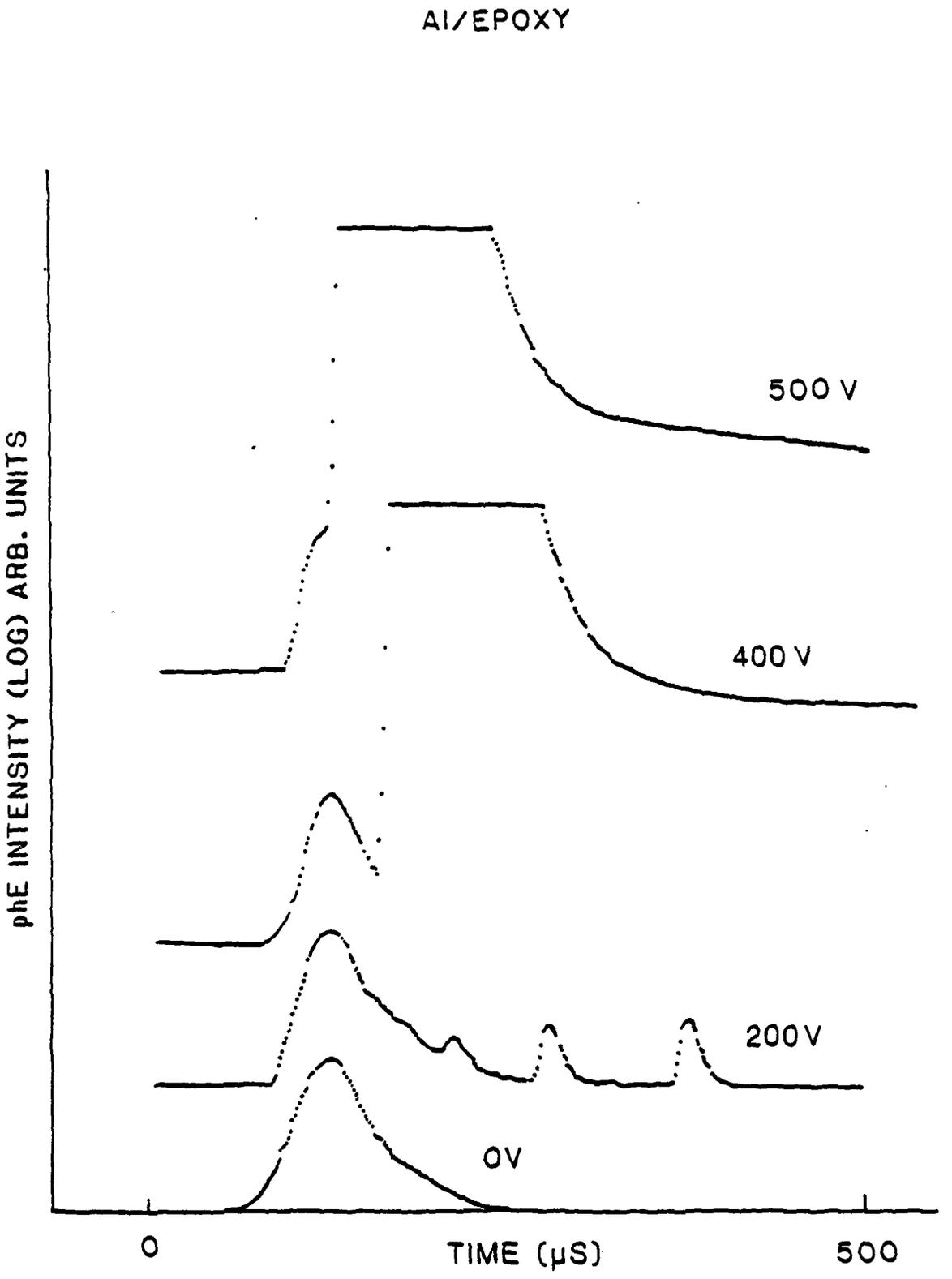
Al/EPOXY
500 V
400 V
200V
0V
phE INTENSITY (LOG) ARB. UNITS
0
TIME (μS)
500

Fig. IV-4

V. TIME AND SIZE CORRELATIONS OF PHOTON AND RADIOWAVE BURSTS FROM PEELING PRESSURE SENSITIVE ADHESIVES IN AIR

E. E. Donaldson, J. T. Dickinson, and X. A. Shen
Department of Physics
Washington State University
Pullman, WA 99164-2814

ABSTRACT

During separation in air of an adhesive from a polymer substrate we have observed intense bursts of photons (phE for photon emission) and long wavelength electromagnetic radiation (RE-for radiowave emission), similar to those reported earlier by Deryagin, et al. In this paper we present detailed measurements of phE time distributions as well as time and size correlations between bursts of phE and RE. These results support the view that patches of electrical charge produced by charge separation between dissimilar materials lead to gaseous breakdown in and near the crack tip. We discuss the role of these discharges in producing sustained phE after the discharge has been extinguished.

Keywords: Fracture, Adhesive Failure, Fracto-Emission, Triboluminescence, Photon Emission, Electromagnetic Radiation, Contact Charging, Electrical Charge Separation, Gaseous Breakdown, Microdischarge.

INTRODUCTION

The emission of a wide variety of particles and radiation has been observed accompanying the fracture of a number of materials.[1-14] The range of materials from which such emission has been detected include crystalline materials such as alkali halides and metal oxides, polymers and composites, as well as several interfaces, including those involving adhesives. The types of emission observed include electrons, positive ions, neutral atoms and molecules, and radiation consisting of visible photons (phE) and long wavelength electromagnetic radiation [radio emission (RE)]. The collective term describing all of these emissions is "fractoemission" because fracture appears to be a necessary prerequisite for its occurrence.

We have recently presented a model[11-14] which explains the intense long lasting electron, positive ion, and photon emission observed during adhesive failure. The sequence of events producing this intense emission is initiated or triggered by the electrical charge separation which is produced when fracture occurs between dissimilar materials. This separation of charge results in discharges in the vicinity of the detachment line or crack tip. These discharges cause excitation of the newly created fracture surfaces as well as any gases present. The microdischarges themselves produce phE and RE directly. In addition, these discharges lead to particle bombardment of the newly created fracture surfaces, thereby exciting them. The de-excitation of these surfaces via thermally stimulated relaxation leads to sustained emission following the discharge.

The production of radiation during the failure of an adhesive joint has been previously observed. Deryagin[15] and co-workers reported that such failure produces light and radio frequency radiation in the form of bursts. They showed that these bursts were produced simultaneously and have the same duration (about 10^{-3} to 10^{-4}s).

Deryagin, Skinner[16], and Huntsberger[17] have examined the role of electrostatic forces as part of the work of adhesion. Clearly these forces exist and may be perceptible in some cases; however, Huntsberger[17] concludes that electrostatic contributions to adhesion will generally be negligible.

In this work we examine the peeling of a common pressure sensitive adhesive, focusing on a detailed characterization of the time distributions of the phE bursts as well as the time and intensity correlations of the phE and RE bursts. We also propose more detailed phE (or triboluminescence) mechanisms in light of these results.

These experiments were conducted in air at 22 + 2 C; similar experiments carried out in vacuum are in progress. Working in air we are limited to the detection of two kinds of fractoemission; namely, phE and RE, which have detectors operable in air. There are several distinct advantages of conducting experiments in air: pump down delays are eliminated; it is easier to refrigerate the PMT and decrease dramatically its background count rate; and the mechanical apparatus was simpler to operate in air. Finally, most practical fracture problems are encountered in air so that any improved knowledge of fracture in air could be used in applications more readily.

The charge separation which leads to microdischarges and fractoemission may arise in a range of situations including adhesive failure and the breaking of chemical bonds. In addition to possible applications to the investigation of failure mechanisms of adhesives, these studies of fractoemission in air may also be applicable to the production and processing of pressure sensitive adhesives as well as to a variety of tribology problems in which surface charges are produced.

EXPERIMENTAL

We selected 3M Scotch Brand Filament Tape No. 893 as a test material. The adhesive is a natural rubber combined with varying amounts of a tackifying agent which is a hydrocarbon resin appearing to be terpene based. More tackifier is used on the face of the adhesive and less in the saturating layer binding the filaments to the backing. The polyester tape backing has been treated with a release coating with a critical surface tension for wetting of approximately 21 dyne/cm. The advantages of this choice of material were its availability, the reproducibility of results in air, and its tendency to produce copious emission. Similar tests on other adhesive-polymer systems

showed that a number of these observations were also applicable to a wide range of materials.

The geometry of the peeling and detectors is shown in Fig. 1. The loading was basically that of a T-peel test. Samples were composed of multiple layers of tape and separated on the axis by the two spools. The samples were arranged so that separation could be produced either between the isoprene based adhesive layers of two tapes or between the adhesive of one tape and the release coated polyester backing of a second tape. A third failure mode involved the delamination of the glass filament layer from the backing of a single layer of tape. During delamination, the filaments appeared to separate cleanly from the inner filament-saturating adhesive layer and this produced emission characteristic of the glass filament-adhesive interface.

The peel forces for this tape were measured in a T peel configuration at a laboratory temperature of 22 C. The average peel force was lowest at slow peel speeds (< 1 mm/s) and higher at greater peel speeds (3 cm/s). For the three tape assemblies just described, the ranges of peel force were:

Two Adhesive Layers Together,	310 - 840 grams (weight)/cm;
One Layer on Coated Backing,	50 - 240 grams (weight)/cm;
Delamination of Filaments,	240 - 470 grams (weight)/cm.

For detection of RE, a flat coil with an inductance of 0.77 mH was placed several cm in front of the tape separation zone (see Fig. 1). Electrical discharges in the vicinity of the coil are like rapidly oscillating charged particles, which produce radiation. Because of our proximity to the source, the coil is sensitive to the changing B field of what is known as the near field. The response of the coil circuit to this stimulation is an

oscillation at a characteristic frequency of 400 KHz. These oscillations are damped in time with an initial amplitude of 1 to 10 mV with the largest lasting for nearly 100 μs. We refer to these ring-down oscillations as RE bursts, realizing that the actual electromagnetic pulse is much shorter.

The RE bursts were amplified by a wide band differential amplifier with low noise and high gain. The amplified signal then entered a discriminator which produced a clean pulse every time an oscillation occurred above the discriminator threshold, usually set just above the noise. These pulses could then be counted; large amplitude RE bursts produced more counts. It was also possible to derive a single pulse at the instant of the initial rise of each RE burst. These single pulses could be used to count the number of RE bursts or to trigger various circuits. The ringing of the RE bursts necessitated a 100 μs dead time between detection of individual successive bursts.

A quartz lens gathered light to the central region of the photomultiplier tube [EMI 9816BQ], which was operated at -40 C to reduce the background or dark count rate. The PMT had a quantum efficiency of approximately 10 percent so the overall detection efficiency for photons coming from the peel region was approximately 10^{-2}. The background was 10 counts/s with all light leaks eliminated.

The thermoelectric refrigerator and PMT housing was provided with an integral amplifier-discriminator which shaped the PMT pulses into 2V pulses about 0.07 μs wide. At low instantaneous levels of phE, pulses from the PMT and its integral amplifier-discriminator could be used directly in a pulse counting mode. Thus, these pulses were fed into a multichannel scaler which provided a direct measure of counts vs time. When the count rate exceeded 10^7 counts/s, the amplifier-discriminator overloaded and an analog current

measurement was used. In this technique the PMT output for a large burst of photons was treated like a rapidly changing DC current. After converting this current to a voltage (by passing it through a resistor), the resulting signal could be amplified by a fast DC amplifier [EGG Ortec 579, <5 ns rise time]. This amplified signal was then digitized at time intervals of 50-100 ns/channel, using a LeCroy 2256-AS Waveform Digitizer. One advantage to this technique is that the PMT gain can be adjusted to prevent saturation when examining the larger bursts.

In one series of experiments the RE bursts were also digitized at 100 ns/channel so that the maximum amplitude of each burst could be measured.

The data from the RE and phE signals were stored in a LeCroy 3500 Data Acquisition System. All of the experiments were conducted in room air at 1 atmosphere of pressure unless otherwise specified.

RESULTS

Time Correlations

When the adhesive is peeled from the release coated polyester backing (substrate) copious phE and RE are observed. In Fig. 2 we show simultaneous phE and RE measurements. The emission occurring in the first 10 s of the plots was for a peel speed of 35 mm/s. Qualitatively, the emission increased at the onset of peeling and decreased rapidly when peeling was stopped. However, careful examination showed that emission continued after the displacement of the ends of the specimen was stopped, principally from additional peeling due to relaxation of the tape.

The emission rising at approximately 25 s on the plots in Fig. 2 was for a second peel at a slower speed (5 mm/s). This shows the strong dependence of phE and RE intensity on the rate of separation of the adhesive

from the substrate. This effect is similar to what we observed earlier in the phE for the same system and for interply delamination in Kevlar-Epoxy composites.[8] In general, the largest maxima in the phE and RE shown in Fig. 2 appear to occur simultaneously.

In Fig. 3, we compare on the same plot the decay of the photons and RE after the displacement was stopped (shown by the arrow). The RE curve shown as a solid line is a fit to the data. The phE that remains after the RE falls is a real "after-glow" and is seen to last on the order of seconds. It should be mentioned that if ones eyes are dark adapted, both the phE during peeling and the "after-glow" can be easily seen.

Fig. 4 shows RE and phE measurements on a faster time scale (0.01 s/channel). We find "oscillations" in both the RE and phE rates, which rise and fall simultaneously. This irregular character in Fig. 4 corresponds to the patchwise failure of the adhesive in an oscillating or low peel rate "stick-slip" mode,[18,19] an effect which is accentuated by the presence of the fibers and stiffness of the adhesive. The peaks in the emission correspond to "slip" and the valleys correspond to "stick".

Upon examination of this emission on yet a faster time scale, one finds that emission such as seen in Figures 2 and 4 actually consist of a superposition of many much faster RE and phE bursts. In order to prevent pile-up of these bursts, we conducted experiments at much slower peeling speeds (1-2 mm/s).

In Fig. 5 we show typical photon bursts measured at 100 μs/channel. We note that bursts of photons appear to rise in a single channel and decay in times of approximately 150 μs. Although not evident here, we were able to

show that the majority of these bursts were saturating our detector electronics so that in fact they are often are considerably larger.

Time correlations between these RE and phE could be investigated using standard coincidence electronics. However, due to the relatively long duration of both the ringing signals from the RE and the phE decay, one would only learn that the two types of bursts were accompanying one another. Instead, we chose to trigger the multichannel scaler with a pulse near the onset of the RE burst and count the accompanying photons. If indeed the two bursts occur "simultaneously" one should observe a peak at or near the RE trigger. In this experiment, the data was accumulated at 1 μs/channel and the process repeated for a number of RE trigger pulses where each phE burst is added on top of the preceding bursts. The results are shown in Fig. 6, indicating, indeed, a correlation between the RE and phE bursts.

We also see that there is a characteristic time distribution of phE accompanying the RE bursts. The problem with the data in Fig. 6 is that the rise in intensity from $t = 0$, or perhaps better put, the depression of the intensity near $t = 0$, is an artifact of the very high photon counting rates accompanying and immediately following the RE trigger, again due to the saturation of the phE detector electronics. At approximately 10 μs after the trigger pulse the electronics recovers; the points beyond this time represent the actual decay in the photon count rate relative to the RE burst on the time scale of several μs. We suggest that this curve eventually blends into the tail shown in Fig. 3. At this point it is not clear whether one single kinetics law could be used to fit this decay curve over such a wide range of times; we note here that the curve in Fig. 6 is non-linear on a log scale and will comment further on these results in a later section.

An improved phE time distribution was obtained by treating the signal in an analog rather than digital mode, using a fast amplifier and a digitizer as described above. The RE trigger served as a convenient stop pulse for the digitizer. The digitized current from a single phE burst is shown in Fig. 7, obtained at 50 ns/channel. As before, we repeatedly ran into saturation problems during the first few channels of the burst. On occasion, we would obtain a small unsaturated phE burst which showed only the initial part of the emission (200-300 ns wide, rising in 50 ns or less). By matching the "tail" of this emission with the curve of Fig. 7 we are able to obtain a "composite" time distribution for the first 50 μs of the burst, which is shown in Fig. 8 (note log scale). The important observation is that the initial spike is extremely intense relative to what is the beginning of a much lower intensity decay. Judging from the data of Fig. 6, this decay lasts for several hundred μs, and in fact in Fig. 3, the collective "tail" of a large number of bursts can be seen to last for seconds.

The position of the RE trigger pulse can be accurately determined with respect to the onset of the front of the phE burst. These were in coincidence to within 100 ns, which was within the uncertainty of determining the start of the RE burst. Thus, to within this time interval, the RE burst and the intense part of the phE burst are occurring simultaneously.

By increasing the time constant of the amplifier (which basically adds some integration to the shape of the signal) we were able to measure the area of an unsaturated burst and calculate the number of photons contained in the bursts. For the larger phE peaks (taking into account the detector efficiency of 10^{-2}), we determine that typically 300 to 400,000 photons are entering the photon detector for each burst. This corresponds to peak counting rates exceeded 10^{10} photons/s. Unfortunately, we do not know the angular

distribution of the phE so that it is difficult to estimate the actual total emission (we need the ratio of photons detected to the total which is given by the integral of the phE angular distribution over the solid angle subtended by the detector divided by the integral of the angular distribution over a sphere). However, assuming isotropic emission, we are detecting only approximately 4% of the total emission.

Correlation Between The Amplitude of RE Bursts and Photon Intensity

A correlation in the amplitudes of the RE and phE bursts was determined in the following way. Each RE burst was digitized and its amplitude was measured. The simultaneous current pulse from the PMT was amplified (with sufficient time constant to capture the major portion of the emission) and digitized. The area, which is directly proportional to the number of photons released, was then measured. One set of data is shown in Fig. 9 which resulted from the peeling apart of two layers of filament tape, (i.e., assembled with their adhesive sides together.) We note two distinct and divergent groups of data points which were fit separately using a linear least squares method. The resulting fits, shown in Fig. 9 as solid lines, had very different slopes yet each exhibited a correlation coefficient of 0.94, implying a high probability of independent and linear behavior.

When we found two sets of data points in the results for this single experiment, we suspected that there were really two kinds of interfacial failure occurring during the test: the failure of the adhesive-glass filament interface and the failure of the adhesive-polyester interface. Other experiments confirmed this fact. By applying glass beads between the layers of adhesive we caused more failure to occur at the adhesive-glass bead interface. (This interface proved to be a very copious source of photons relative to the RE--resulting in a large slope of phE vs RE). We also

delaminated the front adhesive + filament layer from the back adhesive + polyester layer and found that the back adhesive was dramatically different from the front adhesive in that the phE vs RE slope was also very large. Thus, the type of interface which is undergoing failure determines the characteristic slope of the phE vs RE amplitude curve.

It should be mentioned that we also observed a strong positive correlation between the intensity and duration of the decaying part of the phE with the RE intensity. Thus, the excitations necessary to produce the "after-emission" were strongly influenced by the intensity of the discharge.

The Role of the Gaseous Environment

The intense phE which occurred simultaneously with the RE resulted from photons produced during the discharges. We conjectured that the delayed phE might result from particle bombardment of the surfaces followed by a relaxation process which would be a form of phosphorescence. An alternative mechanism for this sustained phE is chemiluminescence. Fanter and Levy's discussion of the role of oxygen in the production of strain-induced phE from polymers[20] suggested to us that a chemiluminescence mechanism would be enhanced by the presence of oxygen. To determine if the decays observed after each discharge were due to a reaction with oxygen, we performed peeling experiments in O_2, N_2, and He at one atmosphere and room temperature. Data for these gases taken under the same peeling conditions (2mm/s) and accumulation time as Fig. 6 (performed in air) are shown in Fig. 10.

When a comparison is made between Figures 10 and 6 the following is noted.

A. The later parts of all curves are qualitatively similar. Each gas displays a slowly varying phE with approximately the same decay kinetics.

B. The position of the early broad peak first observed in air is shifted. For the series of gases O_2, He, Air, and N_2 the peak appears at 1, 5, 8, and 25 μs respectively. This is due to progressively higher initial phE signals which produce progressively longer amplifier saturation.

C. We may calculate the average number of photons per RE burst for the series of gases O_2, Air, He, and N_2; this ratio was 21, 100, 126, and 144, respectively.

The result A shows that chemiluminescence involving oxygen is playing no detectable role in the delayed phE. The results B and C agree with the earlier comments concerning the saturation of the amplifier-discriminator at the highest photon counting intensity. In comparison with air the N_2 produces 40% more photons at each discharge. Thus the phE/RE ratio is greater and the counting is impeded in N_2 for 25 μs on average. In comparison with air, O_2 produces about one-fifth as many photons at each discharge and allows the counter to function after one microsecond. The results for He are intermediate and He appears to support discharges that are slightly more emissive than those in air.

These results are consistent with the electrical breakdown properties of these gases. Oxygen has a fairly high electron affinity and can readily form O^- and O_2^- and perhaps O_3^- and O_4^- when free electrons are present.[21,22] This attachment tends to remove electrons from a discharge before electrons gain sufficient energy to produce additional ion pairs by collision.[23] Thus, this attachment will reduce the intensity of the discharges and therefore reduce the amount of phE accompanying each discharge.

Neither He nor N_2 form negative ions by electron attachment so that they do not quench the avalanche process. N_2 seems to support a particularly emissive discharge. Mambetov and Masuraliev reported[24] some time ago that the

phE from the adhesive failure at the interfaces of natural rubber with aluminum and glass was stronger in He than in air.

We next made a comparison of the RE for the two gases with most disparate properties toward discharge, O_2 and N_2. In order to make this comparison we measured the total number of RE bursts and the size distribution of RE in N_2 and in O_2 under the same peeling conditions (2 mm/s) and accumulation time. The results are shown in Fig. 11. As expected, the N_2 yielded many more bursts and larger bursts than the O_2. For the same new surface area produced, the N_2 atmosphere resulted in the detection of over six times as many bursts as in O_2. On the average, the N_2 RE bursts displayed 1.5 times as many rings or oscillations as the bursts in O_2, indicating considerably larger amplitude RE bursts. The microdischarges are thus more energetic and would produce larger numbers of photons per accompanying RE burst, in agreement with C above.

This fact explains the larger ratio of photons per RE burst for N_2 as opposed to the other gases. We know that there is a positive size correlation between number of phE and the RE burst amplitude. RE bursts which are larger in size should be accompanied by more photons and yield a larger ratio of phE/RE in N_2, precisely the results described in C above. The results of this experiment also allowed us to calculate that on the average in N_2 one RE burst was detected for each 0.3 mm^2 of sample peeled.

DISCUSSION AND CONCLUSION

We interpret these results as follows: Intense charge separation on the fracture surfaces produced by adhesive failure leads to micro-discharges in the region of the crack tip. These micro-discharges are responsible for the production of electromagnetic bursts (RE). These bursts are accompanied

by "spikes" of phE which are extremely rapid and have decay times of less than 50 ns. The peak phE count rate can exceed 10^{10} photons/s. The onset of phE and RE are in coincidence to within 100 ns and correlate in size in a manner that is unique to where the failure has occurred.

During the breakdown event the freshly created surfaces will be exposed to the products of the discharge (charged particles, perhaps uv radiation). This bombardment can have two effects: It can cause the immediate release of more charged particles which enhances the discharge process; and it can cause excitation of the surfaces so that delayed emission can occur. When polymers are stimulated with energetic radiation thermally stimulated processes can lead to photon emission (thermal luminescence). When this occurs immediately after formation of the necessary excitations, it is referred to as phosphorescence. The intensity and duration of the resulting phosphorescence will depend on the "dose" the polymer surface received during the discharge.[25] Thus we conclude that the sustained emission we observe is indeed due to the relaxation of an excited fracture surface, where the surface excitation came from the discharge. In relatively low resolution spectra taken of light accompanying adhesive failure of other adhesive-substrate materials, Ohara et al.[26] and Klyueva et al.[27] have seen evidence of both gaseous and luminescence-like emission. It would be particularly interesting to do time-resolved-spectroscopy to separate the fast and slow components. The latter should be pure luminescence.

To the extent that the intensity of the discharge is influenced by the gaseous environment, we have the observed differences in the intensities for the different gases; i.e., N_2 yielded the strongest emission and O_2 the weakest emission. Furthermore, once the discharge and bombardment of the surfaces were complete, the shape of the delayed decay curves were independent

of the gas and only differed in magnitude depending on the intensity of the discharge. This implies first that the decay kinetics are thus a property of the polymer, and second the "after-glow" is not induced by chemiluminescence from a reaction involving oxygen.

If we peel in a particular gas (e.g., air), we find that other factors can influence the number and size of the RE and phE bursts, e.g., the peel speed. The major effect here is most likely the details of the charge separation process. The faster one separates the two dissimilar materials, the less likely re-neutralization can occur by motion of charge. This leads to higher charge densities and therefore stronger electric fields and more intense discharges. Furthermore, when the separation rate is modulated in time by the "stick-slip" phenomena, corresponding fluctuations result in varying charge densities and discharge intensities. These variations in discharge intensities then lead to corresponding changes in the phE and RE intensities. Current studies on imaging the phE bursts are showing dramatic and extremely sensitive responses to near microscopic features of the mechanics of adhesive failure.

A second factor that influences the net charge separation and resulting emission is variation of the substrate. Thus if different interfaces are involved (adhesive-glass vs adhesive-polyester), for example, we observe a proportionality constant between the magnitudes of RE and phE which is characteristic of the particular interface and may uniquely signify the locus of each individual microscopic failure event.

Finally, we note that a number of the RE and phE characteristics should be similar to the behavior of electron and positive ion emission which are necessarily observed in vacuum. Our major goal is to continue measuring the

characteristics of these emissions, determine in more detail the mechanisms, and identify the dependences of fractoemission on the details of failure.

ACKNOWLEDGMENTS

We wish to thank L. C. Jensen, Washington State University, for his assistance in these experiments.

This work was supported by McDonnell Douglas Independent Development Fund, the Office of Naval Research Power Program under Contract N00014-80-C-0213, NR 659-803, and NASA-Ames Interchange NCA2-OR840-202.

REFERENCES

1. B. V. Deryagin, N. A. Krotova, and V. P. Smilga, Adhesion of Solids; (English Translation), Consultants Bureau, New York (1978).

2. J. Wollbrandt, E. Linke, and K. Meyer, phys. stat. sol. (a) 27, K53-K55 (1975).

3. J. T. Dickinson, D. B. Snyder, and E. E. Donaldson, J. Vac. Sci. Tech. 17, 429 (1980).

4. J. T. Dickinson, E. E. Donaldson, and M. K. Park, J. Mat. Sci. 16, 2897 (1981).

5. J. T. Dickinson, M. K. Park, E. E. Donaldson, and L. C. Jensen, J. Vac. Sci. and Technol. 20, 436 (1982).

6. M. H. Miles and J. T. Dickinson, Appl. Phys. Lett. 41, 924 (1982).

7. J. T. Dickinson, L. C. Jensen, and M. K. Park, Appl. Phys. Lett. 41, 827 (1982).

8. J. T. Dickinson, "Fracto-Emission Accompanying Adhesive Failure," in Adhesive Chemistry--Developments and Trends, ed. by L. H. Lee (Plenum Publishers, New York), 1984.

9. J. T. Dickinson, A. Jahan-Latibari, and L. C. Jensen, "Fracto-Emission from Fiber-Reinforced and Particulate Filled Composites," in Polymer Composites and Interfaces, ed. by N. G. Kumar and H. Ishida (Plenum Publishers, New York), 1985.

10. J. T. Dickinson, L. C. Jensen, and A. Jahan-Latibari, Rubber Chem. and Tech. 56, 927 (1983).

11. J. T. Dickinson, L. C. Jensen, and A. Jahan-Latibari, J. Vac. Sci. Technol.A 2, 1112 (1984).

12. J. T. Dickinson, L. B. Brix, and L. C. Jensen, J. Phys. Chem. 88, 1698 (1984).

13. J. T. Dickinson, A. Jahan-Latibari, and L. C. Jensen, J. Mat. Sci. 20 229 (1985).

14. J. T. Dickinson and L. C. Jensen, J. Poly. Sci.: Poly. Phys. Ed., in print.

15. B. V. Deryagin, L. A. Tyurikova, N. A. Krotova, and Y. P. Toporov, IEEE Trans. Indust. Appl. Vol. IA-14, 541 (1978).

16. S. M. Skinner, J. Appl. Phys. 26 498 (1955).

17. J. R. Huntsberger, "The Mechanisms of Adhesion", in Treatise on Adhesion and Adhesives, Vol. 1, edited by R. L. Patrick (Marcel Dekker, New York, 1967).

18. D. Satas, Handbook of Pressure-Sensitive Adhesive Technology, Chapter 4, edited by D. Satas (Van Nostrand Reinhold Co., New York, 1982).

19. A. J. Duke, J. Appl. Polym. Sci. 18, 3019 (1974).

20. D. L. Fanter and R. L. Levy, ACS Symposium Series No. 95: Durability of Macromolecular Materials, edited by R. K. Eby, 211 (1979).

21. B. M. Smirnov, Negative Ions (McGraw Hill Inc., Newark, NJ, 1982).

22. H. S. W. Massie, Negative Ions (Cambridge Univ. Press, 1976), 3rd edition.

23. A. Von Engel, Ionized Gases (Clarendon Press, Oxford, 1965), 2nd ed., p. 186.

24. D. M. Mambetov and T. Masuraliev, Doklad. Akad. Nauk SSSR 185, 122 (1964).

25. R. Chen and Y. Kirsh, Analysis of Thermally Stimulated Processes (Pergamon Press, 1981), pp. 18-22.

26. K. Ohara and T. Hata, J. Appl. Polym. Sci. 14, 2079 (1970).

27. V. A. Klyueva, E. S. Revina, V. I. Anisimova, Y. A. Khrustalev, and Y. P. Toporov, Colloid Journal (Kolloidn.Zh.) 41, 287 (1979).

FIGURE CAPTIONS

Fig. 1. Schematic diagram of the experiment.

Fig. 2. phE and RE counts vs time measured simultaneouly for fast peeling (35 mm/s) and slow peeling (5 mm/s). Each point represents counts accumulated in a multichannel scaler for 0.12 s.

Fig. 3. Decay of phE and RE signals when fast peel (shown in Fig. 2) was stopped. The phE after the RE has fallen is due to an "after-glow".

Fig. 4. phE and RE counts vs time acquired at 0.01 s/channel.

Fig. 5. phE counts vs time acquired at 100 μs/channel.

Fig. 6. A correlation in time of the RE and phE. At t = 0, each RE trigger pulse started the multichannel scaler counting phE at 1 μs/channel.

Fig. 7. A single phE burst digitized at 50 ns/channel. Note saturation of the signal during the most intense interval (1 μs).

Fig. 8. Composite phE curve using data of Fig. 7 with digitized data from a single, unsaturated phE burst.

Fig. 9. Correlation of the amplitudes of simultaneous RE-phE bursts. Solid lines are linear least squares fits to the two "clusters" of data.

Fig. 10. Accumulated RE-phE correlation curves taken in one atmosphere of N_2, He, and O_2, respectively. Same conditions and accumulation time as Fig. 6 which was taken in air.

Fig. 11. Comparison of total number and relative size of RE bursts in N_2 and O_2. Peeling speed 2 mm/s or 0.36 cm^2/s. For this experiment we detect 333 RE bursts/cm^2 of tape peeled in N_2 and 54 RE bursts/cm^2 in O_2.

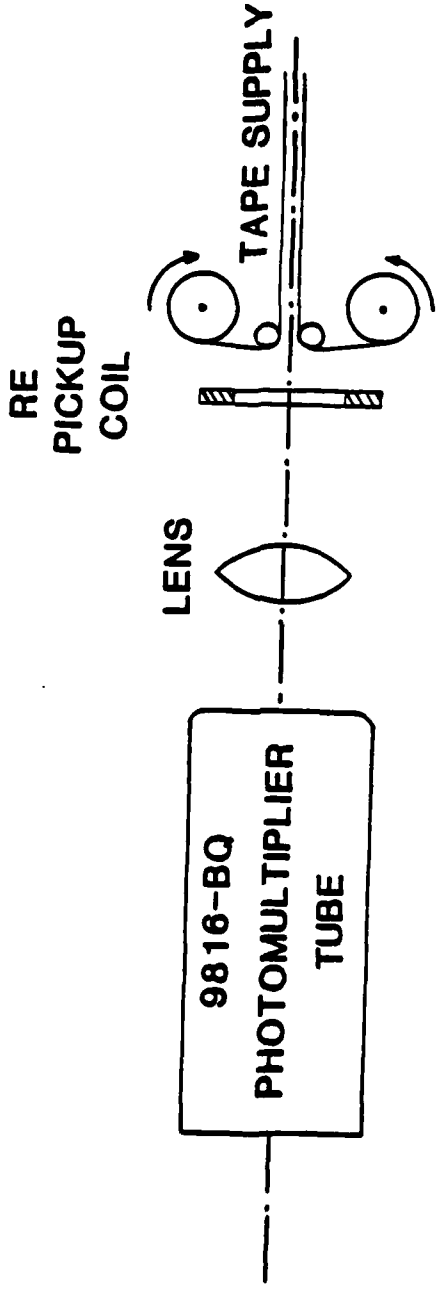
TAPE SUPPLY
RE
PICKUP
COIL
LENS
9816-BQ
PHOTOMULTIPLIER
TUBE

Fig. V-1

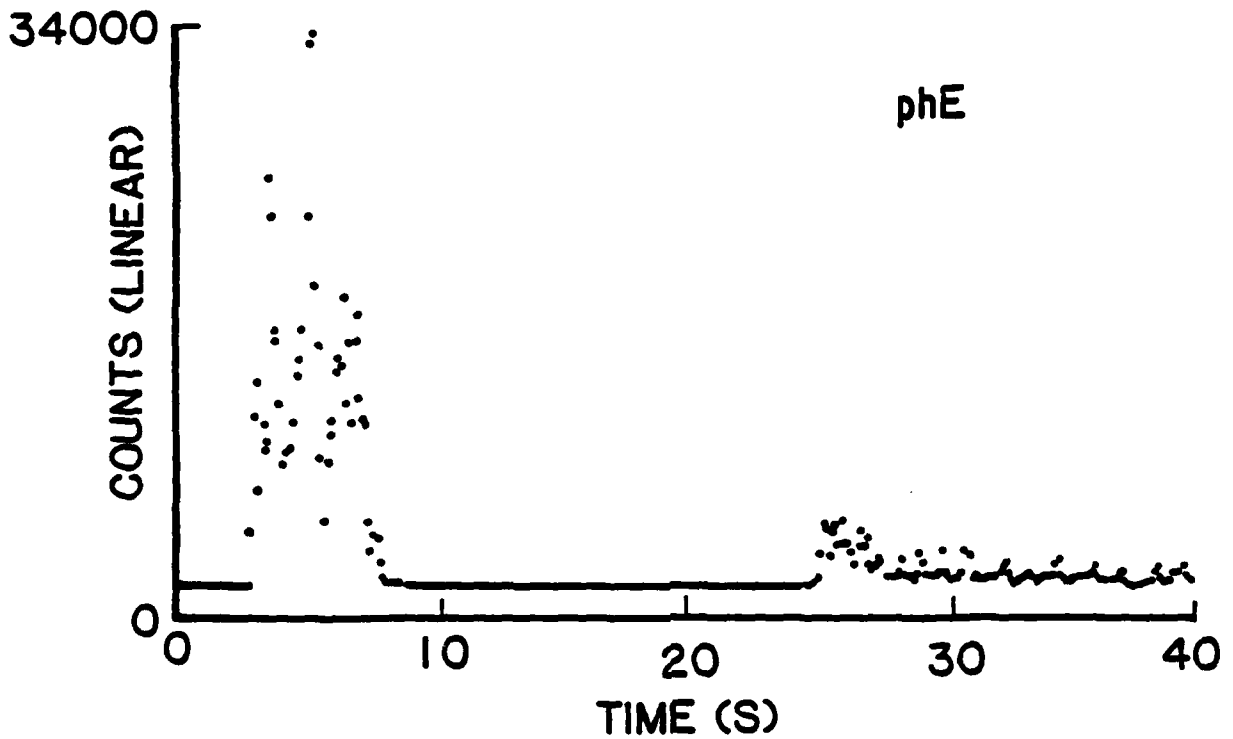
34000
COUNTS (LINEAR)
phE
0
0
10
20
30
40
TIME (S)

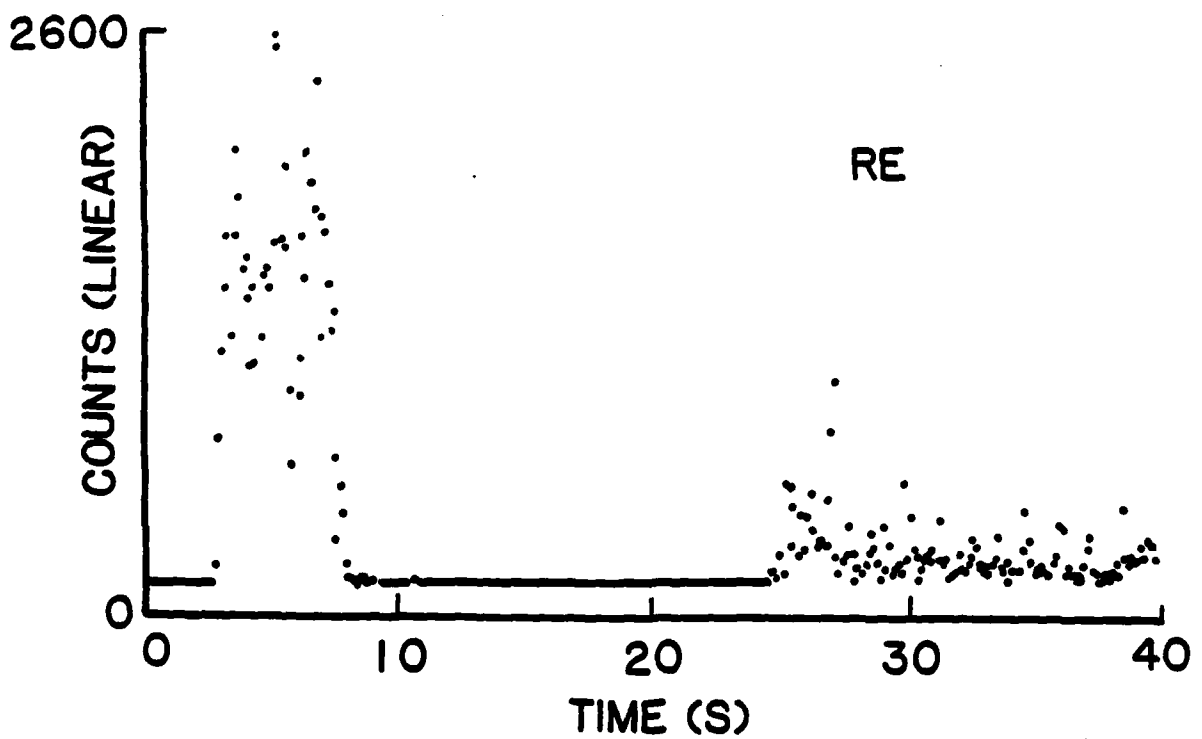
2600
COUNTS (LINEAR)
RE
0
0
10
20
30
40
TIME (S)

Fig. V-2

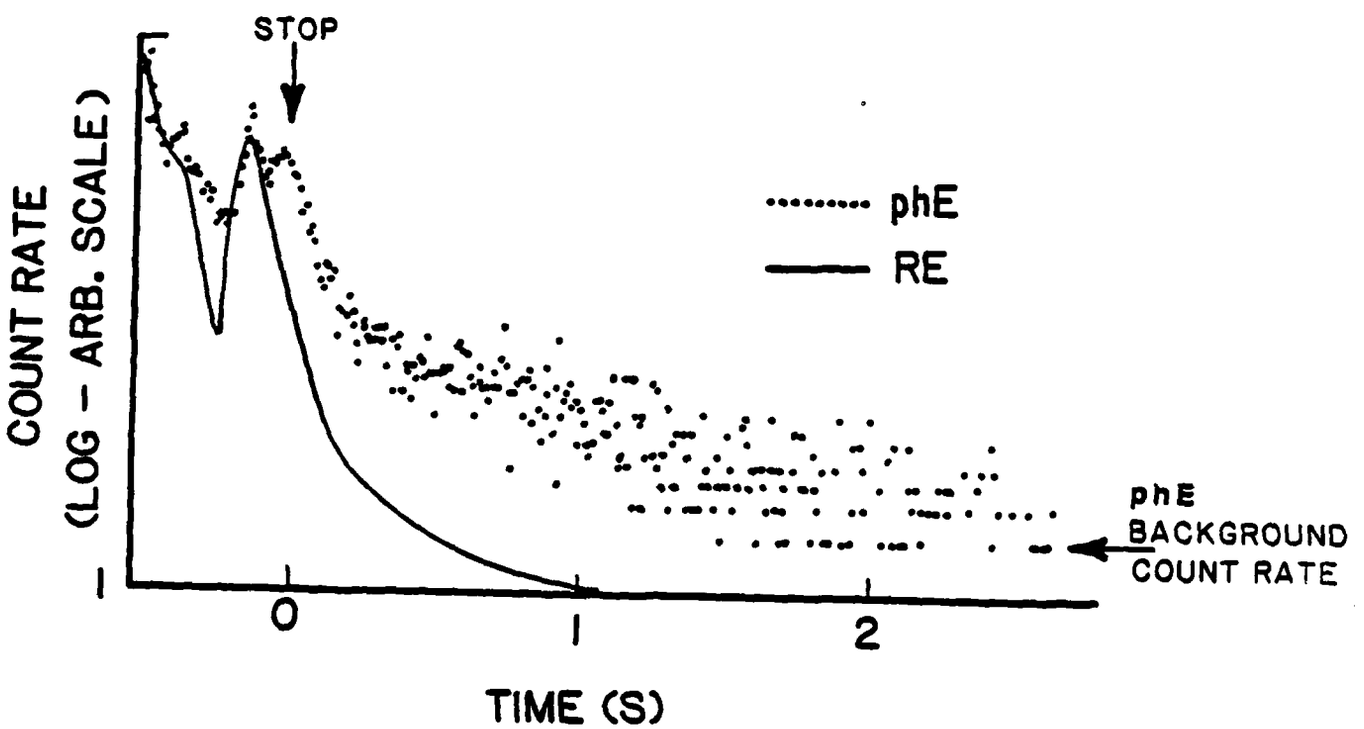
STOP
COUNT RATE
(LOG – ARB. SCALE)
phE
RE
phE
BACKGROUND
COUNT RATE
0
1
2
TIME (S)

Fig. V-3

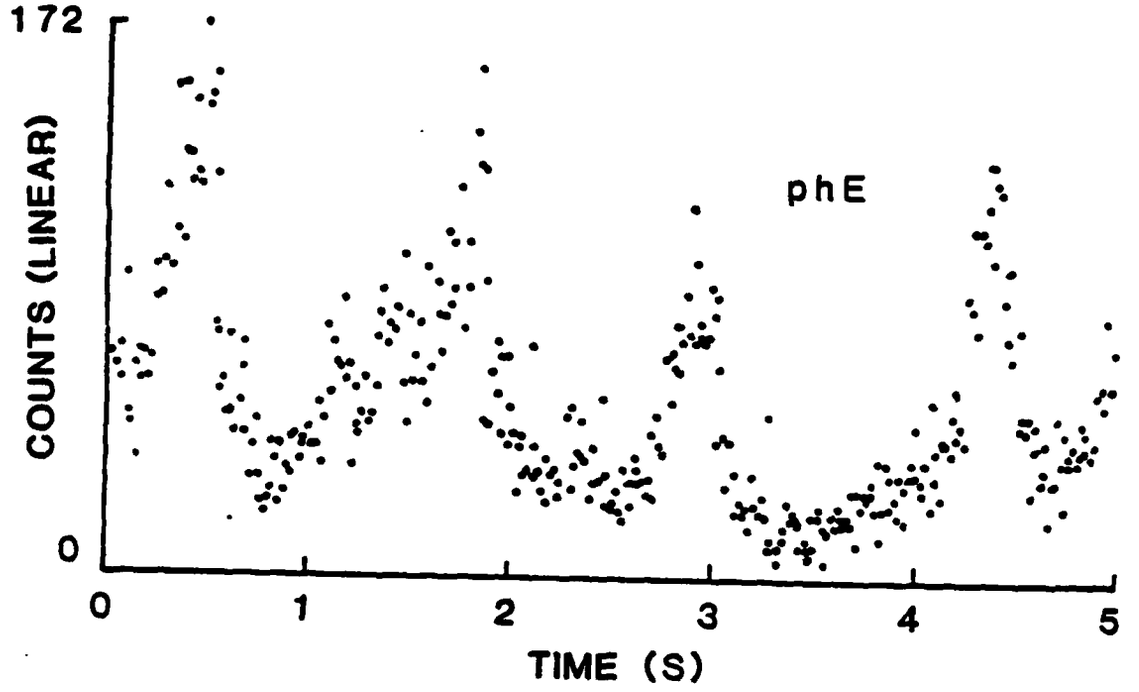
172
COUNTS (LINEAR)
0
phE
0
1
2
3
4
5
TIME (S)

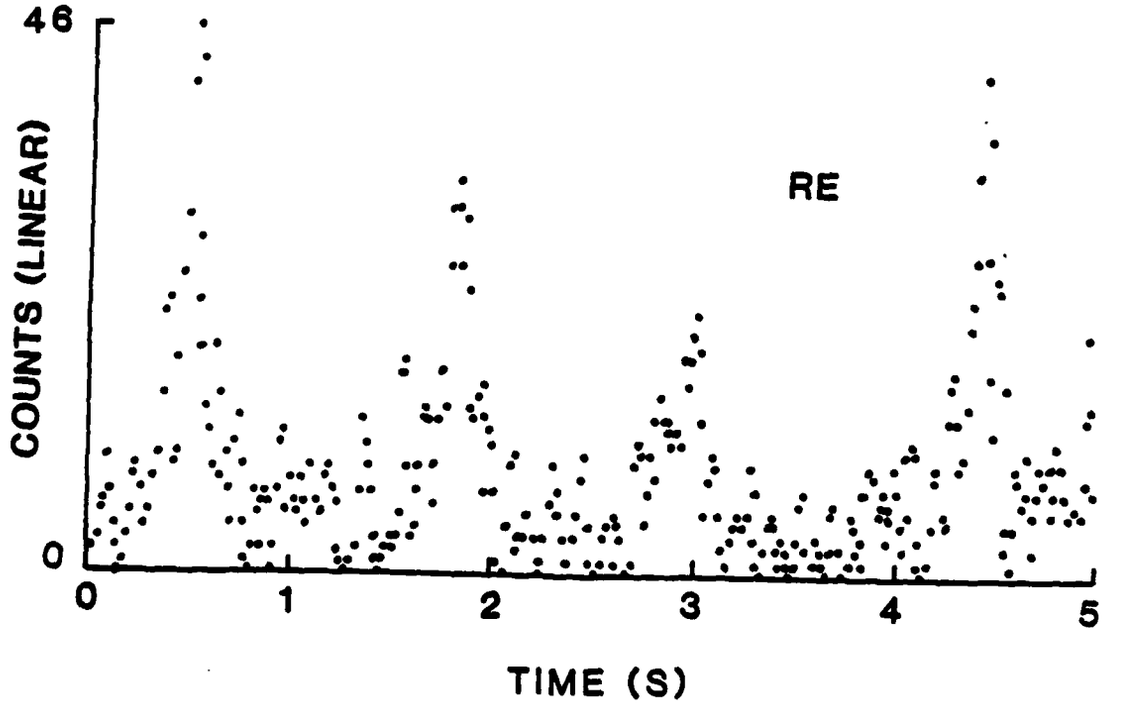
46
COUNTS (LINEAR)
0
RE
0
1
2
3
4
5
TIME (S)

Fig. V-4

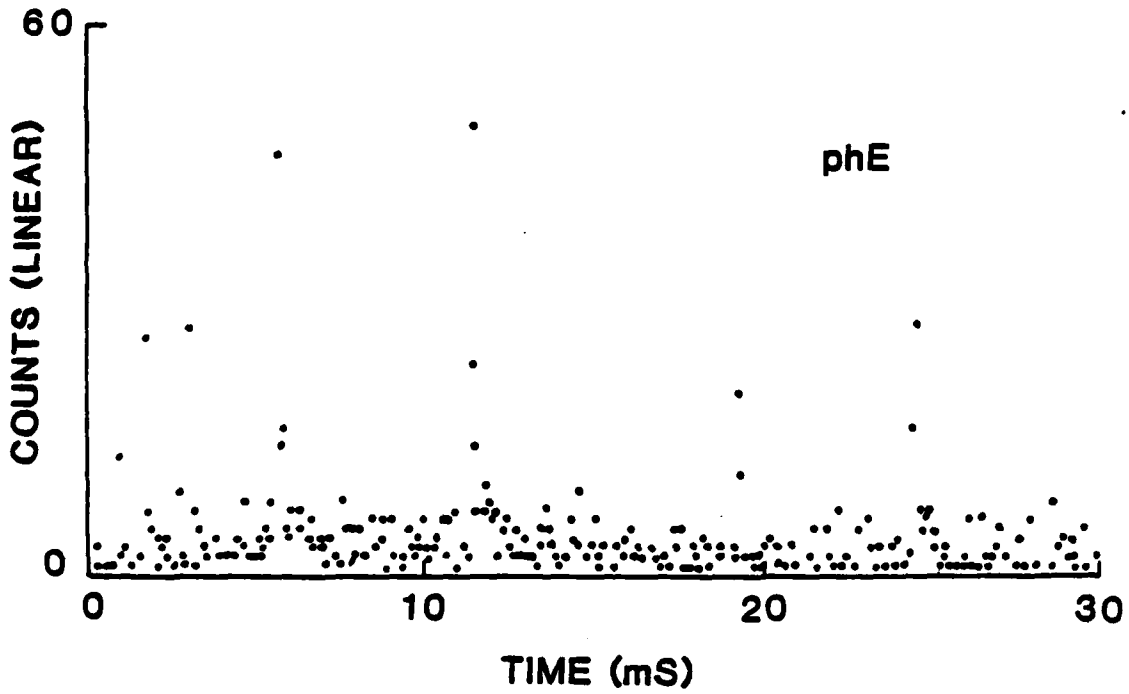

Fig. V-5

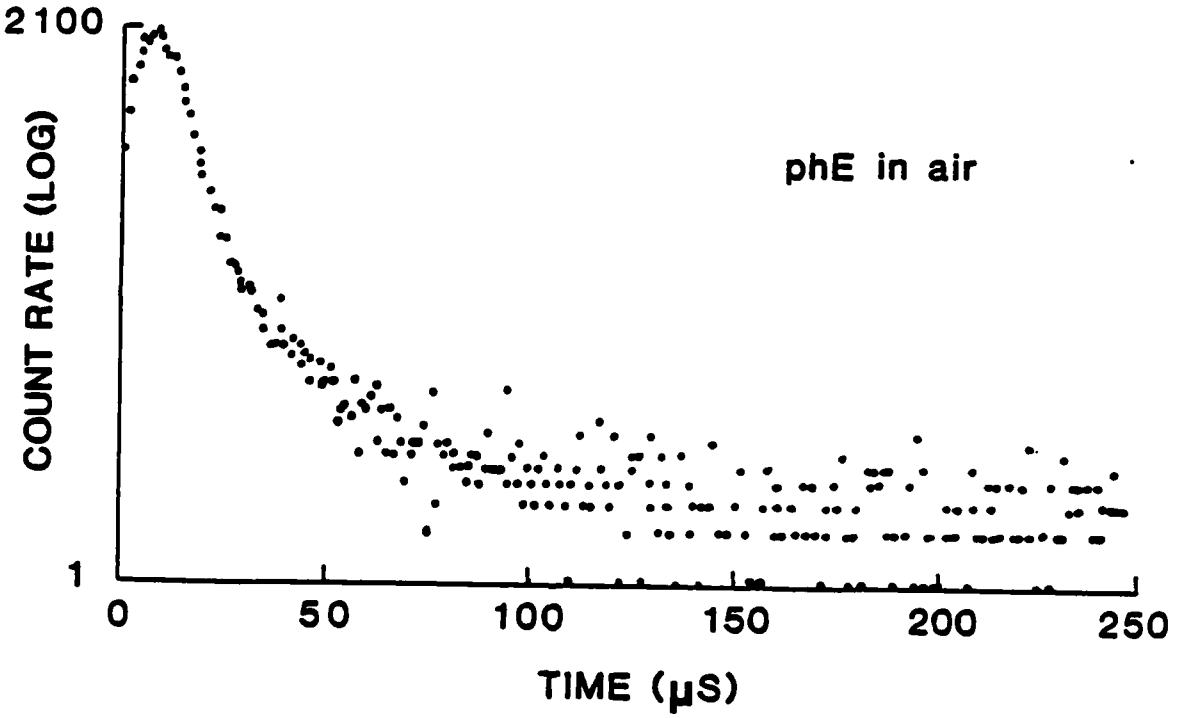

Fig. V-6

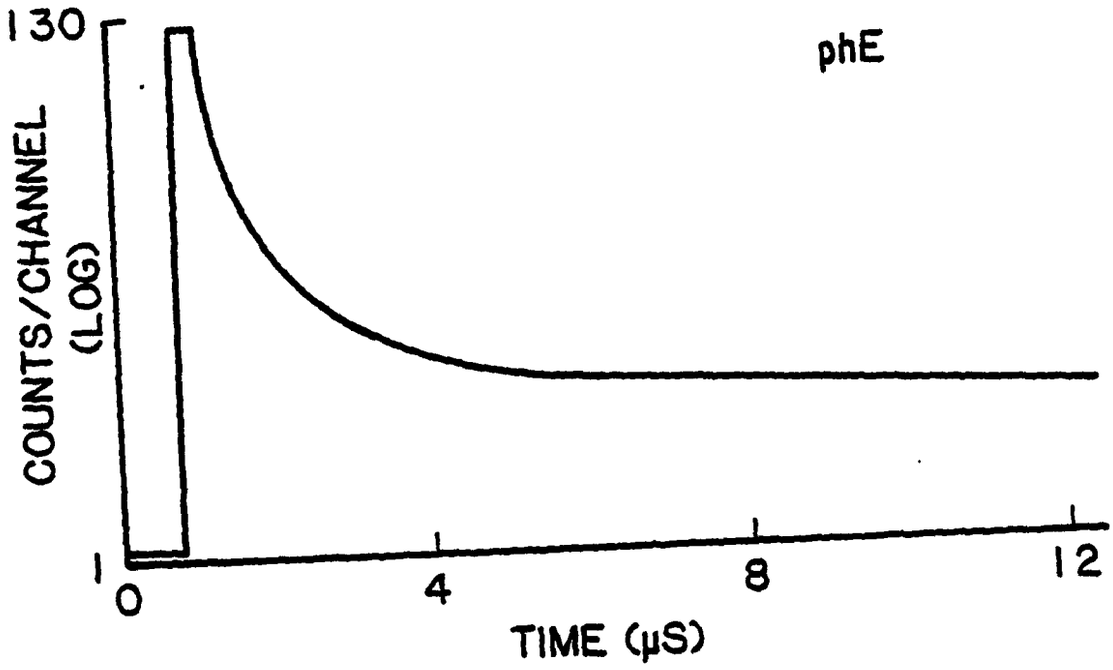

Fig. V-7

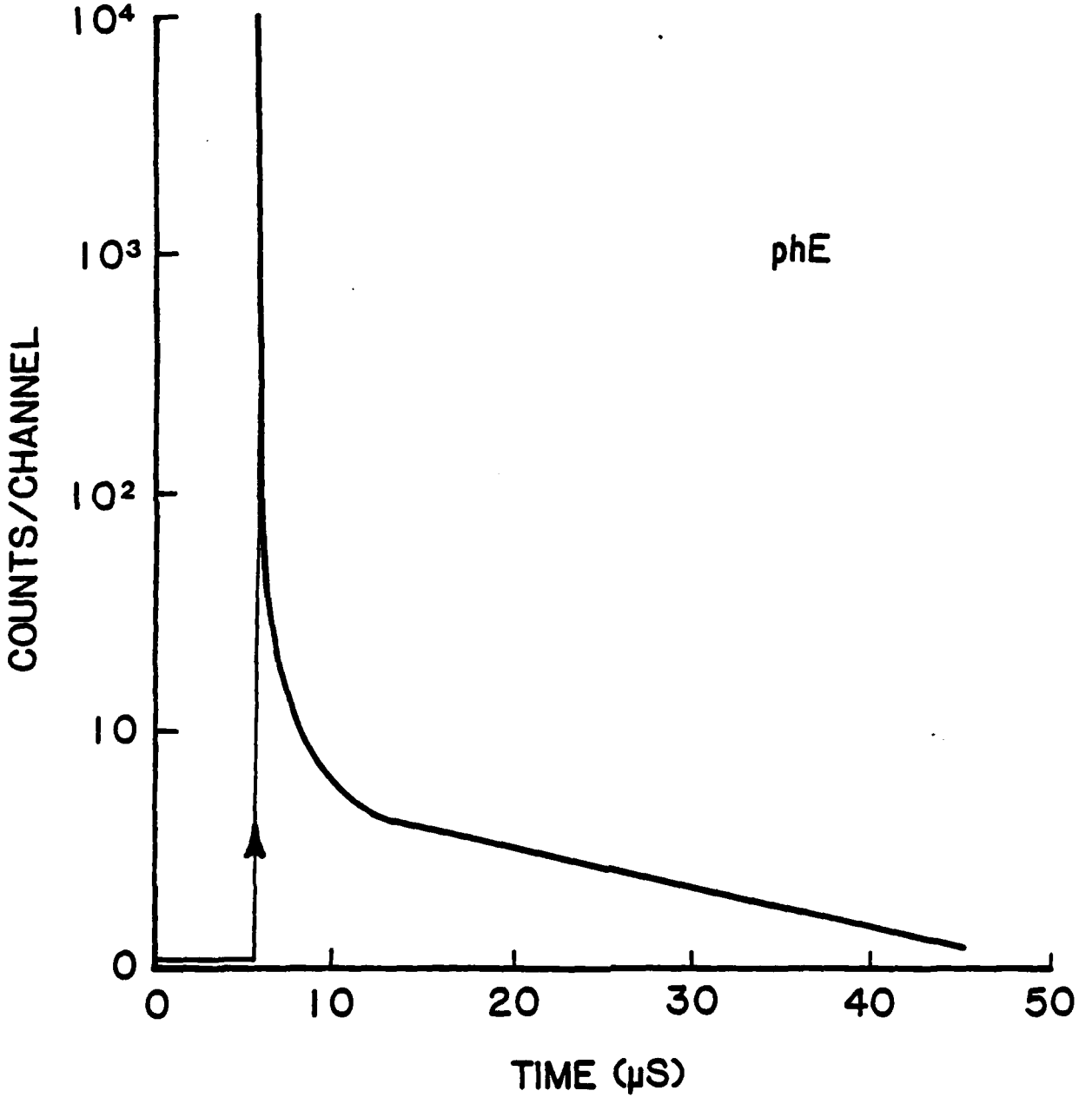

Fig. V-8

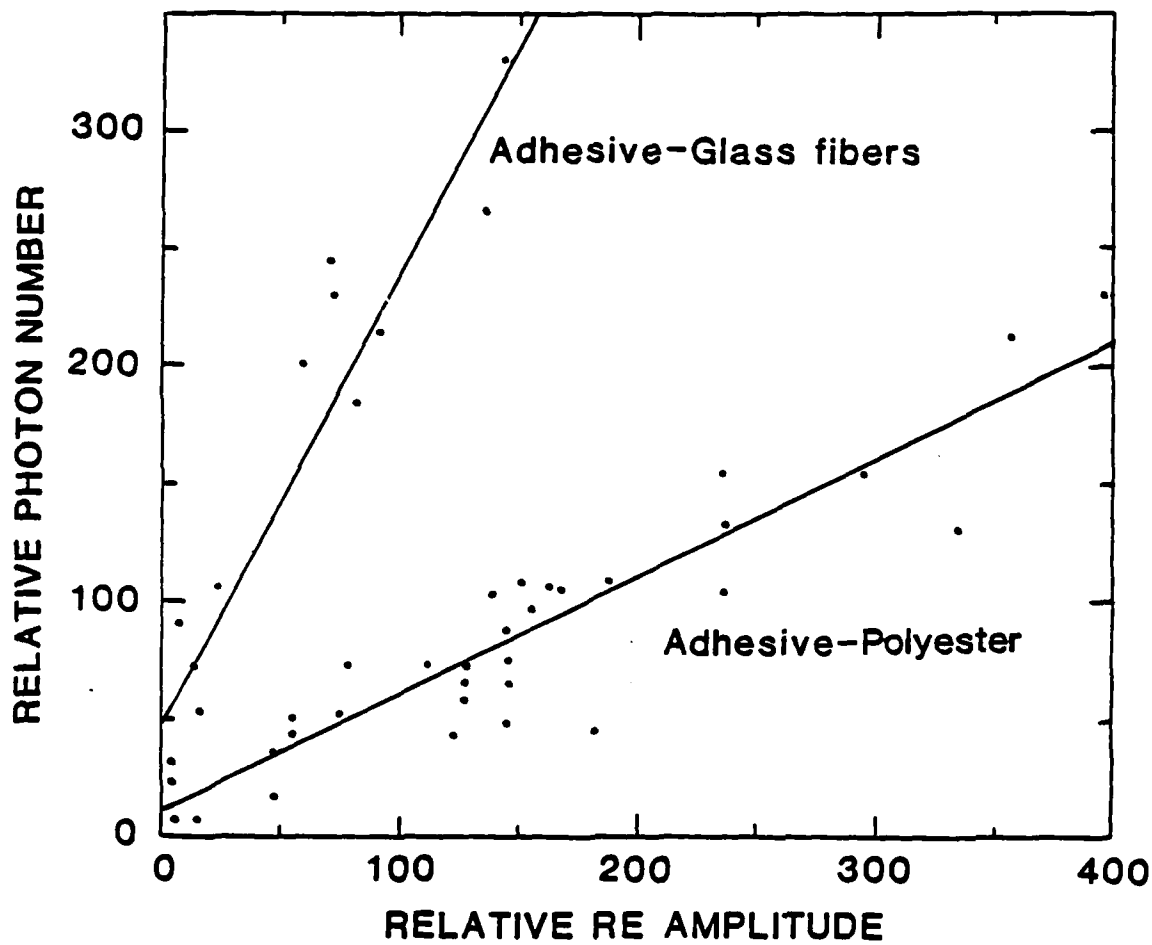
RELATIVE PHOTON NUMBER
300
200
100
0
Adhesive-Glass fibers
Adhesive-Polyester
0
100
200
300
400
RELATIVE RE AMPLITUDE

Fig. V-9

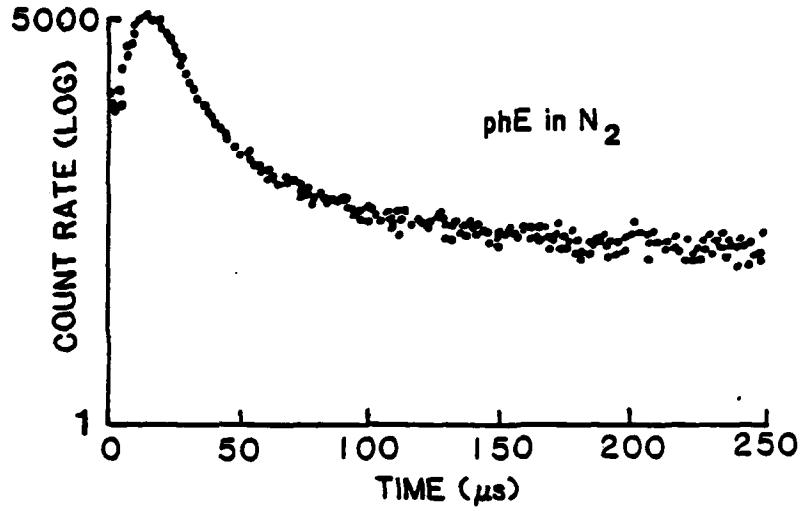
5000
COUNT RATE (LOG)
phE in N_2
1
0
50
100
150
200
250
TIME (μs)

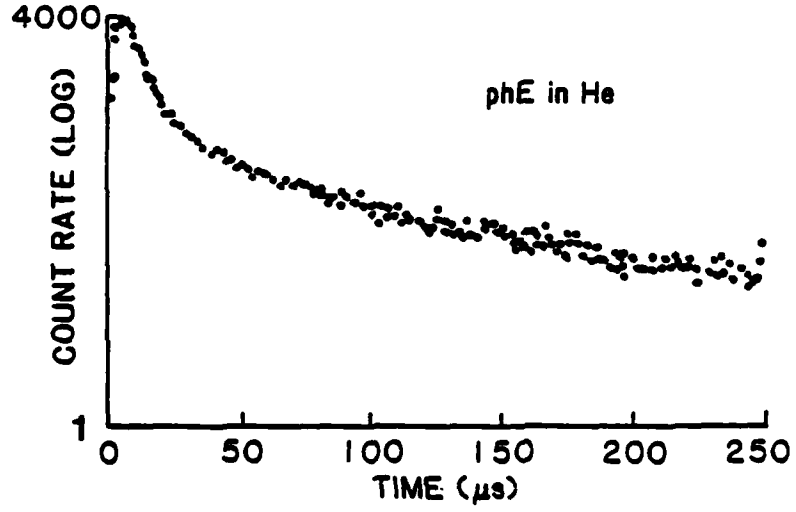
4000
COUNT RATE (LOG)
phE in He
1
0
50
100
150
200
250
TIME (μs)

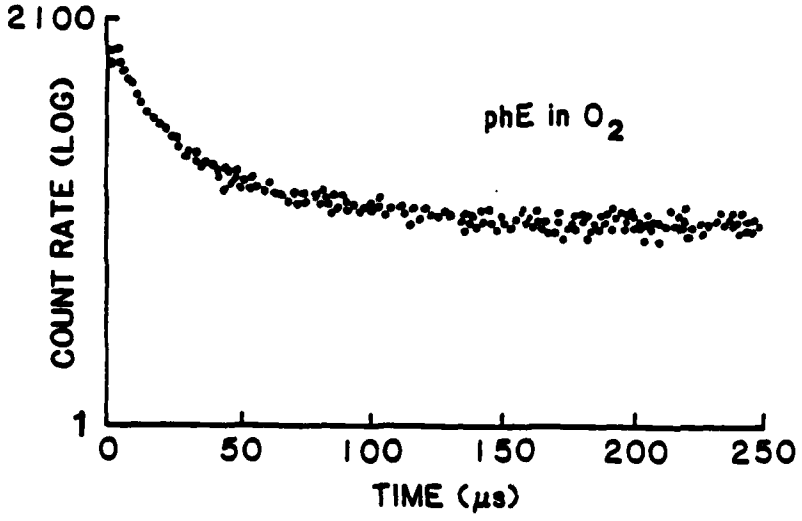
2100
COUNT RATE (LOG)
phE in O_2
1
0
50
100
150
200
250
TIME (μs)

Fig. V-10

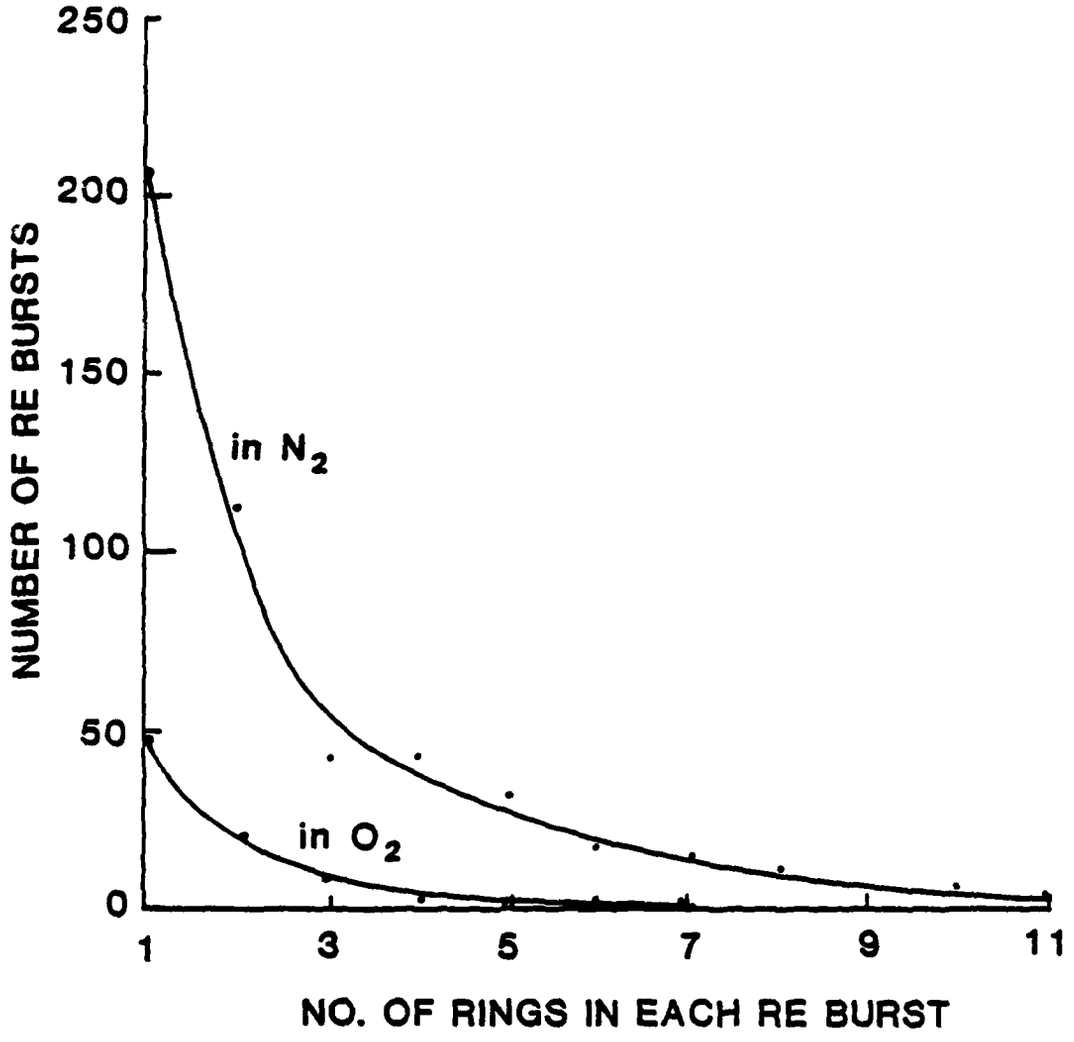
250
200
150
100
50
0
NUMBER OF RE BURSTS
in N_2
in O_2
1
3
5
7
9
11
NO. OF RINGS IN EACH RE BURST

Fig. V-11

VI. THE EMISSION OF ATOMS AND MOLECULES ACCOMPANYING FRACTURE OF SINGLE CRYSTAL MgO

(submitted to J. of Vacuum Science and Technology)

J. T. DICKINSON, L. C. JENSEN, and M. R. MCKAY
Department of Physics
Washington State University
Pullman, WA 99164-2814

F. FREUND*
Institute of Mineralogy
University of Koln
Federal Republic of Germany

ABSTRACT

We have been investigating the emission of particles due to deformation and fracture of materials. We observe the emission of electrons (exoelectron emission), ions, neutral species, photons (triboluminesence), as well as long wavelength electromagnetic radiation; collectively we refer to these emissions as fracto-emission. In this paper, we describe measurements of the neutral emission accompanying the fracture of single crystal MgO. Masses detected are tentatively assigned to the emission of H_2, CH_4, H_2O, CO, O_2, CO_2, and atomic Mg. Other hydrocarbons are also observed. The time dependences of these emissions relative to fracture are presented. We show that the onset of CH_4 emission precedes the fracture event.

*Present Address: NASA Ames Research Center
Mail Stop 239-4
Moffett Field, CA 94035

INTRODUCTION

We have been investigating the emission of particles due to deformation and fracture of materials [1-4 and references therein]. We observe the emission of electrons, ions, neutral species, photons (triboluminesence), as well as long wavelength electromagnetic radiation; collectively we refer to these emissions as **fracto-emission (FE)**. The goals of our research are to characterize the properties of FE, determine the mechanisms for each emission component, and relate the FE behavior to the physics and chemistry of

deformation and fracture of interesting materials and systems. The properties of the emission we measure include identification of the emitted species, total intensities, time distributions relative to crack growth, energies, and correlations in time between various FE components. The dependence of these characteristics on the material properties, locus of fracture, crack velocity, and temperature have also been investigated. The emission effects can be observed over a wide range of materials including inorganic single crystals, ceramics, organic molecular crystals, polymers, composites, and interfaces. In this paper we present recent results on the emission of neutral species: atoms, molecules, and radicals accompanying the fracture of inorganic single crystals, in particular MgO.

A few earlier measurements of the gaseous products accompanying the fracture of materials have been made. In the case of simple cleavage of crystalline inorganic solids, Fox, et. al.[5] first examined carbonates of Ca, Mg, and Pb as well as the azides of Na and Pb. They observed with a time resolution of 0.1 s the decomposition products CO_2 and N_2 only. They attributed their results to thermal decomposition caused by elevated temperatures at the moving crack. Interestingly, they saw no gaseous emission from MgO. Gallon, et. al.[6] showed that during cleavage of alkali halides (MX) one could observe signals corresponding to released M and X. Their response time was relatively long and only crude correlation with the time of fracture was attempted.

Urakaev, et. al.[7] examined the products from cleaving alkali nitrates, nitrites, chlorates, bromates, and iodates. With 0.5 s time resolution, they observed a number of products including substantial amounts of H_2O, CO, and CO_2 with possible atomic emission (low intensities) of such species as O, N, X, and XO (where X represents a halogen atom). In the case of $CsNO_3$ they

observed a delayed (approximately 1.5 s) buildup of NO after fracture. In all their results, no cation-containing species were observed. The dominant decomposition products of nitrates and alkali metal chlorates was O_2; from nitrites: O_2 and N_2. They concluded that the processes occurring during cleavage differ from thermal decomposition. Their proposed mechanism for this neutral emission involving the matrix atoms only involved some form of mechanically induced dissociation between cation-anion accompanied by formation of short-lived excited species, followed by vibrational and electronic transitions leading to neutralization of the anion and its decomposition, which then leads to diffusion and desorption of the products.

In this paper we first present measurements of the total non-condensible gases emitted from MgO, show the wide range of neutral masses seen in the emission spectrum, and take a careful look at the time dependence of various masses relative to fracture. Of considerable interest is our observation of some neutral emission during loading but prior to fracture.

EXPERIMENTAL

Highly transparent, single crystal MgO samples supplied by Spicer Ltd., Cheltenham, England, were synthetically grown by arc fusion with a purity of 99.99%. The samples were cleaved and polished; dimensions were 10 mm x 5 mm x 1 mm. They were mounted in a three point bending apparatus with a 2.5 mm span. The sample holder can hold 20 samples on a carousel arrangement that can be manipulated from outside the vacuum system. Experiments were carried out at a background pressure of 10^{-6} Pa. The sample was stressed by applying a rounded (0.75 mm radius) edge to the sample center at either 0.2 cm/s (three point bending) or 10 cm/s (impact). The fracture was detected with an

acoustic transducer (AET Corporation Model 1500 L) attached to the sample holder.

The neutral emission from the sample was monitored with a UTI 100C quadrupole mass spectrometer and a Bayard-Alpert gauge positioned 1.2 cm and 20 cm from the sample, respectively. Electron emission currents were 2.0 ma and 4.0 ma, respectively. The quadrupole was used both in a scanning mode (1-60 amu every 80 ms) or tuned to a single mass peak. The electrometer outputs from these sources were digitized at 80 μs/channel with a LeCroy Data Acquisition System. The time response of the mass spectrometer electronics was 20 μs; the ion gauge electronics response time was 40 ms.

A double layer of Ni grid mesh which produced an average hole spacing of 5 μm was inserted between the sample and the ionizer block the flight of ejecta (macroscopic particles produced by fracture) into the ionizer. This grounded grid also greatly reduced electron bombardment of the sample from the quadrupole ionizer as well as reducing electrostatic effects on the ionizer from the surface charge on the sample produced by fracture.

On some samples, a 30 nm gold film was sputtered onto the front surface to provide a signal in coincidence with fracture; i.e., when this conductive layer is broken the change in resistance could be converted into a pulse. The uncertainty of this signal is estimated to be within 1 μs of the fracture event, the duration of which is less than 1 μs. For other systems, such a metal film is known to consist of connected islands with a considerable amount of substrate surface area uncovered.[8]

RESULTS AND DISCUSSION

In Fig. 1 we show the total pressure change, p, accompanying the fracture of an MgO single crystal. The gauge was located in the system out of sight of the sample so this signal represents the non-condensible components of the

neutral emission. Tests for artifacts such as motion of bellows, mechanical vibrations, and coating the entire sample with metal produced no evidence that these gases came from any other source than the sample. The observed rise and peak shape could be somewhat slower than the actual p, due to the electrometer time constant. The tail seen in Fig. 1, however, should represent the actual decay of the emitted gases from the fracture. This p curve corresponds to approximately $3x10^{15}$ molecules/cm^2 of sample cross-section. Even with cleavage surface roughness factors as high as 2-3, this is a considerable amount of gas.

Fig. 2 shows a difference spectrum between two mass scans taken immediately before and after fracture of single crystal MgO (total time/scan = 80 ms). We have allowed the mass peaks with relative intensity of 100 to purposefully go off scale so that the smaller peaks can be clearly seen. Frequently observed emission peaks were masses 1, 2, 15, 16, 17, 18, 24, 28, 29, 32, and 44. Tentative assignment of parent species released (based on known cracking patterns) are atomic H_2, CH_4, H_2O, atomic Mg, CO, and CO_2. Other hydrocarbons were also detected as evident by peaks such as 25-27, 30, 38-43, and 53-57, although masses 25 and 26 are also isotopes of Mg. MgO contains a wealth of impurities which contribute to these emissions. Freund et. al. have described the low z impurities in MgO[9,10] due to dissolution of excess O_2, H_2O, and CO_2 and has shown that the H and C are in a reduced state (molecular H_2 and a near zero valance C complex) and the oxygen is found in an oxidized form (spin paired $O^- + O^- = O^{2-}$ peroxy anion). Gas evolution studies done on similar MgO material in powder form[11,12] show that with heating, the evolution of a number of similar compounds occurs, with the probable exception of the metal vapor (atomic Mg).

Based on these results, we would propose that the carbon containing compounds produced by fracture are due to chemical reactions accompanying and following fracture with bulk (impurity) carbon with O type defects (e.g., O^-, which in a O^{2-} lattice represents a defect electron or positive hole) and dissolved hydrogen. It is important to note that the observed compounds do not exist in the crystal prior to fracture. The crystal near the fracture surface is acting as a source of reactants (some of which may have been produced by bond breaking accompanying fracture) and the surface serves as a catalyst for recombination reactions of these reactive species.

Similarly, the H_2O and O_2, which can be very intense, are also products of recombination reactions. However, the atomic Mg observed is more likely a product inherent to bond breaking of the crystalline MgO itself. We envision that patches of the fracture surface are out of stoichiometry with neutral Mg being a desorbed "waste product". A relevant quantity we intend to measure by thermal desorption spectroscopy is the desorption energy of deposited metallic Mg from a freshly cleaved MgO crystal.

The absolute size and the relative peak heights of the mass spectra are strongly variable from sample to sample. Up to this point we have not taken care to control the size and density of microcracks on the crystal surfaces nor controlled the energy being channeled into fracture of the crystals. We find a fairly good correlation between the neutral emission intensity and the strain rate (impact velocity). This generally leads to higher fracture energies and thus, the neutral emission may be a very important probe of the energetics of fracture. Careful simultaneous mechanical measurements are needed and are being developed currently.

One striking variation that was observed was that the mass scan measurements fell into two catagories: A) large mass 32, and B) small

mass 32. The relative peak heights of the major mass peaks or groups for these two cases are shown in Tables IA and IB with tentative assignments to parent molecules. The major uncertainty in the parent identifications is in the specific hydrocarbons contributing to the overall spectrum. Peak heights have been normalized to mass 18 in both categories. We note that when O_2 is strong, CO_2 is very intense and CO is also up, suggesting that the availability of oxygen at the surface regulates these products. Conversely, when O_2 is weak, mass 24 (atomic Mg) is strong; evidently, a lack of oxygen greatly enhances the release of the metal from the surface.

Figure 3a - 3d show the signals observed from the quadrupole mass spectrometer, each taken on different samples, while sitting on single mass peaks,: 16, 24, 32, and 44. The arrows indicate when the fracture event occurred. The inset in Fig. 3a shows on an expanded time scale, the shape of the rise in mass 16, indicating a clearly defined shoulder. A more careful measurement of the time of fracture was carried out using a porous Au film on the surface facing the ionizer, previously described. Such a film would be porous so that gas could still be released from the surface. The arrow in Fig. 4 shows the time of fracture relative to the position of this shoulder; it occurs before fracture. We saw no evidence of this shoulder in mass 32, but is present in mass 15. Thus, we conclude that this pre-failure neutral emission is CH_4 and that it is being produced and driven via dislocations that are appearing at the surface, possibly associated with microcrack growth from dislocation pile-up (MgO can have highly mobile dislocation motion, even at room temperature)[13]. It should be noted that we have seen exactly the same behavior in the photon emission coming from stressed single crystal MgO.

In general, the time dependence of masses 16 (CH_4), 28 (CO)--not shown, 32 (O_2), and 44 (CO_2), behave in a similar fashion, and taking into account the

ionization gauge electrometer time constant these species can account for the shape of the observed total pressure change. It should be noted that the mass 32 emission shown in Fig. 3c is very intense in the initial peak: one to two orders of magnitude greater than other emissions we have observed. As such, the time dependence of the emission appears to be somewhat different than that shown for the other masses; but in fact the tail of the mass 32 emission is similar to the time dependence of the other masses, and it follows the decay of the total pressure change fairly closely.

The mass 24 (Mg) time dependence is quite unique. In Fig. 3b, we show this dependence for the case of a weak O_2 emitter. Mass 24 tends to start growing when the other peaks, particularly those involving oxygen, have decayed. A reasonable explanation for this is that as long as oxygen is available, the Mg prefers to react with it, but as the oxygen disappears the Mg can desorb; this is supported by the observation above that when large 32 peaks are observed, implying that oxygen is more available, mass 24 is small.

Qualitatively, these differences appear to be related to the fracture energy which can vary considerably from sample to sample. If this is the case, these neutral emission signals may be eventually related to the microscopic events occurring during fracture.

CONCLUSIONS

We have shown that a variety of neutral species are emitted when pure, single crystal MgO is fractured. The observed species (e.g., H_2, H_2O, CH_4 and other hydrocarbons, CO, CO_2)) are products of reactions induced by fracture and often involve dissolved low Z impurities (C, H, O-defects) contained in the crystal. The appearance of metallic Mg suggests that neutral Mg is in fact a consequence of bond breaking. In all likelihood, at least some of the

oxygen emitted as O_2, CO and CO_2 is also due to fracture-induced changes in valancy from the lattice O^{2-} state. The appearance of masses 15 and 16 before fracture is believed to be due to dislocations appearing on the surface which drives the formation of CH_4, perhaps due to formation of a highly selective catalytic site. This signal may prove to be a valuable probe of dislocation motion near a surface which is of considerable importance in understanding crack formation in semi-brittle materials.

Further work is being carried out on testing these ideas; e.g., determining the effects on the neutral emission with variations in strain rate and fracture energy, from thermal pre-treatment of the crystals, thermal stimulation of the fractured surface (on the ms time scale), and creation of defects by doping or exposing the crystal to radiation.

In addition to potential applications to fundamental studies of fracture, there are some other important implications of this work that we would like to mention. First, the signals observed are related to one of the most basic dynamic processes of interest to surface science: the transformation of the bulk to a surface. Our fracto-emission studies are examining relaxation phenomena occurring during this transformation on time scales from nanoseconds to milliseconds. Normally, surface science is performed on time scales > seconds. Furthermore, specifically with respect to the atom and molecular emission we have described, the release of metal vapor and organic species by fracture may be of considerable importance in explaining the origin of a number of species seen in intersteller space. Collisions between grains could certainly result in similar fracture induced chemistry we describe here. Finally, we mention that magmatic minerals under high stress can also form and release such gases which could be important in interpreting and even detecting certain geological processes. We have recently examined[14] the neutral

emission from the fracture of crystalline olivine (from San Carlos, AZ). In addition to the species seen from MgO, we also observed atomic Fe and numerous C-H and C-N-H compounds up to mass 210. Perhaps life on earth started with a rockslide rather than a lightning bolt!

ACKNOWLEDGMENTS

This work was supported by the Ceramics and Electronics Materials Division of the National Science Foundation under Grant No. DMR 8210406, the Office of Naval Research (Contract N00014-80-C-0213, NR 659-803), and NASA-Ames Research Center. We thank Dr. Sherwood Chang, NASA-Ames Research Center for his interest in this work.

REFERENCES

1. J. T. Dickinson, L. C. Jensen, and A. Jahan-Latibari, J. Vac. Sci. Technol.A 2, 1112 (1984).

2. J. T. Dickinson, W. D. Williams, and L. C. Jensen, J. Am. Ceramics Soc. 68 235 (1985).

3. L. A. K'Singam, J. T. Dickinson, and L. C. Jensen, "Electron and Photon Emission Accompanying Failure of Metal/Glass Interfaces," to appear in J. Am. Ceramics Soc.

4. J. T. Dickinson and L. C. Jensen, J. Poly. Sci.: Poly. Phys. Ed. 23, 873 (1985).

5. P. G. Fox, and J. Soria-Ruiz, Proc. Roy. Soc. Lond. A317, 79 (1970).

6. T. E. Gallon, I. G. Higgenbotham, M. Prutton, and H. Tokutaka, Surf. Sci. 21, 224 (1970).

7. F. Kh. Urakaev, V. V. Boldyrev, O. F. Pozdnyakov, and V. R. Regel, Kinetika i Kataliz 18, 350 (1977).

8. M. Thomas, J.T. Dickinson, H. Poppa, G.M. Pound, J/ Vac. Sci. Technol. 15(2)568 (1978).

9. H. Kathrein, H. Gonska, and F. Freund, Appl. Phys. A30, 33 (1983).

10. H. Kathrein, F. Freund, and J. Nagy, J. Phys. Chem. Solids 45, 1155 (1984).

11. R. Knobel and F. Freund, Mater. Res. Bull. 15, 1247 (1980).

12. F. Freund, R. Knobel, G. Oberheuser, G. C. Maiti, and R. G. Schafer, Mater. Res. Bull. 15, 1385 (1980).

13. R. W. Davidge, Mechanical Behavior of Ceramics, Cambridge University Press, Cambridge (1979), pp. 54-60.

14. F. Freund, R. M. Knobel, F. Struwe, and J. T. Dickinson, Proceedings of the 12th International Meeting on Organic Geochemistry, Julich, September 16-20, 1985.

FIGURE CAPTIONS

Figure 1. Total pressure change during the fracture of MgO single crystal.

Figure 2. The difference between the mass peaks after fracture and the background prior to fracture.

Figure 3. The time dependence relative to fracture for different MgO crystals of selected single mass peaks: a) 16, b) 24, c) 32, d) 44. The arrows show the time of fracture. The inset in a) shows the rise in mass 16 signal on a faster time scale.

Figure 4. The time dependence of mass 16 emission on a faster time scale. The arrow shows the instant of separation of a 30 nm thin film of Au deposited on the front surface of the crystal. The shoulder (seen also in Fig. 3a) occurs before fracture.

Table I.

A) Large Mass 32

M/q	Relative Intensity	Tentative Assignment
1	20	H_2, C_xH_y, H
2	60	H_2, C_xH_y
4	small	He
15	40	CH_4
16	100	CH_4, O_2
17	40	H_2O
18	100	H_2O
24	small	Mg
25,26	small	C_xH_y, Mg
28	90	CO
29	40	C_xH_y
32	140	O_2
39-42	small	C_xH_y
43	50	C_xH_y
44	90	CO_2
55-57	small	C_xH_y

B) Small Mass 32

M/q	Intensity	Tentative Assignment
1	10	H_2, C_xH_y, H
2	30	H_2, C_xH_y
4	0	none observed
15	20	CH_4
16	25	CH_4
17	25	H_2O
18	100	H_2O
24	45	Mg
25,26	small	Mg, C_xH_y
27	small	C_xH_y
28	80	CO
29	small	C_xH_y
32	small	O_2
39-43	small	C_xH_y
44	10	CO_2
55-57	small	C_xH_y

Table I. Relative intensities of the observed mass peaks with tentative assignments to parent molecules listed in order of decreasing contributions. A) Typical quantities for specimens which were strong mass 32 emitters; B) Quantities for specimens which were weak mass 32 emitters.

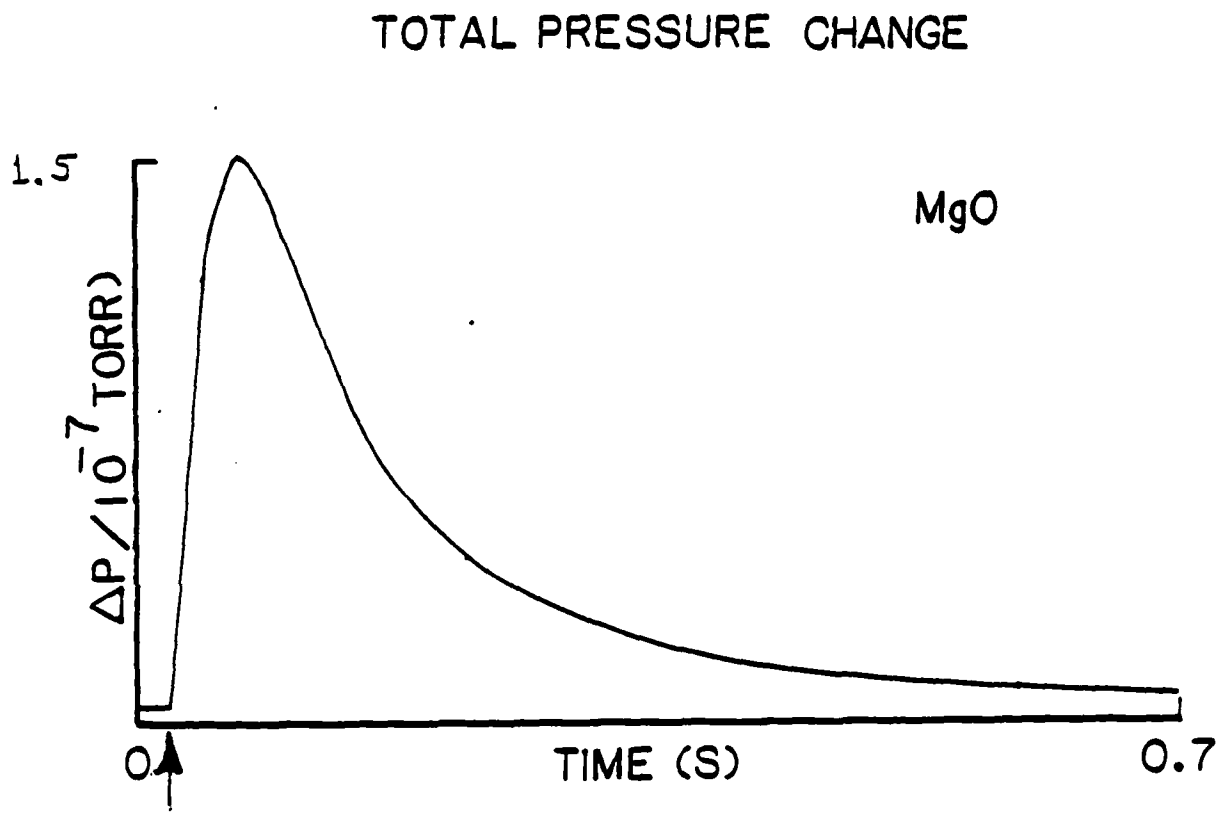

Fig. VI-1

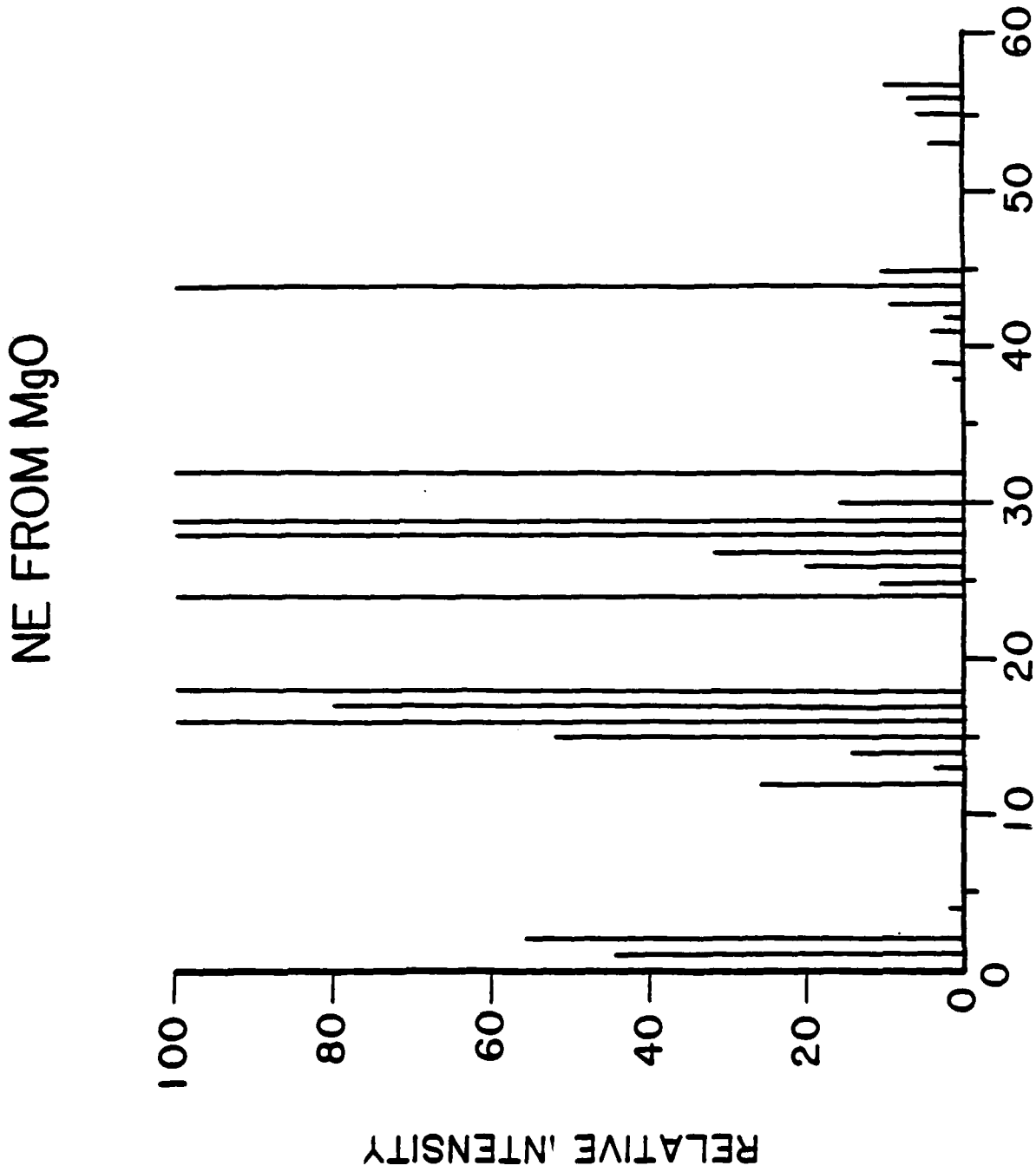
NE FROM MgO
RELATIVE INTENSITY
100
80
60
40
20
0
0
10
20
30
40
50
60
M/q

Fig. VI-2

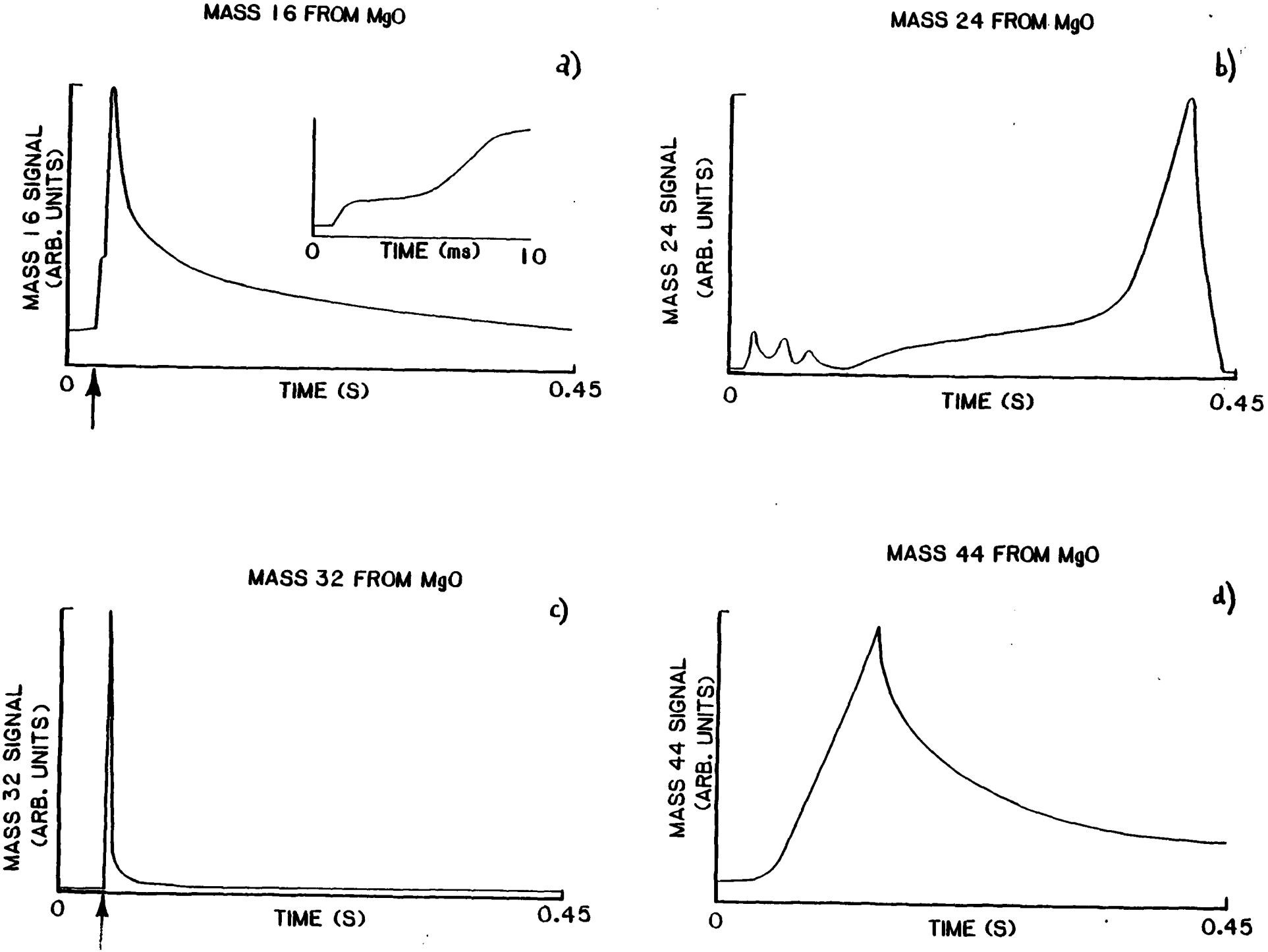
MASS 16 FROM MgO
a)
MASS 16 SIGNAL (ARB. UNITS)
0
TIME (ms)
10
0
TIME (S)
0.45
MASS 24 FROM MgO
b)
MASS 24 SIGNAL (ARB. UNITS)
0
TIME (S)
0.45
MASS 32 FROM MgO
c)
MASS 32 SIGNAL (ARB. UNITS)
0
TIME (S)
0.45
MASS 44 FROM MgO
d)
MASS 44 SIGNAL (ARB. UNITS)
0
TIME (S)
0.45

Fig. VI-3

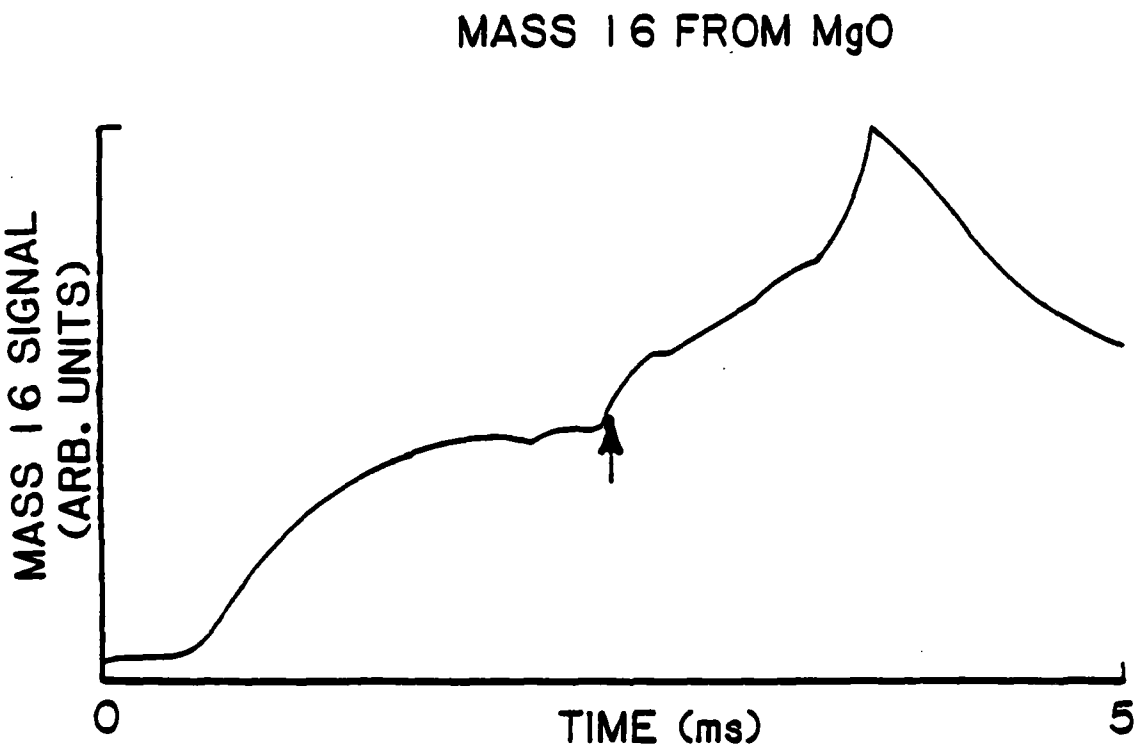

Fig. VI-4

VII. ELECTRON BEAM INDUCED FRACTURE OF KEVLAR* SINGLE FIBERS

(submitted to J. Vacuum Science and Technology)

J. Thomas Dickinson, L. C. Jensen, and M. L. Klakken
Department of Physics
Washington State University
Pullman, WA 99164-2814

ABSTRACT

We examine the unique situation involving the exposure of polymers to both electron bombardment and mechanical stress. Under certain conditions, fracture and crack growth occur due to this combination of stimuli. These studies relate to the performance of a number of materials under hostile environments such as space, plasmas, and propulsion systems. In this paper we present our initial measurements on the response of single Kevlar-49 fibers loaded in tension to bombardment by 3 keV electrons. We present evidence that the resulting electron beam induced fracture is due to bond breaking.

*Kevlar-49 is a trade name of E.I. Dupont de Nemours and Co.

INTRODUCTION

When an energetic electron strikes the surface of a material, inelastic collisions occur leading to energy loss of the primary electron and production of secondary electrons with energies of 1-15 eV. The range of the primary electron is on the order of 0.1 - 10 μm so that the inelastic events can occur quite deep into the material. The processes that can occur include ionization, molecular dissociation, electron stimulated desorption, electron induced diffusion, and various chemical reactions. In addition, an increase in temperature due to the conversion of electronic excitations into thermal vibrations of the material can also occur. This in turn can cause

decomposition, a change in the material physical properties, and additional chemical reactions.

An interesting situation arises when a material is exposed to both electron bombardment and mechanical stress. Under certain conditions, crack growth and fracture can occur due to this combination of stimuli. In certain hostile environments such as space, plasmas, and propulsion systems there are often conditions where materials under stress are exposed to particles and radiation and the consequences can be critical. In this research our initial goals are:

1) To characterize the range of the phenomena (i.e. radiation-induced fracture) in terms of materials and type of incident particle, as well as determine the dependencies of important parameters such as: stress, particle energy, and particle flux.

2) To eventually determine the mechanisms involved and to relate the results to current theories of fracture.

To date, we have concentrated mainly upon determining the mechanical response of a material exposed to stress and energetic electrons[1] in a vacuum of 10^{-5} Pa. When a stressed polymer is bombarded by electrons in the highly concentrated stress region of a notch, crack propagation may occur if the "weakening" factors of the material override the "strengthening" factors. In a polymer, examples of the "weakening" factors are bond scissions, molecular dissociation, thermal degradation, and gas evolution. Additional polymerization, crosslinking, and branching of the material all would tend to "strengthen" the polymer. We have recently measured[1] the propagation of an introduced crack as related to the time of application of the electron beam. Of the materials tested, all have shown a response (i.e. a drop in the total applied load) upon application of the electron beam. The materials tested include: polyisoprene, BAMO/THF (a 50-50 co-polymer of 3,3,bis(azidomethyl)

oxetane and tetrahydroturan), butyl rubber, polybutadiene, and high density polyethylene. Careful calculations of the energy deposition due to the electron beam and subsequent heating of the material showed that the temperature does not increase by more than 10 C within the time observed for a mechanical response. We estimate that given the experimental values of the electron beam's energy and flux and a duration of bombardment of 1 ms, all of the main chain bonds would be broken approximately once. Normally, most of these bonds would reform if the material was not under stress. We hypothesize that when a radiation sensitive material is under stress, fewer of these bonds can reform, which encourages crack propagation.

In this paper, we present our initial results on exposure of single fibers of Kevlar-49 to electron bombardment and stress. Kevlar-49, produced by Dupont, is an important reinforcing fiber for epoxy composites. It has an extremely high strength to weight ratio, and produces a composite with very high fracture toughness (i.e., the material is resistive to growth of an existing crack). Kevlar-49[2-6] achieves its high tensile strength by being a closely packed structure of macromolecular chains that are highly aligned and oriented along the longitudinal axis of the fiber. There are essentially zero crosslinks or chain folds which would tend to reduce the tensile strength of the structure. The angle between the monomer units is parallel (para-type orientation) which allows the stress to be transferred directly down the chain without stretching the bond angle. The macromolecules tend to form crystalline regions of about 200 nm length by 60 nm width. This highly crystalline structure form 200 nm layers that are linked by chain ends. These zones between crystalline regions are defect-like and form the easiest crack propagation path in the transverse direction.

In terms of standard radiation sensitivity tests, where a material is exposed, then mechanically tested, Kevlar-49 is known to be very sensitive to ultraviolet light. Harper and McAlister[7] have reported the strength of bare Kevlar-49 yarn can decrease by more than 25% after one week exposure to ultraviolet radiation. Here, our main interest is to determine if applying both stress and electron bombardment together can cause fracture of Kevlar fibers at stresses below the critical stress (i.e., the tensile strength) on much faster time scales. We are interested in dynamic processes which involve electronic excitations and therefore desire to determine if the mechanism leading to fracture is due to electron collision bond scissions rather than thermal degradation of the material. The latter takes place at temperatures around 500 C on unstressed material.[8]

EXPERIMENTAL

The experimental arrangement shown in Fig. 1 consisted of a small stress/strain device mounted inside a standard vacuum system. Single 12 μm diameter Kevlar-49 fibers (from DuPont) were strained in tension at 0.06%/s. A 0.2 mm diameter copper wire was positioned behind and as close as possible to the fiber and served as a collector for the electron beam which was swept across the fiber. A larger collector was positioned 2 cm from the fiber for measuring the total current in the electron beam.

The electron beam was produced by a Varian Glancing Incidence Auger Electron Gun. The fiber was located at the focus of the electron gun which had a 2 mm spot size. The electron energy used in these studies was 3 keV. Using the deflection plates in the electron gun and a ramp generator, the beam could be swept back and forth across the fiber near its center, typically at a speed of 2.8 to 4.7 mm/s. (We referred to this experiment as our "Pit And The

Pendulum" experiment.) The electron beam profile was measured and determined to be Gaussian in shape. Thus, we can model carefully the spatial and temporal distributions of the electrons hitting the fiber. Because of the small fiber diameter, when the beam is centered on the fiber, only 0.7 % of the total electron current strikes the fiber.

The current to the wire behind the sample and the mechanical load on the fiber were digitized simultaneously, at a sampling rate of 2 ms/channel. Thus, correlations could be made between the electron dose to the fiber and the mechanical response with reasonably high time resolution. These experiments were carried out at pressures of 10^{-5} Pa.

RESULTS

Figure 2a shows the load (force) vs time curve for a typical Kevlar-49 fiber, where the solid line corresponds to an unbombarded fiber. Failure of the fiber occurs at the sudden drop in load. The dotted curve represents the load curve for a fiber where at the arrow we applied a 3000 eV, 120 μA electron beam to the fiber near its maximum stress. The dotted line shows the force dropping immediately, again due to failure. Visual observation of the fiber showed that it had fractured. Similar runs on numerous fibers showed this "coincidence" between application of the beam and fracture. We thus conclude that at high stress, and relatively high current densities, electrons can cause fracture of the fiber.

To gain further insight into this effect, we examined on a faster time scale the response of the load applied to the fiber as the electron beam comes onto the fiber. Fig. 2b shows results for a highly stressed fiber and a beam current of 120 μA. On a ms time scale, the load is seen to drop slightly before failure occurs (the rapid drop in load).

If we keep the electron beam fixed at 100 μA, we can measure the time from the beginning of electron exposure until fracture occurs (time-to-fracture) as a function of the load when the exposure begins. Fig. 3 shows these results. There is initially a substantial drop in the time-to-fracture, then a slow decrease, indicating that the response to the beam is indeed dependent on the stress state of the fiber. At lower loads, the time to failure is essentially infinite. A simple interpretation of this data is that at higher stresses one needs to do less "damage" to the fiber (where by damage we mean the severing of bonds in the region of the fiber being bombarded) before fracture is initiated. It is possible that the efficiency of the electrons in producing irreversible bond breaking is higher when the bonds are more highly stretched.

Similarly, there is a strong dependence of the time-to-fracture on the electron beam current, as seen in Fig. 4, taken at constant beam energy of 3 keV and constant load of 0.75 N. Here we see a dramatic initial decrease in time-to-fracture, followed by a slow decrease at higher currents. In the latter part of the curve, the doses (total number of electrons striking the fiber before fracture) for the points shown are approximately the same. Since the number of broken bonds would be proportional to the dose, this suggests that at constant load the number of bond scissions induced by electron collisions required to cause fracture is a constant.

SEM photographs of the fracture surface show that the fiber ends look quite different in the electron bombarded fibers vs fibers broken without the beam. The unbombarded samples split into many fibrals, as shown in Fig. 5a, often for 700 μm down the fiber, with many very small "hairs" protruding from these fibrals. This is a well known tendency of Kevlar[2-5]. Morgan[6] et al have described the same type of fibral formation, observing that the outer

skin of the fiber tears in the longitudinal fiber direction to form a continuous ribbon for hundreds of μm along the fiber surface.

The fibers that were exposed to the electron beam, shown in Fig. 5b, tend to break in the transverse direction. The small "hair" like fibrals along the larger fibrals are totally absent. With some samples broken with the electron beam there is some fibral formation but it tends to be more transverse than the unbombarded samples and completely without the smaller side fibrals.

In order to examine the role of heating of the fiber by the electron beam, we modeled the energy deposition, conduction, and temperature rise in the fiber, using known thermal properties of Kevlar-49. The typical calculated temperatures at the first sign of a drop in load was less than 100 C. The typical calculated temperature at fracture is less than 150 C. In Table I we show the results of these calculations for various samples. The calculated temperature at failure is always much less than the 500 C needed for thermal decomposition of the unstressed fiber.

CONCLUSIONS

We have presented initial results of the mechanical response of single fibers of Kevlar-49 under tension to exposure to energetic electrons. We have shown that there is an initial drop in load followed by failure of the fiber. The sensitivity of the failure process increases with applied load and with the rate of electron impingement, with threshold-like behaviors in each of these dependences. Temperature calculations indicate that the effect is not dominated by thermal processes but is clearly assisted greatly by electron collision bond breaking of stressed polymer chains. Our results indicate that the damage to these chains is more likely to lead to failure at higher strains

Table 1. Sample Description and Composition as Formulated by NWC. Taken from Reference 7.

NWC TP 6619

TABLE 1. Sample Status.

Mix No.	Binder system	Specimens shipped					
		RDX wt, %	NWC various tests	WSU fracto-emission	PSU burn rates	Lockheed SAX[a]	Lockheed acoustic studies
BLX-1	R45M/IPDI	75.5[b]	+[c]	+	+	+	+
BLX-2	R45M/IPDI	80.0	+	+	+	+	+
BLX-3	R45M/IPDI	75.0	+	+	+	+	+
BLX-4	GAP/TMETN[d] (1:3)	74.8	+	+	+	+	+
BLX-5[e]	Acrylic polymer	72.5	-	-	-	-	-
BLX-6[f]	Acrylic polymer	72.5	+	+	+	+	+
BLX-7	GAP	68.6	-	-	-	-	-
BLX-8	GAP	68.6	+	+	+	+	+
BLX-9	GAP/BTTN[g] (1:2)	65.9	+	+	+	+	+
BLX-10[h]	BAMO/THF (1:2)	66.3	-	-	-	-	-
BLX-11[i]	R45M/IPDI	75.0	-	-	-	-	+

[a] Small angle X-ray.

[b] Large particles.

[c] + Sent for testing; - not sent for testing.

[d] Metriol trinitrate.

[e] Small hand mix.

[f] System gelled before it could be cast.

[g] Butanetriol trinitrate.

[h] Plasticizer exuded from cured formulation.

[i] Special mix for acoustic studies.

the materials sent to us for testing are given in the tables (NWC Tables 1-5) copied from reference 7, designated here collectively as Table 1.

EXPERIMENTAL

The measurements described here were performed on materials fractured in a vacuum of 1×10^{-5} Pa. Tensile specimens were of dimensions 2 mm x 6 mm x 15 mm, notched with a sharp blade in the center (1 mm deep) with a sharp blade so that fracture would occur in front of the detectors. Tensile tests were carried out at three strain rates (referred to as slow, medium and fast): 0.2 /s, 10/s, and 100/s. The latter was achieved by attaching a massive aluminum frame to the pull rod that entered the vacuum chamber via a bellows separating vacuum from the atmosphere. A sharp rap with a heavy hammer rapidly elongated the sample with subsequent faster crack growth.

Compressional impact was achieved by attaching the above impact device to a stainless steel fixture with parallel steel faces which rapidly closed when the aluminum frame was impacted. Compared to drop-hammer test devices, our system was rather "soft" and would not lead to as high a compressional load as these devices. We will soon have ready a much more rigid compressional impact device mounted in our vacuum system.

An electron detector was placed on one side of the sample and a photomultiplier placed on the other side. For electrons, we used a channeltron electron multiplier (CEM) which produces fast pulses (10 ns in duration with 90% absolute detection efficiency. For photons, a Thorn 9924Q photomultiplier was used without cooling. The photocathode was of type S20 with sensitivity in the visible and soft uv region. The photomultiplier background count rate was typically 1000-1500 counts/s. Standard nuclear

AD-A160 510 FRACTO-EMISSION FROM POLYMERS(U) WASHINGTON STATE UNIV 2/2
PULLMAN DEPT OF PHYSICS J T DICKINSON 15 OCT 85
N00014-80-C-0213

UNCLASSIFIED F/G 7/4 NL

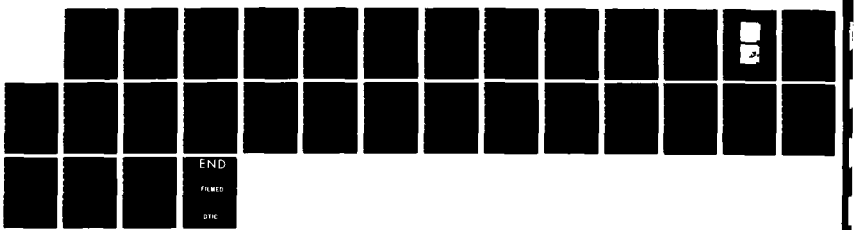

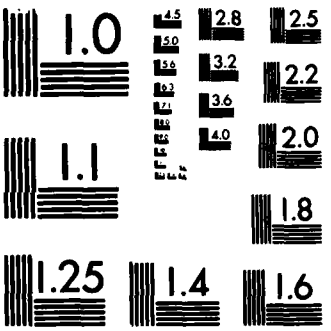

MICROCOPY RESOLUTION TEST CHART
NATIONAL BUREAU OF STANDARDS-1963-A

materials were part of a Navy Weapons Center program to investigate the effects of surface interactions and mechanical properties of plastic bonded explosives on explosive sensitivity.

In section IV we examine the electron, photon, and long wavelength electromagnetic emission accompanying the failure of interfaces between aluminum and a polymer (epoxy). The effect of applying an external electric field across the interface is examined and shown to greatly enhance the resulting emissions. This enhancement provides further evidence that the surface charge on the fracture surfaces can strongly influence the resulting fracto-emission.

In Section V, we present a study on the time and size correlations of photon and radiowave bursts from the peeling of pressure sensitive adhesives in air. The interfaces consisted of tackified natural rubber separating from various polymers, thus serving as a model of any adhesive failure system involving two polymers. Considerable detail on the nature of these emissions was gained by examining their correlations and time and acquiring time distributions of the photon emission.

In Section VI, we present our first results on the emission of atoms and molecules accompanying the fracture of single crystal inorganic materials. In this case, high purity MgO. MgO serves as a model material for semi-brittle crystals. We report evidence for fracture induced decomposition as well as recombination reactions involving impurities.

In Section VII, we show recent results on inducing crack growth in polymers with the combination of stress and electron bombardment. These studies, in addition to being of a fundamental nature in terms of the physics of fracture, address in a new way the response of materials under stress in a hostile environment. In this study, we show that at stresses below critical

II. INTRODUCTION

Crack propagation through an insulating material or at an interface produces regions of high electronic and chemical activity on the freshly-created surfaces. This activity causes the emission of particles, i.e. electrons, ions, and neutral species, as well as photons, from the surfaces both during and after crack propagation. This emission is called fracto-emission. Our primary goals have been to a) further characterize fracto-emission from filled and unfilled polymers, as well as from crystalline materials which model energetic molecular crystals, b) to further our understanding of the fracto-emission mechanisms, and c) to examine the dependence of fracto-emission on the nature of the fracture event and material properties. These effects are very sensitive to locus of fracture, crack velocity, crack tip temperature, and materials properties. As we learn more about the mechanisms of fracto-emission, we are able to provide detailed information about crack propagation and failure mechanisms. Our ultimate goal is to use fracto-emission to probe fracture on an atomic and molecular level. Furthermore, the physical effects involving charge separation, electrostatic effects, and the consequences of fracture in energetic materials is of considerable interest because of possible ties to rapid energy release mechanisms.

In addition, we have undertaken the study of radiation-induced crack propagation in polymers and molecular crystals. We wish to determine the sensitivity of materials under stress to bombardment by electrons, ions, and energetic photon and investigate the mechanisms for inducing crack propagation with such radiation.

In this report we include our recent work on measuring the electron and photon emission from RDX-filled polymeric binders (Section III). These

due to a lower probability of reforming the broken bonds. The most susceptible structures in the fiber are the tie molecules between the crystalline regions, and we therefore suspect that the electron damage leading to failure is concentrated in these regions. In the crystalline portions of the fiber, the polymer chains are not under as large a strain and therefore may be less likely to be permanently broken. Additional work is continuing on improving these measurements, applying them to other materials, and developing computer models of the electron beam induced fracture process.

ACKNOWLEDGMENTS

This work was supported by the Office of Naval Research, Contract (N00014-80-C-0213, NR 659-803) and the McDonnell Douglas Independent Research and Development Program. One of us (MLK) wishes to thank the NASA-Johnson Space Center for Graduate Student Fellowship support.

REFERENCES

1. J. T. Dickinson, M. L. Klakken, M. H. Miles, and L. C. Jensen, to appear in J. Poly. Sci.: Poly. Phys. Ed.

2. A. R. Bunsell, J. Mater. Sci. 10, 1300 (1975).

3. J. W. S. Hearle and B. S. Wong, J. Mater. Sci. 12, 2447 (1977).

4. L. Konopasek and J. W. S. Hearle, J. Appl. Poly. Sci. 21, 2791 (1977).

5. L. Penn and F. Larson, J. Appl. Poly. Sci. 23, 59 (1979).

6. R. J. Morgan, C. O. Pruneda, and W. J. Steele, J. Poly. Sci.: Poly. Phys. Ed. 21, 1757 (1983).

7. W. L. Harper and C.E. McAlister, "The Effect of Radiation on Kevlar-49," DOE report, Oak Ridge, TN, Y-DA-6527 (1975).

8. J. Preston, in Encyclopedia of Chemical Technology, Volume 3, pp. 213-216, John Wiley & Sons, New York, 1978.

FIGURE CAPTIONS

Fig. 1. Experimental setup for electron bombardment of a single Kevlar-49 fiber under stress.

Fig. 2. a) Load vs time curve for a single Kevlar-49 fiber under stress. The dashed line indicates the fracture of the fiber upon application of the electron beam (vertical arrow). The solid line represents the drop in load occurring during fracture of the fiber with no electron bombardment.
b) Load vs time curve on a faster time scale. The vertical arrow indicates the time when the electron beam was applied. Note that the load prior to complete failure drops slightly, indicating that damage is occurring.

Fig. 3. A plot of the time-to-fracture vs applied load for single Kevlar-49 fibers all bombarded by a 3000 eV, 100 μA electron beam.

Fig. 4. A plot of the time-to-fracture vs electron beam current (at 3 keV) for a single Kevlar-49 fiber under an applied load of 0.75 N.

Fig. 5. SEM photographs of a single fiber of Kevlar-49 a) fractured without the application of an electron beam, and b) fractured during the application of a 120 μA, 3000 eV electron beam.

TABLE I.

ELECTRON BEAM CURRENT uA	TEMP AT ONSET OF YIELDING C	TEMP AT FAILURE C
75	60	90
100	90	130
100	120	160
200	100	150
200	55	170

Table I. Calculated temperatures at the onset of yielding and at failure of single Kevlar fibers for various electron beam currents. Electron energy is 3 keV. The applied force is 0.75 N.

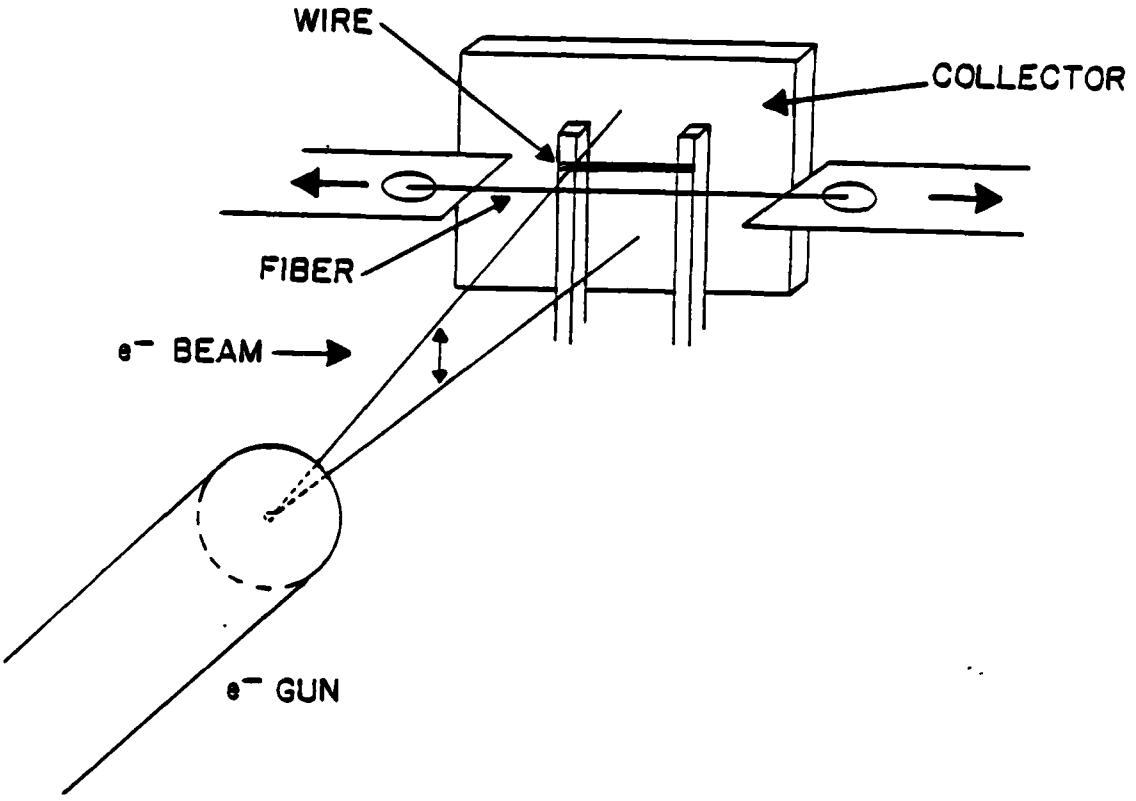

Fig. VII-1

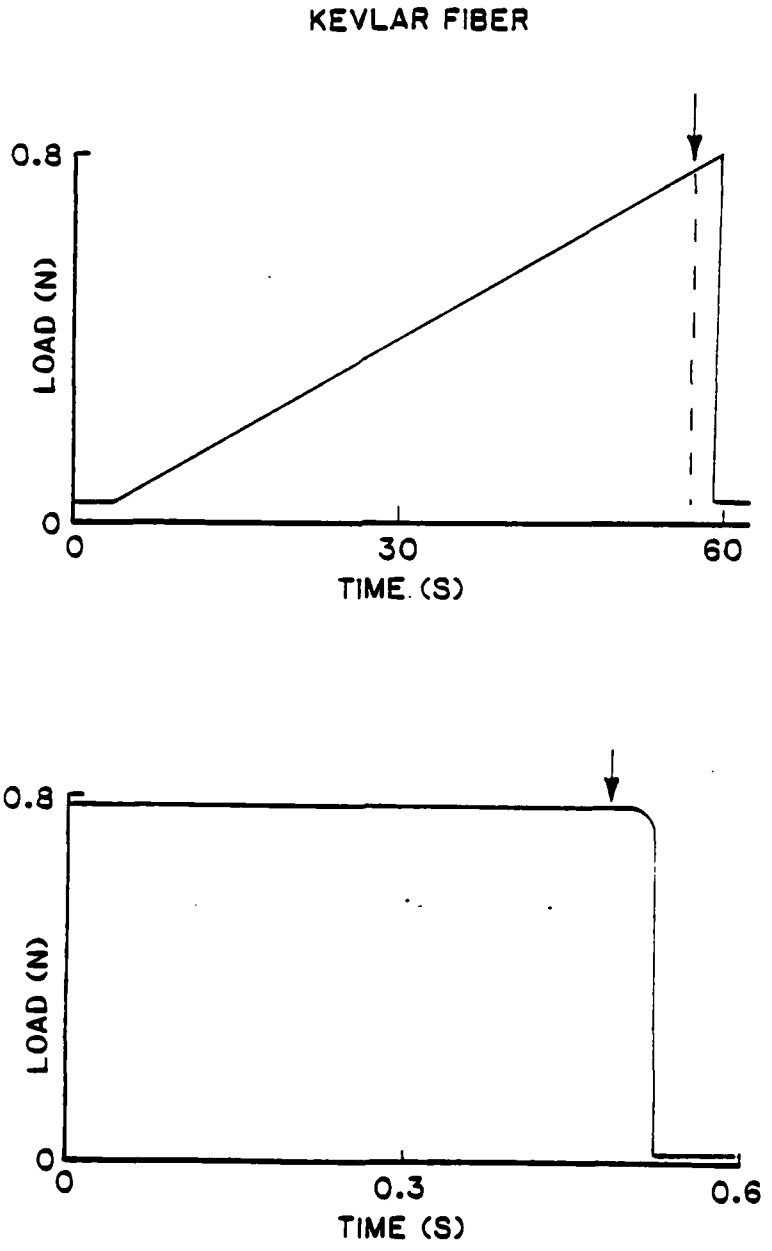

Fig. VII-2

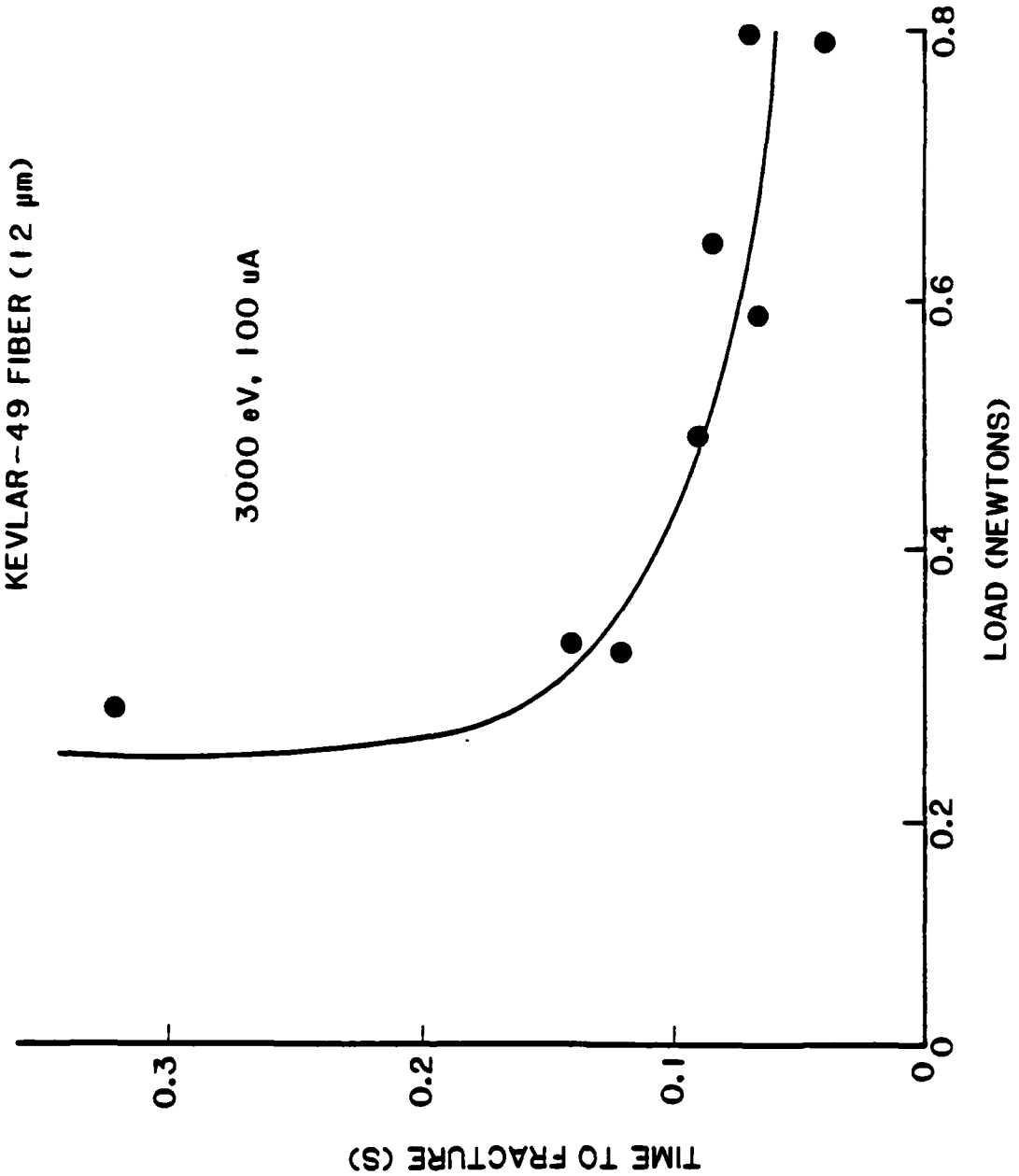
KEVLAR-49 FIBER (12 μm)
3000 eV, 100 uA
TIME TO FRACTURE (S)
LOAD (NEWTONS)
0
0.1
0.2
0.3
0.2
0.4
0.6
0.8

Fig. VII-3

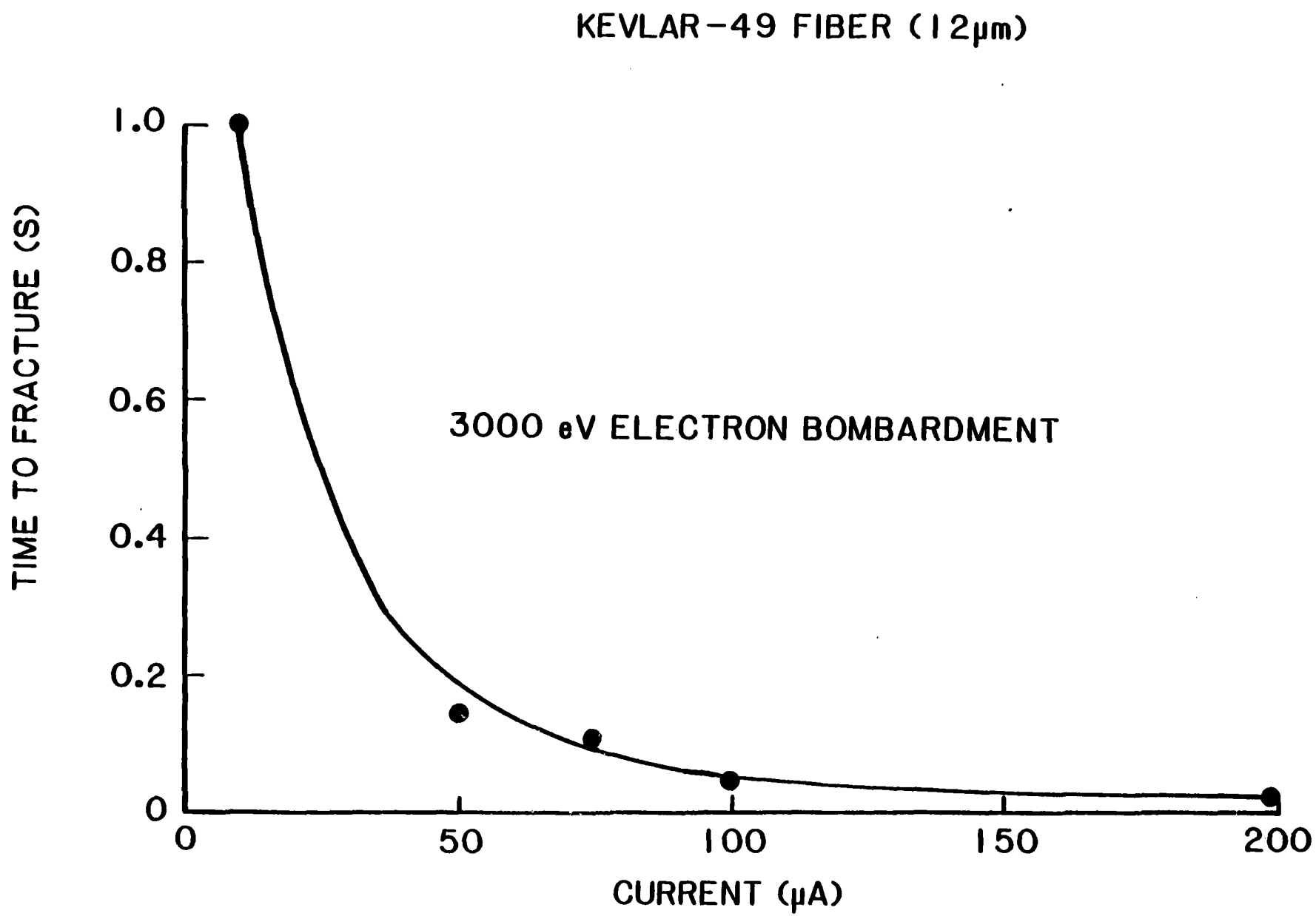
KEVLAR-49 FIBER (12μm)
3000 eV ELECTRON BOMBARDMENT
TIME TO FRACTURE (S)
1.0
0.8
0.6
0.4
0.2
0
0
50
100
150
200
CURRENT (μA)

Fig. VII-4

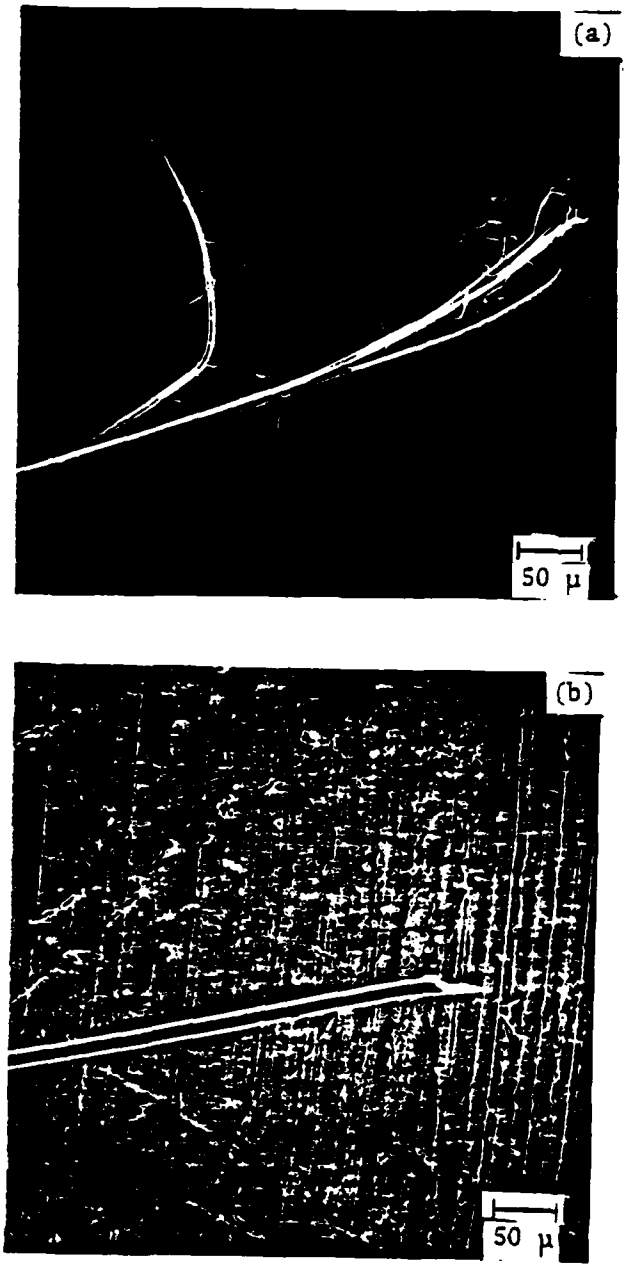

Fig. VII-5

VIII. WORK IN PROGRESS

Mechanism Studies. We have continued our studies of electron and positive ion emission mechanisms, extending our studies to single crystal substances that serve as model materials for energetic molecular crystals. We have found that a number of inorganic single crystal substances have emission characteristics similar to polymers. For intense emitters of charged particles we find accompanying intense photon emission. We have measured simultaneously electron radiowave and photon versus time for the fracture in vacuum of materials such as alkali halides, MgO, MgF_2, and SiO_2. These results show that during fracture there are radio waves and accompanying visible photons due to a weak electrical discharge caused by charge separation and the desorption of gaseous species into the crack tip.

The electron emission rises with the photon emission and radiowave emission but then decays with a long tail. Recent measurements with larger photocathode photomultipliers show that the photon emission from MgO and SiO_2 have identical decay kinetics to the electron decay. Such emission is most evident in crystals where charge separation on the fracture surfaces is strong and a discharge is more likely to occur, we hypothesized that during the discharge the fracture surfaces are bombarded by electrons and ions with relatively high energies. It is this bombardment which is the key stimulus for the electron emission, positive ion emission and photon emission which follows fracture. Calculations of emission kinetics for these inorganic crystals are ongoing using iterative curve fitting techniques to models involving three to four coupled rate equations. We are utilizing known defect structures and energy transfer mechanisms for these materials, assuming that the electron/photon emission event accompanies a recombination process (e.g., electron hole pairs, complementary defect annihilation). These models predict

the effect of increasing the sample temperature after fracture for comparison with ongoing measurements.

Neutral Emission from Polymers and from Inorganic Single Crystals. Using new techniques that we have developed, we have measured the gases released from deformation and fracture of two types of materials: a) Elastomers modeling binder material, and b) Inorganic single crystals of alkali halides and various oxides. In the case of elastomers, we have examined BAMO/THF and polybutadiene. We observe a wide range of product peaks in the mass spectrum. We are sorting out two sources for these species: 1. residual content of volatile compounds, and 2. mechanically produced products due to bond scissions. The evolved products produced by mild thermal stimulation are used to identify 1. Also, purification techniques are being explored to reduce 1 to a minimum. The experiments on inorganic single crystals are showing impurity products, also, but they are not in the crystals as assembled molecules. There is fracture induced chemistry occurring, producing a wealth of species. For example, O_2, H_2, CO_2 from single crystal MgO. In addition, we are seeing atomic species emitted from the crystals, e.g., Mg from MgO, Na and Cl from NaCl, and Li and F from LiF. These products are certainly due to bond breaking of the ionic lattices.

Impact Studies on PETN. In work recently published (J. Appl. Phys. 57, 5048 (1985), we showed a strong dependence of the fracto-emission intensities from single crystal PETN on the mode of fracture, where fast compression (impact) yielded the strongest response. This mode of loading led to considerable pulverization, accompanied by shear and frictional grinding of the crystal fragments. We have instrumented an impact device for our vacuum system and have started correlations of the emission with intensity of the

impact. One unexpected result was the properties of the ejecta (small microscopic fragments thrown out of the vice by the impact) was found to be highly charged and we have evidence that the fragments are emitting charge and photons with high intensities. As part of this study, we are attempting to collect such ejecta for both energetic materials and model crystalline substances and measure the total residual charge on the ejecta as well as the emission from these particulates.

Photon and Radiowave Emission During Peeling of Pressure Sensitive Adhesives in Vacuum. As a further test of some of the features of our models involving systems that yield a high degree of charge separation, we are examining several details of the photons, electrons, and radiowave signals emitted from a commercial pressure sensitive adhesive peeled from a polyester surface IN VACUUM, similar to the study described in Section V, which was performed in air. We are seeing many of the same effects, with the added feature that we can now measure the correlations of the electron emission with either the photons or radiowaves. The signals are quite strong, and we hope to find relations between the occurrence, intensities, and decays of the electron bursts with those of the other fracto-emission components. Furthermore, the kinetic energy of the charged particle emission (including the positive ion emission) and identification of the masses of the positive ions are also being measured. We are also imaging some of these emissions and find that they are often highly localized.

Fracto-Emission from Propellents. In collaboration with the Navy Weapons Center, we are continuing to measure fracto-emission from a few more formulations of the RDX filled polymeric binders which are being sent to us by R. Y. Yee, NWC. Also, Dr. Yee has produced for us macroscopic binder/single

crystal RDX specimens with a surface area at the interface of about 1 cm^2, which will be sent soon. We will perform peel tests on these samples, pulling the binder off of the crystal, searching for emission similar to what we observed in polybutadiene from macroscopic metal and glass surfaces and in peeling pressure sensitive adhesives. Such experiments will prove that such failure can produce intense, long lasting emission. If these experiments confirm our predictions, we would like to determine from which surface, if any, dominates in the emission process. More fundamental measurements on the origin of various fracto-emission components from this particular system will be pursued.

Fracto-Emission from Metal Filled Binder. In collaboration with H. Stacer, Air Force Rocket Propulsion Labs, we are studying the fracto-emission from binders filled with small aluminum particles. The purpose of these studies is to study the fracto-emission and related effects due to adhesive failure at the interface between the matrix and particle. To date, we have studied the electron, photon, and radiowave emission from urethane cross-linked polybutadiene, both filled and unfilled. The emissions differ by several orders of magnitude and the duration of the decay after fracture change from ms (unfilled) to several hundred seconds (filled). Microscopy of the fracture surfaces show that considerable interfacial failure occurs during fracture. The systematic study of this system will be continued with variations in filler concentration and binder cross-linking.

In addition, related to the metal filled elastomer studies, macroscopic specimens of metal surfaces and common binders (e.g., urethane cross-linked polybutadiene) are being studied as a function of metal particle surface condition (with/without oxide coating), crack velocity, and presence of an external electric field. These studies relate to both metal filled

propellents and the interaction of propellents with metal walled casings. Similar studies could be made on other rocket motor casing materials as substrates (e.g., filled epoxies), if there is interest.

Radiation Induced Fracture. We have further explored the consequences of combining the application of stress and electron bombardment to a polymer. Alan Gent, University of Akron, is collaborating with us on the next phase of the work. We have been measuring tear energies of rubbers with and without electron bombardment in such a way that we can quantify the bond breaking effect of the electron beam. We have examined additional materials to sort out the mechanisms. These materials include polybutadiene, polyisobutyl rubber, a ethylene-propylene co-polymer, and a number of fibers other than Kevlar: Nylon 66, Graphite, E-glass, quartz, and soda-lime glass. Each of these materials can be broken with the electron beam. However, there is evidence that in the case of non-polymeric fibers, rapid heating is taking place which may be causing failure. In the case of E-glass, the calculated temperatures at failure are below the temperatures required to cause the fiber to flow, yet yielding is observed. We have hypothesized the presence of a "hot spot", presumably a flaw in the fiber in the region being bombarded, that leads to an instability (local yielding). In the case of the polymers, we have modeled the energy deposition and thermal conduction occurring during bombardment and concluded that the effects we are observing are not thermal. We believe that bond scissions due to electronic interactions are the dominant effect leading to crack growth. The critical requirement is that the electronic processes occur at vulnerable bonds, i.e., those under stress. To answer questions concerning the stress dependence, radiation induced cross-linking and other chemistry, we are modeling the phenomenon using a molecular

dynamics code in collaboration with Timur Halicioglu, NASA-Ames Research Center.

We will soon be using an additional source of radiation for these experiments, namely a high powered excimer laser as a driver. We now have our excimer laser working with KrF as the active gas. We will explore the effects of such uv radiation focused into cracks in elastomers. We predict that under proper loading conditions, we can cause crack propagation. Examination of the relevant parameters and mechanisms will be made.

IX. CONCLUSIONS

We continue to make progress in our understanding of the emission of electrons, positive ions, and photons during and following fracture of polymers, inorganic crystals, and organic crystals. The concepts fracture induced excitations due to bond breaking, the occurrence of charge separation, gas desorption, gaseous discharges yielding additional excitations of the fracture surfaces, followed by subsequent relaxation processes have allowed us to make predictions which have proven to bear out experimentally. Additional quantitative models and numerous additional experiments are also suggested. In addition we have shown that material properties, e.g. adhesion strength between binder and filler particles can influence FE greatly. Also, the detection of atomic and molecular species from single crystals of MgO and other inorganics indicate considerable bond-scission induced chemistry occurring on fracture surfaces. As further understanding develops on the mechanisms of fracto-emission and the factors influencing the emission characteristics, a growing interest in applications of our techniques is developing. Finally, the studies of radiation-induced fracture are progressing towards contributing to the physics of fracture as well as to providing new insights of materials under stress in hostile environments.

X. RECENT PRESENTATIONS AND PUBLICATIONS, PARTICIPANTS

Invited Presentations

"Fracto-Emission," IBM Research Laboratories, San Jose, CA, April 1984.

"Fracto-Emission from Adhesive Failure," Gordon Conference on the Science of Adhesion, New Hampshire, August, 1984.

"The Emission of Particles Due to Fracture," 3M Corp., St. Paul, MN, October 1984.

"Particle Induced Chemistry at Dielectric Surfaces", NWC, China Lake, CA, November, 1984.

"Particle Emission from Fracture", SAMPE-Seattle Section, November, 1984.

"Fracto-Emission Accompanying Adhesive Failure", SAMPE Symposium, Anaheim, CA, March, 1985.

"Photon and Radio-wave Emission Accompanying Peeling of Pressure Sensitive Adhesives", National SAMPE Symposium, Anaheim, CA, March, 1985.

"Fracto-Emission from Inorganic Solids", Department of Materials Science, Penn State, April, 1985.

"Atomistics of Fracture", Johnson Space Center, Houston, TX, June, 1985.

Atomistics of Fracture", ONR Workshop on Fracture and Deformation of Energetic Materials, Great Oak Harbor, MD, June, 1985.

"Fracture of Fibers and Composites," Owens/Corning Technical Center, Gainsville, OH, August, 1985.

"Fracto-Emission Accompanying Adhesive Failure," National AIChE Meeting, Seattle, WA, August, 1985.

"Fracto-Emission From Composites," McDonnell Douglas Research Center, St. Louis, MO, September, 1985.

"Fracto-Emission from Energetic Systems", Army Munitions Research & Development Center, Dover New Jersey, September, 1985.

"Fracto-Emission and Fracture Surfaces", AT&T Bell Labs, Murray Hill, NJ, Sept. 1985.

"Fracto Emission from Polymers and Interfaces", Goodyear Tire Co., Akron, OH Sept. 1985.

Contributed Papers

"Electron Beam Induced Fracture of Polymers," American Physical Society, Detroit, MI, March 1984.

"Charge Separation and Fracto-Emission from Polybutadiene," American Physical Society, Detroit, MI, March 1984.

"Fracto-Emission from Ferro-electric Ceramics," American Physical Society, Detroit, MI, March 1984.

"Mechanisms for the Emission of Electrons and Positive Ions During the Fracture of Brittle Materials," American Ceramics Society, Pittsburgh, PA, May 1984.

"Electromagnetic Radiation and Induced Electrical Breakdown from the Fracture of Ceramics," American Ceramics Society, Pittsburgh, PA, May 1984.

"Measurements of the Mass-to-Charge Ratio of Positive Ions from the Fracture of Glass," American Ceramics Society, Pittsburgh, PA, May 1984.

"Electron Induced Damage of ThF_4 Thin Films in Presence of XeF_2", (with Mike Loudiana), American Vacuum Society, Reno, Nov. 1984.

"Fracto-Emission From Failure of Metal/Epoxy Interfaces", American Vacuum Society, Reno, Nov. 1984.

"Electron Beam Induced Fracture of Glass Fibers", American Ceramics Society, Cincinnati, OH, May, 1985.

"Atom and Molecular Emission Accompanying Fracture of Crystalline Inorganic Solids", American Ceramics Society, Cincinnati, OH, May 1985.

"Fracto-Emission Accompanying Failure of Metal/Glass Interfaces", American Ceramics Society, Cincinnati, OH, May, 1985.

Recent Emission and Fracture Related Publications

J. T. Dickinson, L. C. Jensen, and A. Jahan-Latibari, "Fracto-Emission from Filled and Unfilled Elastomers," Rubber Chem. and Tech. 56, 927 (1984), Review Article.

J. T. Dickinson, L. C. Jensen, and A. Jahan-Latibari, "Fracto-Emission: The Role of Charge Separation," J. Vac. Sci. Technol. A 2, 1112 (1984).

J. T. Dickinson, L. B. Brix, and L. C. Jensen, "Electron and Positive Ion Emission Accompanying Fracture of Wint-O-Green Lifesavers and Single Crystal Sucrose," J. Phys. Chem. 88, 1698 (1984).

J. T. Dickinson, L. C. Jensen, and A. Jahan-Latibari, "The Effect of Cross-Linking on Fracto-Emission from Elastomers," J. Mat Sci. 19, 1510 (1984).

J. T. Dickinson, Response to: "On the Question of Emission of Charged Particles in the Case of Failure of Solids," Mat. Sci. Lett. 19, 2426 (1984).

J. T. Dickinson, M. H. Miles, W. L. Elban, and R. G. Rosemeier, "Fracto-Emission from RDX Single Crystals", J. Appl. Phys. 55, 3994 (1984).

J. T. Dickinson, "Fracto-Emission Accompanying Adhesive Failure," in Adhesive Chemistry--Developments and Trends, ed. by L. H. Lee (Plenum Publishers, New York), 1984, Review Article.

J. T. Dickinson, A. Jahan-Latibari, and L. C. Jensen, "Fracto-Emission from Single Fibers of Kevlar-49", J. Mat. Sci. 20, 1835 (1985).

M. L. Klakken, J. T. Dickinson, and L. C. Jensen, "Electrical Breakdown Induced by Fracture", IEEE Transactions on Electrical Insulation, EI-19, 578 (1984).

J. T. Dickinson, A. Jahan-Latibari, and L. C. Jensen, "Electron Emission and Acoustic Emission from the Fracture of Graphite/Epoxy Composites," J. Mat. Sci. 20, 229 (1985).

J. T. Dickinson, L. C. Jensen, and S. Bhattacharya "Fracto-Emission from the Failure of Metal/Epoxy Interfaces", J. Vac. Sci. Technol. A3, 1398 (1985).

J. T. Dickinson, W. D. Williams, and L. C. Jensen, "Fracto-Emission from Lead Zirconate-Titanate", J. Am. Cer. Soc., 68 235 (1985).

J. T. Dickinson, X. A. Shen, and L. C. Jensen, "Peeling of Pressure Sensitive Adhesives," Proceedings of the 30th National SAMPE Symposium, 1985.

E. E. Donaldson, X. A. Shen, and J. T. Dickinson, "Photon and Radiowave Emission from Peeling Pressure Sensitive Adhesives in Air", Proceedings of the 30th National SAMPE Symposium, 1985.

M. H. Miles, J. T. Dickinson, and L. C. Jensen, "Fracto-Emission from Single Crystals of PETN", J. Appl. Phys. 57, 5048 (1985).

J. T. Dickinson, A. Jahan-Latibari, and L. C. Jensen, "Fracto-Emission from Fiber-Reinforced and Particulate Filled Composites," in Polymer Composites and Interfaces, ed. by N. G. Kumar and H. Ishida (Plenum Publishers, New York), 1985, Review Article.

J. T. Dickinson and L. C. Jensen, "Fracto-Emission from Filled and Unfilled Polybutadiene", J. Poly. Sci.: Poly. Phys. Edition 23, 873 (1985).

J. T. Dickinson, M. L. Klakken, M. H. Miles, and L. C. Jensen, "Electron Beam Induced Fracture of Polymers," to appear in J. Poly. Sci.: Poly. Phys. Ed.

M. A. Loudiana, J. Bye, J. T. Dickinson, and D. A. Dickinson, "Chemisorptive Emission from Fluorine Adsorption on Tungsten," Surf. Sci. 157, 459 (1985).

L. A. K'Singam, J. T. Dickinson, and L. C. Jensen, "Electron and Photon Emission Accompanying Failure of Metal/Glass Interfaces," to appear in J. Am. Ceramics Soc.

J. T. Dickinson, M. J. Dresser, and L. C. Jensen, "Time Correlation of Ion and Electron Emission from Surfaces Following Fracture," in Desorption Induced by Electronic Transitions (DIET II), W. Brenig and D. Menzel, ed., Springer-Verlag, Berlin, (1985).

J. T. Dickinson, S. Bhattacharya, and L. C. Jensen, "Fracto-emission from Neat Epoxy", submitted to J. Mat. Sci.

E. E. Donaldson, J. T. Dickinson, and X. A. Shen, "Time and Size Correlations of Photon and Radiowave Bursts from Peeling Pressure Sensitive Adhesives in Air", submitted to J. Adhesion.

J. T. Dickinson, L. C. Jensen, and M. R. McKay, "Emission of Atoms and Molecules Due To Fracture of Single Crystal MgO," submitted to J. Vac. Sci. and Technol.

J. T. Dickinson, L. C. Jensen, and M. L. Klakken, "Electron Beam Induced Fracture of Kevlar Single Fibers, submitted to J. Vac. Sci. and Technol.

F. Freund, R. M. Knobel, F. Struwe, and J. T. Dickinson, "Abiogenic Synthesis of Hydrocarbons from Carbon and Hydrogen Structurally Dissolved in Minerals," submitted to Proceedings of 12th International Meeting on Organic Geochemistry, Julich, West Germany, Sept. 1985.

(DYN)

DISTRIBUTION LIST

Dr. R.S. Miller
Office of Naval Research
Code 432P
Arlington, VA 22217
(10 copies)

Dr. J. Pastine
Naval Sea Systems Command
Code 06R
Washington, DC 20362

Dr. Kenneth D. Hartman
Hercules Aerospace Division
Hercules Incorporated
Alleghany Ballistic Lab
P.O. Box 210
Washington, DC 21502

Mr. Otto K. Heiney
AFATL-DLJG
Elgin AFB, FL 32542

Dr. Merrill K. King
Atlantic Research Corp.
5390 Cherokee Avenue
Alexandria, VA 22312

Dr. R.L. Lou
Aerojet Strategic Propulsion Co.
Bldg. 05025 - Dept 5400 - MS 167
P.O. Box 15699C
Sacramenta, CA 95813

Dr. R. Olsen
Aerojet Strategic Propulsion Co.
Bldg. 05025 - Dept 5400 - MS 167
P.O. Box 15699C
Sacramento, CA 95813

Dr. Randy Peters
Aerojet Strategic Propulsion Co.
Bldg. 05025 - Dept 5400 - MS 167
P.O. Box 15699C
Sacramento, CA 95813

Dr. D. Mann
U.S. Army Research Office
Engineering Division
Box 12211
Research Triangle Park, NC 27709-2211

Dr. L.V. Schmidt
Office of Naval Technology
Code 07CT
Arlington, VA 22217

JHU Applied Physics Laboratory
ATTN: CPIA (Mr. T.W. Christian)
Johns Hopkins Rd.
Laurel, MD 20707

Dr. R. McGuire
Lawrence Livermore Laboratory
University of California
Code L-324
Livermore, CA 94550

P.A. Miller
736 Leavenworth Street, #6
San Francisco, CA 94109

Dr. W. Moniz
Naval Research Lab.
Code 6120
Washington, DC 20375

Dr. K.F. Mueller
Naval Surface Weapons Center
Code R11
White Oak
Silver Spring, MD 20910

Prof. M. Nicol
Dept. of Chemistry & Biochemistry
University of California
Los Angeles, CA 90024

Mr. L. Roslund
Naval Surface Weapons Center
Code R10C
White Oak, Silver Spring, MD 20910

Dr. David C. Sayles
Ballistic Missile Defense
Advanced Technology Center
P.O. Box 1500
Huntsville, AL 35807

(DYN)

DISTRIBUTION LIST

Mr. R. Geisler
ATTN: DY/MS-24
AFRPL
Edwards AFB, CA 93523

Naval Air Systems Command
ATTN: Mr. Bertram P. Sobers
NAVAIR-320G
Jefferson Plaza 1, RM 472
Washington, DC 20361

R.B. Steele
Aerojet Strategic Propulsion Co.
P.O. Box 15699C
Sacramento, CA 95813

Mr. M. Stosz
Naval Surface Weapons Center
Code R10B
White Oak
Silver Spring, MD 20910

Mr. E.S. Sutton
Thiokol Corporation
Elkton Division
P.O. Box 241
Elkton, MD 21921

Dr. Grant Thompson
Morton Thiokol, Inc.
Wasatch Division
MS 240 P.O. Box 524
Brigham City, UT 84302

Dr. R.S. Valentini
United Technologies Chemical Systems
P.O. Box 50015
San Jose, CA 95150-0015

Dr. R.F. Walker
Chief, Energetic Materials Division
DRSMC-LCE (D), B-3022
USA ARDC
Dover, NJ 07801

Dr. Janet Wall
Code 012
Director, Research Administration
Naval Postgraduate School
Monterey, CA 93943

Director
US Army Ballistic Research Lab.
ATTN: DRXBR-IBD
Aberdeen Proving Ground, MD 21005

Commander
US Army Missile Command
ATTN: DRSMI-RKL
Walter W. Wharton
Redstone Arsenal, AL 35898

Dr. Ingo W. May
Army Ballistic Research Lab.
ARRADCOM
Code DRXBR - IBD
Aberdeen Proving Ground, MD 21005

Dr. E. Zimet
Office of Naval Technology
Code 071
Arlington, VA 22217

Dr. Ronald L. Derr
Naval Weapons Center
Code 389
China Lake, CA 93555

T. Boggs
Naval Weapons Center
Code 389
China Lake, CA 93555

Lee C. Estabrook, P.E.
Morton Thiokol, Inc.
P.O. Box 30058
Shreveport, Louisiana 71130

Dr. J.R. West
Morton Thiokol, Inc.
P.O. Box 30058
Shreveport, Louisiana 71130

Dr. D.D. Dillehay
Morton Thiokol, Inc.
Longhorn Division
Marshall, TX 75670

G.T. Bowman
Atlantic Research Corp.
7511 Wellington Road
Gainesville, VA 22065

Ser 432/84/211DYN
Revised January 1985

(DYN)

DISTRIBUTION LIST

R.E. Shenton
Atlantic Research Corp.
7511 Wellington Road
Gainesville, VA 22065

Brian Wheatley
Atlantic Research Corp.
7511 Wellington Road
Gainesville, VA 22065

Mike Barnes
Atlantic Research Corp.
7511 Wellington Road
Gainesville, VA 22065

Mr. G. Edwards
Naval Sea Systems Command
Code 62R32
Washington, DC 20362

Dr. Lionel Dickinson
Naval Explosive Ordinance
Disposal Tech. Center
Code D
Indian Head, MD 20340

C. Dickinson
Naval Surface Weapons Center
White Oak, Code R-13
Silver Spring, MD 20910

Prof. J.T. Dickinson
Washington State University
Dept. of Physics 4
Pullman, WA 99164-2814

Prof. John Deutch
MIT
Department of Chemistry
Cambridge, MA 02139

M.H. Miles
Dept. of Physics
Washington State University
Pullman, WA 99164-2814

Dr. E.H. deButts
Hercules Aerospace Co.
P.O. Box 27408
Salt Lake City, UT 84127

Dr. T.F. Davidson
Vice President, Technical
Morton Thiokol, Inc.
Aerospace Group
110 North Wacker Drive
Chicago, Illinois 60606

David A. Flanigan
Director, Advanced Technology
Morton Thiokol, Inc.
Aerospace Group
110 North Wacker Drive
Chicago, Illinois 60606

Mr. J. Consaga
Naval Surface Weapons Center
Code R-16
Indian Head, MD 20640

Dr. L.H. Caveny
Air Force Office of Scientific
Research
Directorate of Aerospace Sciences
Bolling Air Force Base
Washington, DC 20332

Naval Sea Systems Command
ATTN: Mr. Charles M. Christensen
NAVSEA-62R2
Crystal Plaza, Bldg. 6, Rm 806
Washington, DC 20362

W.G. Roger
Code 5253
Naval Ordance Station
Indian Head, MD 20640

Mr. R. Beauregard
Naval Sea Systems Command
SEA 64E
Washington, DC 20362

Dr. Donald L. Ball
Air Force Office of Scientific
Research
Directorate of Chemical &
Atmospheric Sciences
Bolling Air Force Base
Washington, DC 20332

Ser 432/84/211DYN
Revised January 1985

(DYN)

DISTRIBUTION LIST

Dr. Anthony J. Matuszko
Air Force Office of Scientific Research
Directorate of Chemical & Atmospheric Sciences
Bolling Air Force Base
Washington, DC 20332

Dr. Michael Chaykovsky
Naval Surface Weapons Center
Code R11
White Oak
Silver Spring, MD 20910

J.J. Rocchio
USA Ballistic Research Lab.
Aberdeen Proving Ground, MD 21005-5066

G.A. Zimmerman
Aerojet Tactical Systems
P.O. Box 13400
Sacramento, CA 95813

B. Swanson
INC-4 MS C-346
Los Alamos National Laboratory
Los Alamos, New Mexico 87545

Dr. James T. Bryant
Naval Weapons Center
Code 3205B
China Lake, CA 93555

Dr. L. Rothstein
Assistant Director
Naval Explosives Dev. Engineering Dept.
Naval Weapons Station
Yorktown, VA 23691

Dr. M.J. Kamlet
Naval Surface Weapons Center
Code R11
White Oak, Silver Spring, MD 20910

Dr. Henry Webster, III
Manager, Chemical Sciences Branch
ATTN: Code 5063
Crane, IN 47522

Dr. A.L. Slafkosky
Scientific Advisor
Commandant of the Marine Corps
Code RD-1
Washington, DC 20380

Dr. H.G. Adolph
Naval Surface Weapons Center
Code R11
White Oak
Silver Spring, MD 20910

U.S. Army Research Office
Chemical & Biological Sciences Division
P.O. Box 12211
Research Triangle Park, NC 27709

G. Butcher
Hercules, Inc.
MS X2H
P.O. Box 98
Magna, Utah 84044

W. Waesche
Atlantic Research Corp.
7511 Wellington Road
Gainesville, VA 22065

Dr. John S. Wilkes, Jr.
FJSRL/NC
USAF Academy, CO 80840

Dr. H. Rosenwasser
AIR-320R
Naval Air Systems Command
Washington, DC 20361

Dr. Joyce J. Kaufman
The Johns Hopkins University
Department of Chemistry
Baltimore, MD 21218

Dr. A. Nielsen
Naval Weapons Center
Code 385
China Lake, CA 93555

Ser 432/84/340
Revised January 1985

(DYN)

DISTRIBUTION LIST

K.D. Pae
High Pressure Materials Research Lab.
Rutgers University
P.O. Box 909
Piscataway, NJ 08854

Dr. John K. Dienes
T-3, B216
Los Alamos National Lab.
P.O. Box 1663
Los Alamos, NM 87544

A.N. Gent
Institute Polymer Science
University of Akron
Akron, OH 44325

Dr. D.A. Shockey
SRI International
333 Ravenswood Ave.
Menlo Park, CA 94025

Dr. R.B. Kruse
Morton Thiokol, Inc.
Huntsville Division
Huntsville, AL 35807-7501

G. Butcher
Hercules, Inc.
P.O. Box 98
Magna, UT 84044

W. Waesche
Atlantic Research Corp.
7511 Wellington Road
Gainesville, VA 22065

Dr. R. Bernecker
Naval Surface Weapons Center
Code R13
White Oak
Silver Spring, MD 20910

Prof. Edward Price
Georgia Institute of Tech.
School of Aerospace Engineering
Atlanta, GA 30332

J.A. Birkett
Naval Ordnance Station
Code 5253K
Indian Head, MD 20640

Prof. R.W. Armstrong
University of Maryland
Dept. of Mechanical Engineering
College Park, MD 20742

Herb Richter
Code 385
Naval Weapons Center
China Lake, CA 93555

J.T. Rosenberg
SRI International
333 Ravenswood Ave.
Menlo Park, CA 94025

G.A. Zimmerman
Aeroject Tactical Systems
P.O. Box 13400
Sacramento, CA 95813

Prof. Kenneth Kuo
Pennsylvania State University
Dept. of Mechanical Engineering
University Park, PA 16802

T.L. Boggs
Naval Weapons Center
Code 3891
China Lake, CA 93555

Ser 432/84/340
Revised January 1985

(DYN)

DISTRIBUTION LIST

Dr. C.S. Coffey
Naval Surface Weapons Center
Code R13
White Oak
Silver Spring, MD 20910

D. Curran
SRI International
333 Ravenswood Avenue
Menlo Park, CA 94025

E.L. Throckmorton
Code SP-2731
Strategic Systems Program Office
Crystal Mall #3, RM 1048
Washington, DC 23076

Dr. R. Martinson
Lockheed Missiles and Space Co.
Research and Development
3251 Hanover Street
Palo Alto, CA 94304

C. Gotzmer
Naval Surface Weapons Center
Code R-11
White Oak
Silver Spring, MD 20910

G.A. Lo
3251 Hanover Street
B204 Lockheed Palo Alto Research Lab
Palto Alto, CA 94304

R.A. Schapery
Civil Engineering Department
Texas A&M University
College Station, TX 77843

J.M. Culver
Strategic Systems Projects Office
SSPO/SP-2731
Crystal Mall #3, RM 1048
Washington, DC 20376

Prof. G.D. Duvall
Washington State University
Department of Physics
Pullman, WA 99163

Dr. E. Martin
Naval Weapons Center
Code 3858
China Lake, CA 93555

Dr. M. Farber
135 W. Maple Avenue
Monnovia, CA 91016

W.L. Elban
Naval Surface Weapons Center
White Oak, Bldg. 343
Silver Spring, MD 20910

G.E. Manser
Morton Thiokol
Wasatch Division
P.O. Box 524
Brigham City, UT 84302

R.G. Rosemeier
Brimrose Corporation
7720 Belair Road
Baltimore, MD 20742

Ser 432/84/340
Revised January 1985

Administrative Contracting
Officer (see contract for
address)
(1 copy)

Director
Naval Research Laboratory
Attn: Code 2627
Washington, DC 20375
(6 copies)

Defense Technical Information Center
Bldg. 5, Cameron Station
Alexandria, VA 22314
(12 copies)

Dr. Robert Polvani
National Bureau of Standards
Metallurgy Division
Washington, D.C. 20234

Dr. Y. Gupta
Washington State University
Department of Physics
Pullman, WA 99163

END

FILMED

12-85

DTIC